FINAL TECHNICAL REPORT

NASA Grant NSG-7329

Application of Laser Ranging and VLBI Data to a Study of Plate Tectonic Driving Forces

Principal Investigator: Sean C. Solomon
Associate Professor of Geophysics
Department of Earth and Planetary Sciences
Massachusetts Institute of Technology
Cambridge, MA 02139

617/253-3786

Period of Grant: April 1, 1978 to March 31, 1979

Date of Submission: May 30, 1980

This is a final technical report for the period 1 April 1978 - 30 April 1979 for the NASA Grant NSG-7329 "Application of Laser Ranging and VLBI Data to a Study of Plate Tectonic Driving Forces." As outlined in our original proposal, our broad goals have been to investigate the conditions under which changes in plate driving or resistive forces associated with plate boundary earthquakes will be measurable with laser ranging or VLBI and to pinpoint those aspects of plate forces that can be characterized by such measurements.

The bulk of this technical report consists of detailed reports of three aspects of our work as of the end of the grant year: (1) analytic solutions for two-dimensional stress diffusion in a plate following earthquake faulting on a finite fault; (2) two-dimensional finite-element solutions for the global state of stress at the Earth's surface for possible plate driving forces; and (3) finite-element solutions for three-dimensional stress diffusion in a viscoelastic Earth following earthquake faulting.

I. TWO DIMENSIONAL ANALYTICAL STUDY OF STRESS PROPAGATION WITHIN PLATES

Introduction

The migration of large earthquakes along plate boundaries has been a significant discovery in global tectonics (Mogi, 1968; Kelleher, 1970; Delsemme and Smith, 1979). Since the occurrence of plate boundary earthquakes is associated with the state of stress at the convergingplate boundaries, it is necessary to understand the response of the lithosphere to application or removal of horizontal boundary stresses (or displacements) in space and time. The new geodetic data offered by the VLBI network will give us the opportunity to observe these displacements in time.

There have been several studies on stress and strain diffusion from plate boundaries. The results depend largely on the type of material properties used to represent the asthenosphere. Bolt and Dean (1973) investigated a one dimensional model of an elastic plate underlain by a viscous layer. They confirm that the viscous shearing stress of the asthenosphere on the base of the lithosphere plays an important role in stress and strain diffusion through the lithosphere. They also predict the possible occurrence of a new type of strain wave in the lithosphere.

Melosh (1976) extends the study to a nonlinear viscous asthenosphere, again without an elastic component. Unlike the previous two viscous models, we introduce a Maxwellian behavior to the asthenosphere for the one-dimensional model; thus, an initial elastic response is possible. The results are significantly different from the previous models and suggest that, with the thickness of the asthenosphere at about 80 km and a viscosity of 10^{20} poise, the fluctuations in velocity and stress are greater than 50% of the equilibrium level for distances within 1000 km from the boundary disturbance (final report, NASA grant no. NSG-7329, April 1978).

One-dimensional models, however, can provide only limited insight into the plate response; the model ignores the finite length of the fault rupture. Moreover, the migration of major earthquakes is essentially parallel to the plate boundaries. In this study we examine displacements and stress propagation in two directions, parallel and perpendicular to the plate boundaries. Using this simple model will allow a qualitative understanding of the effect introduced by a finite fault on the plate dynamics.

Two dimensional stress and strain propagation

The earth's plates can be considered as shells covering the spherical surface of the earth. In order to simplify the problem, the earth's curvature is neglected and plane stress is assumed within the lithosphere. Figure 1 shows a finite two dimensional plate of thickness H_1 overlying a second layer, the asthenosphere, of thickness H_2. The boundary x=0 corresponds to the converging boundary (or trench) and the boundary x=L represents the ridge. The width of the plate in the y direction (along the arc) is 2C. Now consider a small element of the plate with volume dV=dxdydz.

The forces in the x and y directions are

$$f_x = \left(\frac{\partial \sigma_x}{\partial x} + \frac{\partial \tau_{xy}}{\partial y}\right) dV$$

$$f_y = \left(\frac{\partial \sigma_y}{\partial y} + \frac{\partial \tau_{yx}}{\partial x}\right) dV$$

The forces along the lithosphere per unit are are

$$F_x = \left(\frac{\partial \sigma_x}{\partial x} + \frac{\partial \tau_{xy}}{\partial y}\right) H_1 \qquad (1)$$

$$F_y = \left(\frac{\partial \sigma_y}{\partial y} + \frac{\partial \tau_{yx}}{\partial x}\right) H_1$$

For the driving mechanism of the plates, the above forces must be balanced by interplate friction and basal shear stresses. In most studies the basal shear stress is a primary factor in balancing the forces (Richter, 1977; Davies, 1978), the interplate friction appear to be smaller (Davies, 1978). Although it is still not known whether the basal

shear drives or drags the plates, we will assume that it drags the plate motion and ignore the transform friction.

If the asthenosphere is a simple elastic media with shear modulus μ , the basal shear on the top of the asthenosphere per unit area is

$$f_{xz} = \mu \frac{u}{H_2} \qquad (2)$$

$$f_{yz} = \mu \frac{v}{H_2}$$

where u and v are displacements in x and y directions respectively, and H_2 is the thickness of the asthenosphere.

Combining (1) and (2) and writing the stresses in terms of displacements, we obtain the equations of motion:

$$2\frac{\partial^2 u}{\partial x^2} + (1-\nu)\frac{\partial^2 u}{\partial y^2} + (1+\nu)\frac{\partial^2 v}{\partial x \partial y} = \frac{2\mu(1-\nu^2)}{E H_1 H_2} \qquad (3)$$

$$2\frac{\partial^2 v}{\partial y^2} + (1-\nu)\frac{\partial^2 v}{\partial x^2} + (1+\nu)\frac{\partial^2 u}{\partial x \partial y} = \frac{2\mu(1-\nu^2)}{E H_1 H_2} \qquad (4)$$

We can further simplify the equations of motion into

$$\nabla^2 \psi = \frac{k^2}{2}\psi \qquad (5)$$

$$\nabla^2 \varphi = \frac{k^2}{1-\nu}\varphi \qquad (6)$$

where ∇^2 is the Laplacian operator in two dimensions, and

$$\psi = \frac{\partial u}{\partial x} + \frac{\partial v}{\partial y} \qquad (7)$$

$$\varphi = \frac{\partial u}{\partial y} - \frac{\partial v}{\partial x} \qquad (8)$$

$$k^2 = \frac{2\mu(1-\nu^2)}{E H_1 H_2} \qquad (9)$$

Solving for $\psi(x,y)$ and $\varphi(x,y)$ gives the displacement fields u(x,y) and v(x,y).

A set of solutions that satisfies (5), (6), (7), and (8) is:

$$u(x,y) = \sum_{m=0}^{\infty} \cos\alpha y \left\{ \frac{a}{a^2-\alpha^2}\left(A_1 e^{ax} - A_2 e^{-ax}\right) + \frac{\alpha}{b^2-\alpha^2}\left(B_3 e^{bx} + B_4 e^{-bx}\right)\right\}$$

$$+ \sum_{m=0}^{\infty} \sin\alpha y \left\{ \frac{a}{a^2-\alpha^2}\left(A_3 e^{ax} - A_4 e^{-ax}\right) - \frac{\alpha}{b^2-\alpha^2}\left(B_1 e^{bx} + B_2 e^{-bx}\right)\right\} \quad (10)$$

$$v(x,y) = \sum_{m=0}^{\infty} \cos\alpha y \left\{ \frac{\alpha}{a^2-\alpha^2}\left(A_3 e^{ax} + A_4 e^{-ax}\right) - \frac{b}{b^2-\alpha^2}\left(B_1 e^{bx} - B_2 e^{-bx}\right)\right\} \quad (11)$$

$$+ \sum_{m=0}^{\infty} \sin\alpha y \left\{ \frac{-a}{a^2-\alpha^2}\left(A_1 e^{ax} + A_2 e^{-ax}\right) - \frac{b}{b^2-\alpha^2}\left(B_3 e^{bx} - B_4 e^{-bx}\right)\right\}$$

where

$$\alpha = m\pi/c \quad (12)$$

$$a = \sqrt{\alpha^2 + k^2/2} \quad (13)$$

$$b = \sqrt{\alpha^2 + k^2/1-\nu} \quad (14)$$

The coefficients $A_1, A_2, \ldots, B_3, B_4$ are functions of m.

Boundary conditions

In order to obtain non-trivial solutions, the boundary conditions require careful attention. The problems of geometry restrict the applications to general cases with rectangular boundaries. Great earthquakes and their aftershocks only occury a small portion of the boundary. To simulate this boundary condition, we assume a unit displacement along the x=0 corresponding to the arc. The displacement is applied from y=-d to y=d throughout the thickness H_1. The remainder of this boundary remains fixed. We assume frictionless boundaries

at $y=\pm C$. The ridge ($x=L$) is also assumed to be stress free. Mathematically, these conditions become

$$u(0,y) = \begin{cases} u_0 & \text{at} \quad -d \le y \le d \\ 0 & \text{elsewhere} \end{cases} \tag{15}$$

$$\text{or} \quad u(0,y) = u_0 \frac{d}{c} + \sum_{m=1}^{\infty} \frac{2u_0 \sin(\alpha d)}{\alpha c} \cos \alpha y$$

$$\tau_{xy} = 0 \qquad \text{at} \quad y = \pm c \tag{16}$$

$$\sigma_x = \tau_{xy} = 0 \qquad \text{at} \quad x = L \tag{17}$$

Using these boundary conditions we obtain:

$$A_3 = A_4 = B_1 = B_2 = 0$$

$$A_1(0) = -A_2(0)\, e^{-2aL} \qquad \text{for} \quad m = 1, 2, \ldots, \infty$$

$$A_1(m) = A_2(m)\, e^{-2aL}$$

$$B_3(m) = B_4(m)\, e^{-2bL}$$

Solving for A_2 and B_4 is accomplished with the matrix equation:

$$\begin{bmatrix} \frac{2\alpha a}{a^2-\alpha^2} e^{-aL} & -\frac{(b^2+\alpha^2)}{b^2-\alpha^2} e^{-bL} \\ \frac{-a}{a^2-\alpha^2}(1+e^{-2aL}) & \frac{\alpha}{b^2-\alpha^2}(1+e^{-2bL}) \end{bmatrix} \begin{bmatrix} A_2 \\ B_4 \end{bmatrix} = \begin{bmatrix} 0 \\ 2\mu_0 \frac{\sin(\alpha d)}{\alpha \cdot c} \end{bmatrix} \tag{18}$$

The solution has the form of a Fourier series. In practice we truncate the series to obtain a solution. The truncation introduces a Gibb's phenomena which is reduced through a Lanczo's factor. With 120 terms, the solutions for the displacements and stresses at the boundary x=0 (the 'arc') are plotted in Figure 2. The figure shows u displacement applied as the boundary condition on the converging 'arc'. The corresponding displacement v along the 'arc' is shown in Figure 3. The displacements increase sharply near the "earthquake".

Examining the stress distribution along the boundary in Figure 4, we note that the stress normal to the arc (σ_x) is compressional in the 'earthquake' region and changes to tension at the edge of the rupture zone.

The distribution of stress σ_y along the arc x=0 (figure 5) fits our interpretation of the displacements in figure 3. A sharp increase in shear stress at the edge of the 'earthquake' rupture is also expected and is shown in figure 6. In each case these are the elastic deformations expected for the simple plate model at the plate boundary.

We now wish to examine how deeply this instantaneous elastic deformation penetrates into the plate. Figure 7 and 8 are the distributions of the displacement u and stress σ_x along the x axis, that is, perpendicular to the arc. Both diagrams suggest that the elastic deformations are significant within a distance equivalent to the length of the fault rupture. This qualitatively agrees with exact solutions for the elastic deformations. If we now transform our elastic solution with the correspondence principle of viscoelasticity, we can obtain the time-dependent solutions for a Maxwellian asthenosphere. Our approach is analogous to the one-dimensional problem outlined in the previous report (final report, NASA grant no. NSG-7329).

FIGURES

Figure 1

Two dimensional model for an elastic lithosphere of thickness H_1 and Young's modulus E overlying a viscoelastic asthenosphere of thickness H_2, viscosity η, and shear modulus μ. The lithosphere has a finite length L in the x direction perdendicular to the arc. The width is 2C in the y direction along the 'arc'. A unit displacement simulates the 'earthquake' at the boundary x=0 between y=-d and y=d. Consequently, the earthquake rupture zone has length 2d.

Figure 2

Displacement u (in x direction) at the boundary x=0 corresponding to the 'arc'. The displacement is plotted along the y axis, distance along the 'arc'. For this model we assume that d = 800 km and C = 4000 km. The length of the plate is 5000 km . The displacement u along the rupture is 10 m,

Figure 3

Displacement v parallel to the arc along the boundary x=0. In the 'rupture' zone, the displacement increases rapidly until the termination of the rupture is reached at $y=\mp d$. Beyond the rupture, the displacement v decreases.

Figure 4

The stress σ_x normal to the arc as a function of distance along the arc (x=0). As expected, compression occurs in the earthquake zone and tension occurs outside this area. If the converging boundary is initially under compression, the 'earthquake' rupture increases the stress level outside the earthquake zone.

Figure 5

The stress σ_y parallel to the arc as a function of distance along the boundary (x=0).

Figure 6

Shear stress as a function of distance along the arc (x=0). Near the edge of the rupture zone the shear stress reaches a maximum.

Figure 7

Displacement normal to the arc (u) as a function of x, the distance from the converging arc.

Figure 8

Stress σ_x normal to the 'arc' as a function of x, the distance from the converging arc.

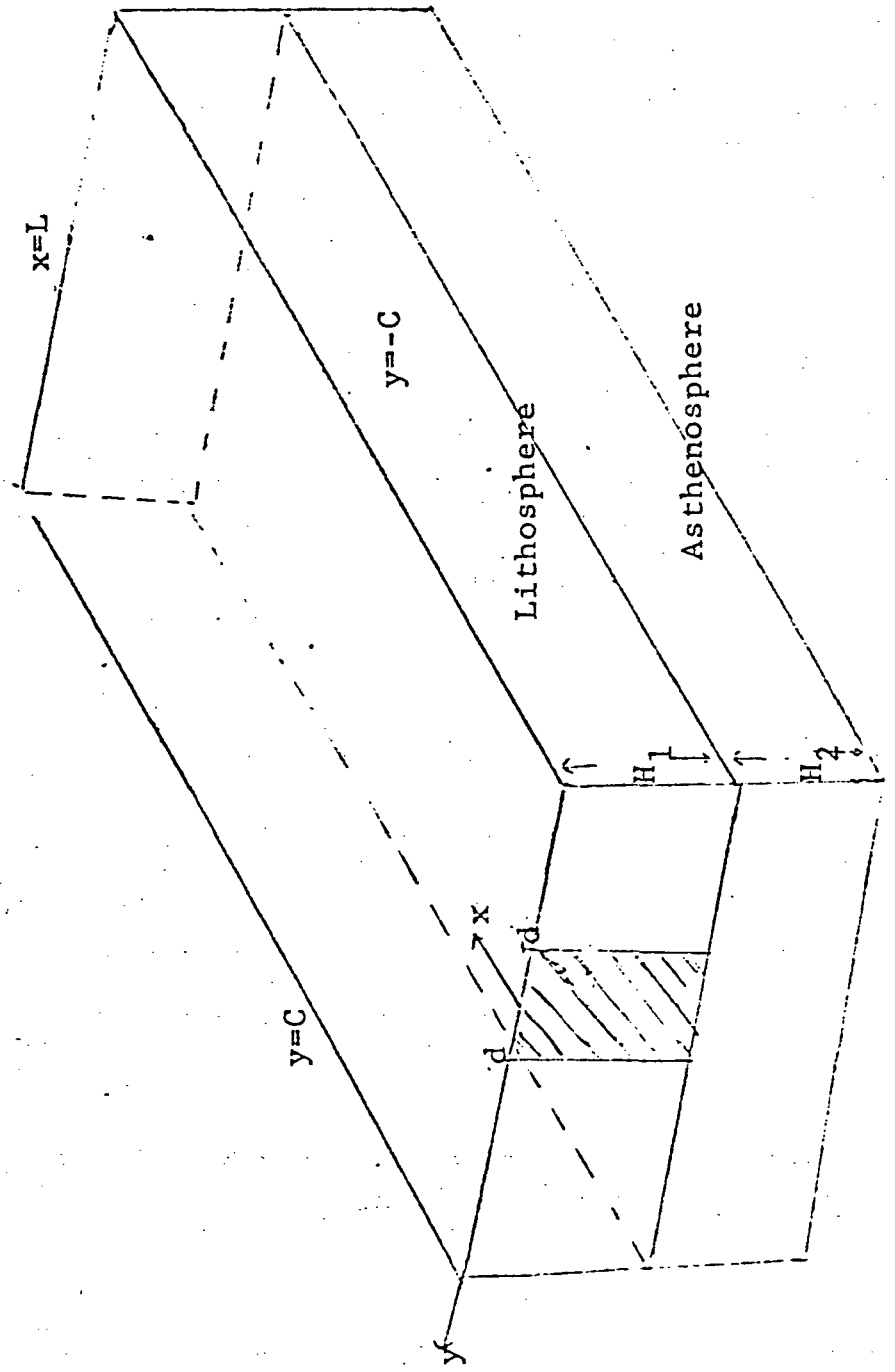

Fig. 1

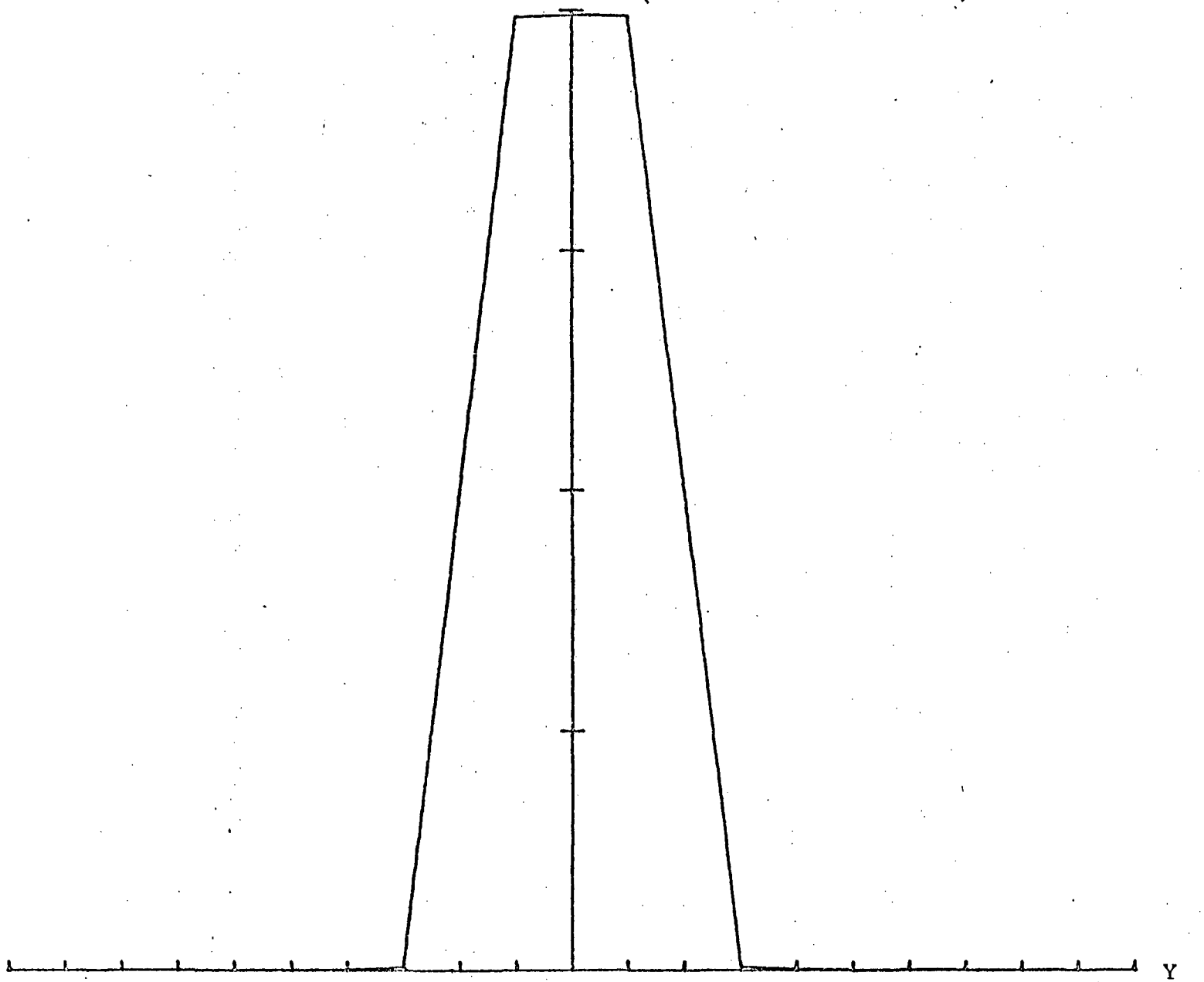
DISPLACEMENT U (PERPENDICULAR TO ARC)
Y
4000 km
DISTANCE ALONG ARC
Fig. 2

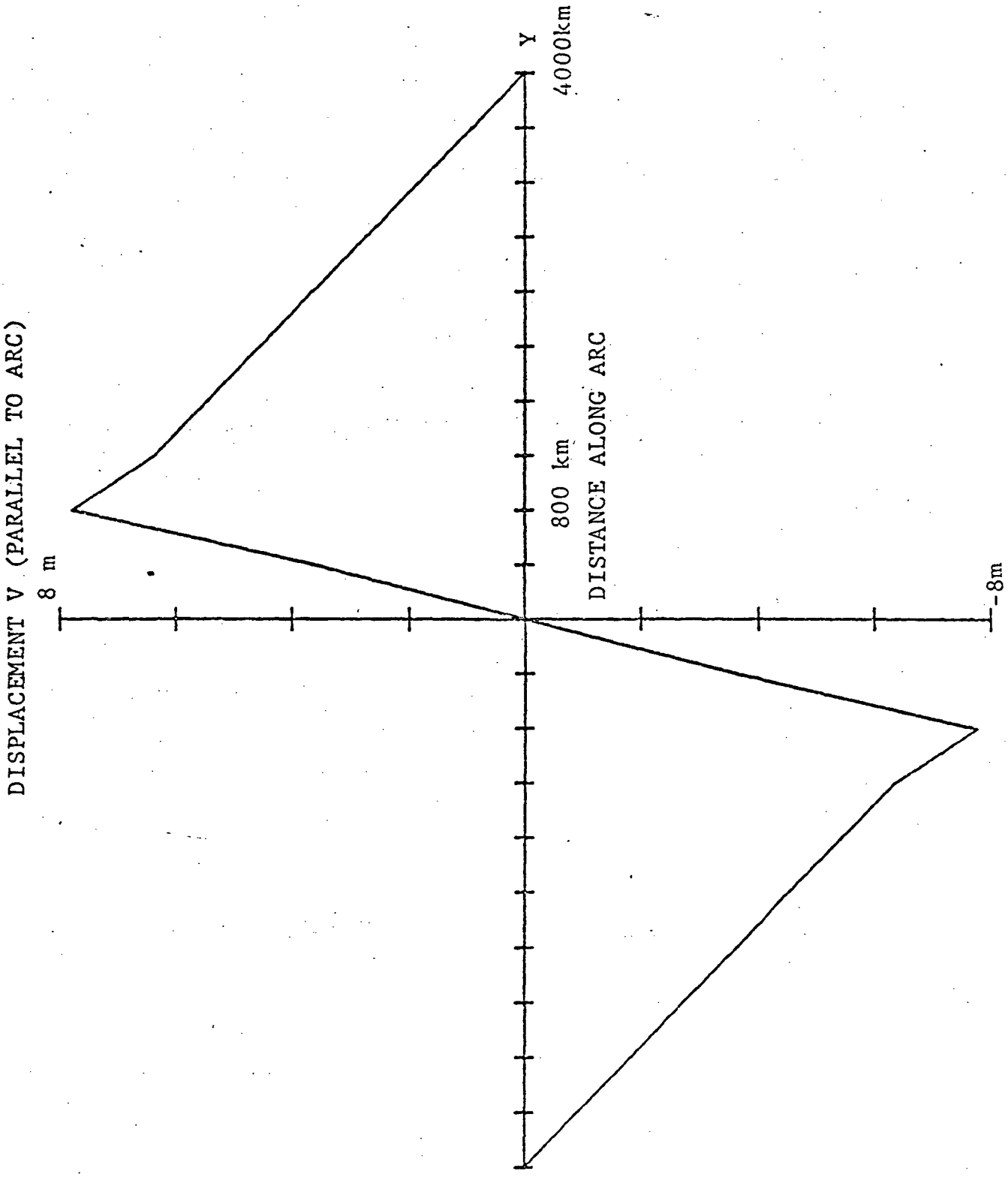
DISPLACEMENT V (PARALLEL TO ARC)
8 m
-8m
Y
4000km
800 km
DISTANCE ALONG ARC

Fig. 3

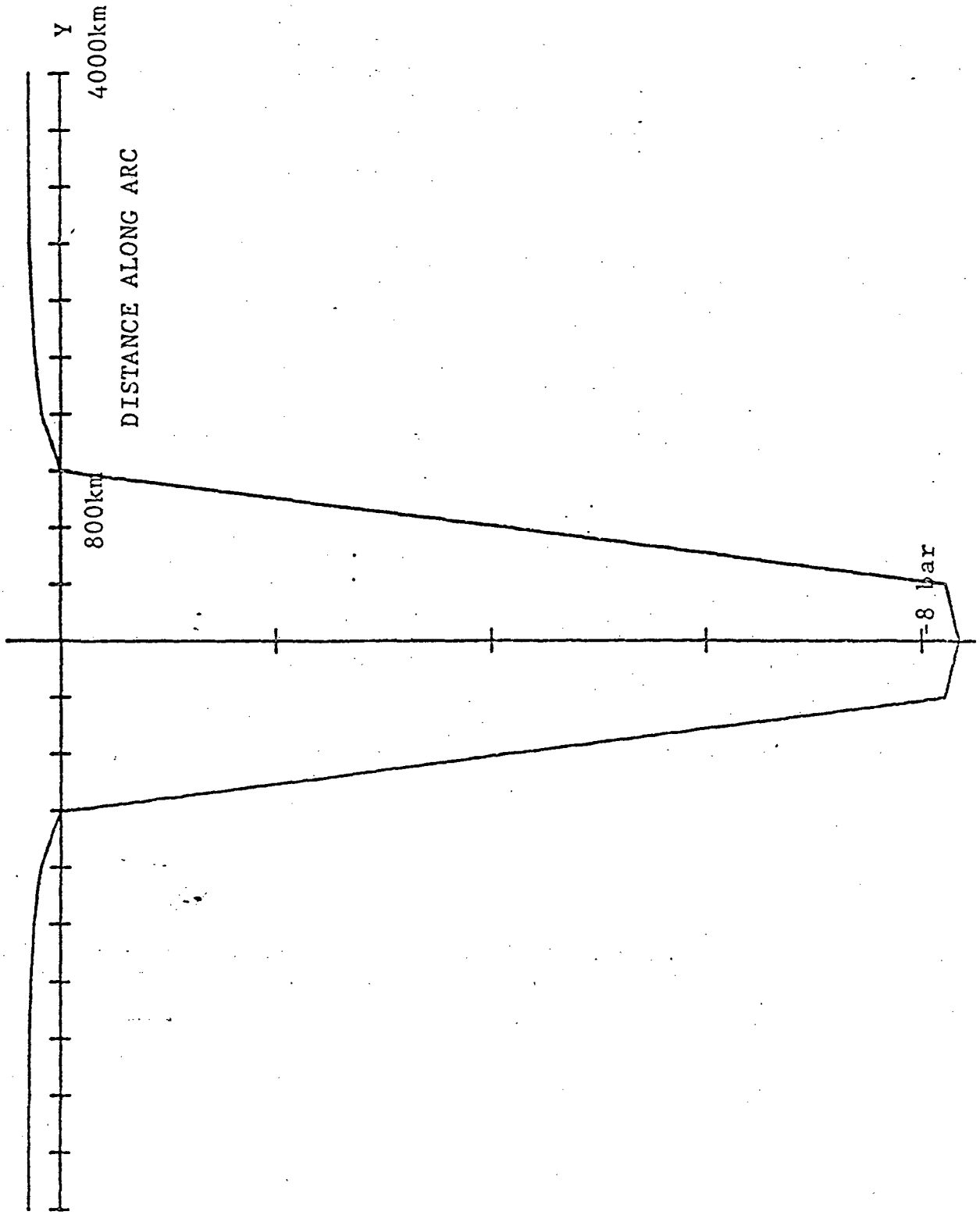

Fig. 4

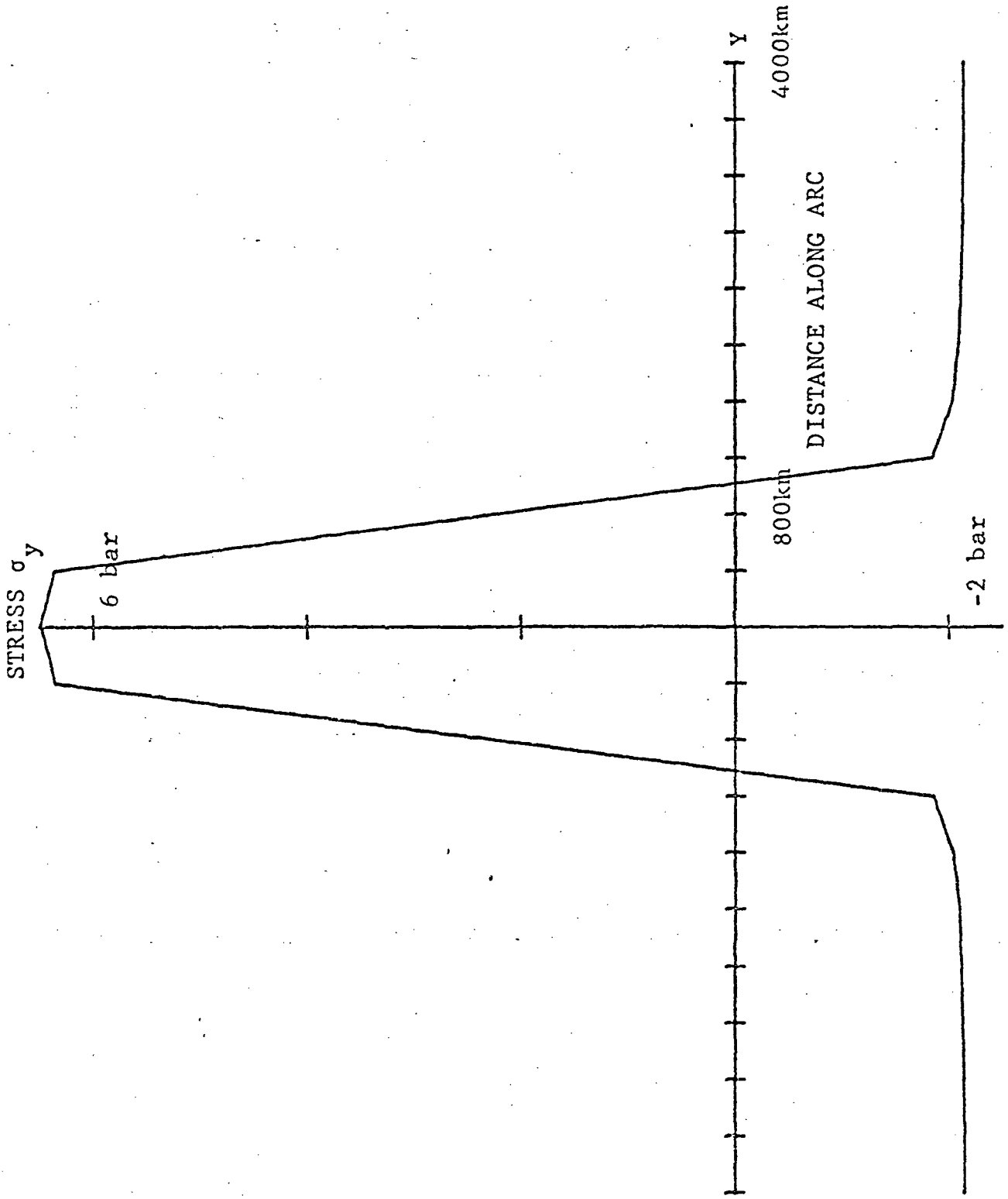

Fig. 5

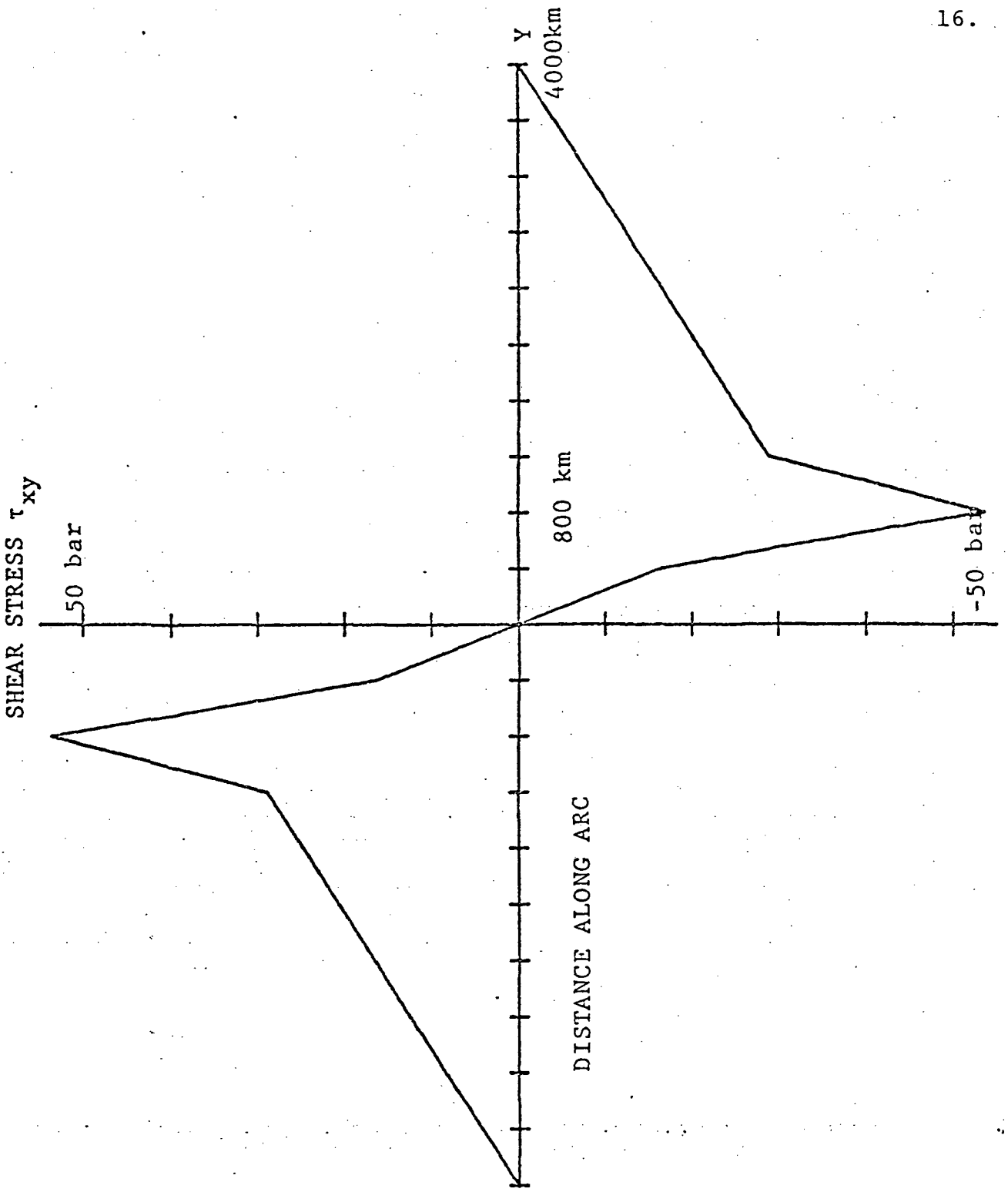
SHEAR STRESS τ_{xy}
50 bar
-50 bar
800 km
Y
4000km
DISTANCE ALONG ARC

Fig. 6

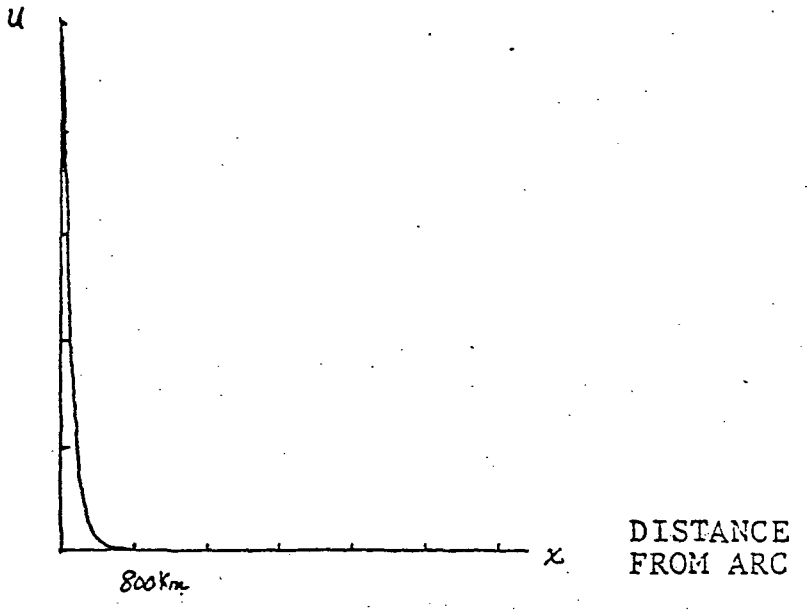

Fig. 7

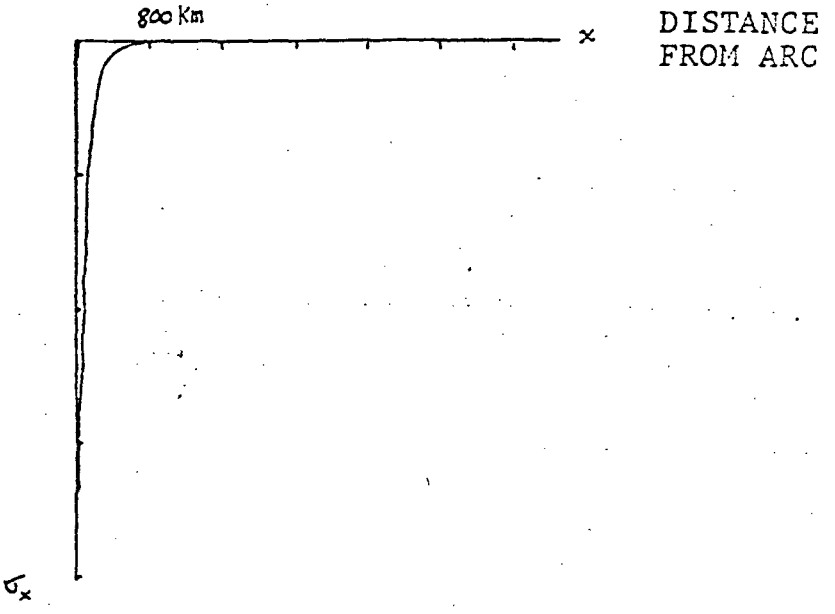

Fig. 8

INTRODUCTION

The state of stress in the lithosphere is the product of the many forces on a variety of scales that act on the plates. Foremost in importance among such forces are those responsible for plate motions, often collectively termed the driving mechanism. For specific models of the plate tectonic driving mechanism, the intraplate stress field may be calculated and compared against those indicators of stress in the earth most likely to reflect tectonic forces. The comparison of predicted and observed stresses, a powerful test of driving force models, is the subject of this paper.

In earlier works, we calculated intraplate stresses for various driving mechanism models, using a finite difference technique, a coarse grid for the earth, and a body of observations consisting primarily of midplate earthquake mechanisms [Solomon et al., 1975,1977b; Richardson et al., 1976]. In this paper we offer several substantial improvements over the earlier work, including the use of a more versatile finite element computational technique with better spatial resolution, particularly near plate boundaries; a more extensive catalog of intraplate stress observations; and a wider range of tested driving force models.

We begin with a review of the important tectonic driving and resistive forces capable of stressing the plates, with due consideration also for sources of intraplate stress not related to the driving mechanism. The constraints set on

these forces by the relative and absolute velocities of the plates are briefly summarized.

The various methods for inferring the orientations and/or magnitudes of the principal intralithospheric stresses are next reviewed, including earthquake mechanisms, in situ measurements, and observation of stress-sensitive geological features. Based on these techniques, the regional stress orientation field and its observational basis is synthesized for each plate.

The logical leap to the notion that the directions of principal stresses inferred from observations may be used as quantitative tests of driving force models as posed in this paper is based on three premises: (1) that a regionally consistent stress field exists within large fractions of the lithosphere; (2) that such a stress field is steady on a time period of less than $\sim 10^6$ years; and (3) that the dominant forces which give rise to most of that stress field are plate tectonic in origin.

The first premise, regional consistency of stress orientations, is the most readily established for several important intraplate areas, on the basis of many determinations by a variety of independent techniques. The second premise, steadiness of the regional stress field over time periods long compared to the period of observation, depends on the response of the plate to plate-boundary earthquakes through the rheology of the asthenosphere and lithosphere [c.f., Anderson, 1975] and is not well established at this time. Determination by laser ranging [Bender and Silverberg, 1975] or by very long baseline interferometry [Coates

et al., 1975] that the motion is steady between the stable interiors of different plates would lend strong support to the concept of a steady regional stress field.

The third premise, that an identifiable portion of the regional stress field arises from plate tectonic forces, is the most difficult to ascertain. We argue below that this premise is most likely to be correct in regions well removed from such other notable sources of stress as recent tectonic or thermal activity, recent topographic loading or unloading, and pronounced structural heterogeneities.

If these three premises hold, then the comparison of calculated to observed intraplate stresses offers a sensitive test of driving mechanism models. If one or more of the premises is unfounded, then the calculations of stresses presented in this paper may still be viewed as a guide to that contribution to the stress field from steady plate driving forces.

The stress calculations are based on a finite element technique, described below and also in Richardson [1978]. The lithosphere is modeled as a thin shell, and the plates are regarded as distinct elastic units which terminate at plate boundaries. Net driving forces at spreading centers and subduction zones are abstracted as line forces at plate boundaries. Global intraplate stresses determined for a large number of possible force models, and the comparison of predictions with observations, are used as a basis to

modify and reject models.

The results of the modeling may be summarized as follows: pushing forces related to the topography of ridges are required of all models that match the inferred intraplate stress field. The net pulling force exerted on the plates by subducted lithosphere is at most a few times greater than other forces acting on the plates, even if net slab forces decrease with increasing subduction rate because of resistive forces that depend on velocity. Forces acting at continental convergence zones that resist further convergence are important for models of the intraplate stress field in Europe, Asia, and the Indian plate. Viscous drag at the base of the plate is best modeled as a resistive force, with a drag coefficient that is non-zero beneath oceanic lithosphere, but which may be concentrated by a factor of up to ten beneath continental lithosphere. Models of the driving mechanism in which drag forces drive the plates are in poor agreement with the observed data for most regions. A model in which drag balances the net torque produced on each plate by boundary forces, including slab pull concentrated on the subducted plate, yields good agreement between predicted and observed stresses in the continents but a poor fit in oceanic regions.

DRIVING FORCES AND STRESSES

The specification of the driving mechanism for plate tectonics should ideally be a fully dynamic description, in which plate motions and plate geometries do not have to be assumed but follow from a quantitative theory for mantle convection that includes plate recycling as a natural element. Such a specification is unfortunately not yet within our grasp. As an alternative, perhaps adequate at this stage in our knowledge, we abstract the true driving mechanism as simply parameterized forces acting at plate boundaries and at the base of the lithosphere. The plate boundary forces depend upon boundary type, and perhaps on other parameters such as relative velocity or local plate age, and the basal forces depend on the nature of the interaction between the lithosphere and the asthenosphere.

Ridge Forces

Mid-ocean ridges can exert a net compressive stress on the adjacent spreading plates because of their elevation with respect to abyssal sea floor. The magnitude of this stress has been estimated at several hundred bars [Hales, 1969; Frank, 1972; McKenzie, 1972; Artyushkov, 1973], and likely dominates any resistance to spreading at the ridge axis [Sleep and Biehler, 1970; Lachenbruch, 1973] as expressed in the extensional tectonics [Sykes, 1967].

The driving force associated with spreading centers is distributed over oceanic lithosphere young enough so that the

plate density structure continues to change with age [e.g., Hager, 1978], but we approximate it for simplicity as a line force at the ridge. The force is normal to the topographic strike of the ridge (i.e., generally in the direction of spreading), and is symmetric about the ridge axis. Since the height of most ridges far from hot spots is nearly uniform [Sclater et al., 1971], the ridge force is approximately independent of spreading rate.

Subduction Zone Forces

A major potential driving force for plate motions is the negative buoyancy of subducted lithosphere. The density contrast due to the temperature difference between subducted slab and surrounding mantle is capable of exerting a tensile stress of up to several kilobars on the subducted surface plate [McKenzie, 1969a; Turcotte and Schubert, 1971], an important component of which is the elevation of major phase changes within the slab [Smith and Toksöz, 1972; Solomon and Paw U, 1975].

For the determination of intraplate stress, the effective force at subduction zones is the net difference between the negative buoyancy of the slab and the variety of resistive forces acting to oppose subduction. These resistive forces include friction along the island arc thrust zone, drag against the sides of the slab, and the excess pressure on the leading edge of the slab [Isacks and Molnar, 1971; Smith and Toksöz, 1972; Richter, 1977]. It is also possible that large normal-

faulting earthquakes may decouple sections of the slab from the surface plate [Kanamori, 1971; Abe, 1972]. Evidence both from the speeds of subducted plates and from the focal mechanisms of intraslab earthquakes suggest that the negative slab buoyancy is approximately balanced by these resistive forces for most subduction zones [Smith and Toksöz, 1972; Forsyth and Uyeda, 1975; Richter, 1977]. The net pulling force at trenches resulting from this approximate balance is likely to depend on convergence rate, the angle of subduction, and the age of the subducted lithosphere [Richter and McKenzie, 1979].

The extent to which the subducted slab exerts a 'pull' on the overthrust plate is an important but poorly resolved issue. That such a force exists is strongly suggested by the trenchward component of absolute motion for nearly all overthrust sides of subduction zones, particularly if inter-arc spreading is considered [Chase, 1978b]. This force may be associated with a convective cell generated by shear on the asthenosphere by the descending slab [Richter, 1973]. The relative magnitudes of net pull on the subducted plate and any pull on the overriding plate are not well constrained.

The topography of the outer rise seaward of many trenches has been explained in terms of plate flexure. Hanks [1971] argued on the basis of a thin elastic plate model that both large (kilobars) bending stresses and a superposed regional compressive stress of comparable magnitude are required. Lower bending stresses, however, are possible for thicker viscoelastic plates [DeBremaecker, 1977], and a regional compressive stress has been shown to be unnecessary for several forms of plate rheology [e.g., Chapple and Forsyth, 1979].

It is likely that boundary forces at zones of active continental convergence such as the Alpine-Himalayan belt are not of the same form as along oceanic subduction zones. The absence of a substantial length of slab and the elevated topography at the collision zone suggest that such boundaries may offer a net resistance to further convergence. Detailed models of the Himalayan zone [Bird, 1976]give 1 kbar net compressive stress due to the load of the mountain belt.

Drag Forces

Viscous shear forces will be present at the base of the plates if the lithosphere is in motion with respect to the asthenosphere. The magnitude of such forces will depend upon plate velocity and asthenosphere viscosity and the directions will depend upon the velocity of local mantle flow relative to the plate. The mantle may be convecting and dragging the plates along the tops of convection cells; it may be passively resisting the motion of the plates; or it may have a complex flow pattern perhaps only loosely related to current plate geometries and surface motions. These possibilities are intimately tied to the questions of the radial extent of upper mantle convection and to the depth dependence of viscosity in the Earth.

Convection in the earth was suggested as early as Holmes [1929] as the driving mechanism for continental drift. The simple early notion that the plates were dragged along the tops of large Rayleigh-Benard cells can be shown to be inadequate

for plates of large horizontal extent [Richter, 1973], though this result depends on the assumed depth extent of convection. Mantle 'plumes,' are another form of convection proposed as a plate driving mechanism [Morgan, 1972], though the identification of 'hot spots' with plume traces leads to geometries not compatible with plumes playing a major driving force role for most plates. A major objection to sublithospheric convective shear as a major driving mechanism is the amount of time required for the flow pattern to change, 10^7 to 10^9 years [Richter, 1973], compared to times of 10^6 years or less over which substantial changes in spreading rates and directions occur [e.g., Sclater and Fisher, 1974]

If the lithosphere is moving with respect to a generally passive asthenosphere, there will be a viscous force resisting plate motion. The force will be in the direction opposite to absolute plate motion and the magnitude of the drag will depend on the plate speed and on the law relating shear stress to strain rate. The simplest assumption is that viscosity is independent of strain rate, so that the drag force is linearly proportional to the plate velocity. In the actual mantle, a non-linear relationship between stress and strain-rate seems likely [Stocker and Ashby, 1973], and shear heating may also be important [Schubert et al., 1976].

The asthenosphere viscosity may also vary spatially, with potentially higher viscosity beneath continental lithosphere compared to oceans [Jordan, 1975] or beneath old oceanic lithosphere compared to young seafloor [Schubert et al., 1976].

Most likely the asthenosphere is neither passive nor actively dragging the surface plates along their present directions of movement, but rather has a complicated flow pattern with respect to the surface plate geometries. On a large scale, there must be flow to balance the creation and destruction of plates. There are several solutions to this asthenospheric 'counterflow' [Harper, 1978; Chase, 1979; Hager and O'Connell, 1979], depending principally on the assumed penetration depth of upper mantle convection. The direction of the counterflow is, for at least a few plates, substantially different from antiparallel to the 'absolute' plate motion vector [e.g., Chase, 1979; Hager and O'Connell, 1979]. An alternative approach to the problem of large scale drag is to find that drag for each plate that balances the torques due to boundary forces [Davies, 1978]. There may also be a smaller secondary scale of convection [Richter and Parsons, 1975; McKenzie and Weiss, 1975] associated with mantle heat transfer, though this result, too, is sensitive to the question of the radial extent of upper mantle convection.

Thus drag forces are among the most difficult to specify with any confidence. Shear stress associated with secondary scales of convection that may not be important for net momentum transfer to large surface plates may still be important for intraplate stress. At best, the calculation of intraplate stress can serve as a test of any specific mantle flow model. As knowledge of the flow pattern improves, this test can be refined.

Transform Fault Forces

Shear stress on transform faults separating two plates will resist the relative motion of the plates. The seismic activity observed on transform faults is a clear indication that transform faults resist plate motion. The magnitude of that resistance, however, is less clear. If shear stresses in the kilobar range exist along major transforms and thrust faults at subduction zones, the forces of ridge pushing and slab pulling are insufficient to drive the plates and a driving mechanism involving shear by mantle convection must be involved [Hanks, 1977].

Laboratory measurement of the shear strengh of rocks at pressures and temperatures corresponding to crustal depths indicates that several kilobars of shear stress are required to produce failure of samples, even when pre-existing faults exist [Brace and Byerlee, 1970; Stesky et al., 1974]. The requirement of high shear stresses is relaxed if the ambient effective stress is lowered by high fluid pore pressures.

Shear stresses in the hundreds of bars range on transform faults are indicated, however, by several lines of reasoning. Heat flow measurements across the San Andreas fault [Brune et al., 1969], along with a model of shear heating, indicate a maximum shear stress of a few hundred bars acting on the fault. The generally orthogonal relationship between transform faults and spreading centers has been used to conclude that resistance to motion along transforms is less than the resistance to plate separation at spreading centers [Lachenbruch and Thompson, 1972]; to the extent that ridges are the site of upwelling of material of low

strength, this result implies that the shear stresses on transforms are small. From the inversion of observed plate motions, Forsyth and Uyeda [1975] found that shear forces on transform faults were not an important part of the driving mechanism, because plate velocities do not depend on the length of transform for each plate. For these reasons and because the total length of transform boundaries is less than ridge or trench boundaries, we shall adopt the view here that transforms are a relatively minor component of the driving mechanism.

Other Sources of Stress

Central to the idea that the intraplate stress field can be used to study the driving mechanism is the assumption that the effect of sources of stress other than plate driving forces can be removed or neglected. Such other sources of intraplate stress include thermal stresses associated with a cooling lithosphere [Turcotte and Oxburgh, 1973], stresses arising from the motion of an elastic plate on an ellipsoidal earth [Turcotte and Oxburgh, 1973], inhomogeneities in crustal thickness [Artyushkov, 1973], lithospheric loading by glaciers, sea level changes, and volcanic constructs [Walcott, 1970; Watts and Cochran, 1974], sedimentation and erosion [Voight and St. Pierre, 1974; Haxby and Turcotte, 1976], and residual strains [Swolfs et al., 1974; Tullis, 1977].

Tensile thermal stresses parallel to the ridge may arise as the plate spreads away from the ridge and cools. This stress has been estimated to be potentially as large as 40 kbar in magnitude [Turcotte and Oxburgh, 1973]. Thermal stresses, however, must be relaxed by deformation on the grain size level because of anisotropic thermal expansion of mineral grains, a process that should also relax the larger scale thermal stress without coherent lithospheric failure and large intraplate earthquakes [Solomon et al., 1975].

As a plate moves in a north-south direction, it will experience a change in radius of curvature due to the ellipticity of the earth. This effect will be at a maximum at a latitude of ±45°, where estimates of the magnitude of ensuing tensile stresses at the edge of the plate, based on thin shell theory, are as large as 6 kbar [Turcotte and Oxburgh, 1973]. Most of the earth's plates have velocities with large east-west components compared to north-south motions, which would minimize the effect of ellipticity. For northward plate velocities of a few centimeters a year, it would take about 10^8 years for the plate to travel from the equator to 45°N. In such a time, the plate may deform plastically and relieve these membrane stresses. Such stresses may have been important in Africa, however; the East African rift system may have been generated by the slow northward motion of the African plate over the last 100 million years [Oxburgh and Turcotte, 1974].

Horizontal variations in the density of the crust or mantle will result in stresses in the lithosphere. The stresses generated by the topographic relief of mid-ocean ridges and continental

convergence zones arise in this way. Features such as mid-plate mountains, large plateaus, and continental shelves also produce stress, even if the structures are isostatically compensated [Artyushkov, 1973]. Intraplate stress observations as indicators of plate driving forces should be well removed from such features.

The addition and removal of mass from the surface of the lithosphere will also give rise to stress. Important processes capable of producing measurable stress in this fashion are glaciation, addition of volcanic constructs, sedimentation and erosion. For the case of erosion, the thermal stress associated with material cooling as it approaches the earth's surface is opposite in sign and may be comparable to the unloading stress [Haxby and Turcotte, 1976]. Evidence on the driving mechanism from intraplate stresses should be sought from sites where none of these processes are likely to dominate the stress field.

There is evidence that strains can be locked into rocks after the forces producing the strains have ceased to operate [Swolfs et al., 1974; Tullis, 1977]. Known as residual strains, these may be the result of ancient tectonic processes and may mask strains associated with present tectonic forces. The magnitudes of residual strains can be estimated using double overcoring techniques. Uncertainties in the origin of the stress field may thus be reduced if residual strains are found to be small. Further, if the intraplate stress field is uniform over a large area including regions of very differeng geologic history, the effects of residual strains are probably small. The possibility of some regionally consistent remnant stresses indicative perhaps of an old plate

tectonic event cannot, however, be dismissed.

EVIDENCE FROM PLATE VELOCITIES

A primary data base for testing the relative importance of the various forces acting on the edges and the bases of the plates has been the set of plate motions. Information on these forces has been derived from (i) the prediction of absolute plate velocities given the relative motions, (ii) statistical correlations between plate speeds and force distributions, (iii) the prediction and/or the inversion of relative plate velocities, and (iv) several of the above at geologic times different from the present.

The motions of the plates with respect to the underlying mantle, often termed their 'absolute' motions, are derivable from plate driving force models as long as the set of forces includes some that are dependent on absolute plate velocity. The latitudinal component of predicted absolute velocities may be compared with paleomagnetic [McElhinny, 1973; Jurdy and Van der Voo, 1974] or paleosedimentation [Clague and Jarrard, 1973; van Andel, 1974] data, and the full velocity vector may be compared with the motion predicted from the fixed hot-spot hypothesis [Morgan, 1972]. Global calculations of absolute motions have the advantage that plate boundary forces symmetric about the boundary do not enter into the net torque balance for the lithosphere [Solomon and Sleep, 1974].

Global models of absolute plate models have been determined assuming a variety of relationships for lithosphere-asthenosphere interactions, including a uniform viscous drag law [Solomon and Sleep, 1974; Liboutry, 1974]; enhanced drag

beneath continental lithosphere; viscous drag balancing slab pull concentrated on the subducted plate at convergence zones [Solomon and Sleep, 1974; Solomon et al., 1975]; minimization of the horizontal translation of ridges and slabs [Kaula, 1975]; and viscous drag characterized by a non-linear relationship between stress and strain rate [Solomon et al., 1977b]. The models with no net torques due to drag also correspond to a minimization of the energy dissipated by drag [Solomon et al., 1975]. For virtually all of these absolute motion models, the predicted velocities are indistinguishable on the basis of present data and are similar to the velocities calculated in a fixed hot-spot frame [Minster et al., 1974]. Thus global models of present absolute plate motions do not yield much information about driving forces except to provide alternatives to deep mantle plumes as a physical basis for a hot-spot reference frame.

Present root-mean-square absolute speeds of the plates show several interesting correlations with boundary or force distributions that may have physical significance. The plate speeds generally decrease with increasing area of continental lithosphere [Minster et al., 1974] and increase with the percentage of plate boundary connected to a subducted slab [Forsyth and Uyeda, 1975]. The plate speed has also been recently shown to be generally proportional to the sum of the percentages of plate boundary occupied by ridges and connected to downgoing slabs [Aggarwal, 1978].

Direct relationships between the relative plate motions and driving force models have been sought both as forward and inverse problems. A fair fit to observed motions was obtained

by Harper [1975] using a ridge pushing force, subduction zone pull, and resistive drag; and an improved fit if subduction zone forces depend on the age of subducted lithosphere. Formal inversions of relative angular velocities to obtain the magnitudes of parameterized driving forces have been presented by Forsyth and Uyeda [1975], Chapple and Tullis [1977] and Harper [1978]. The solutions of both Forsyth and Uyeda [1975] and Chapple and Tullis [1977], using slightly different formulations, indicated that the negative buoyancy of the downgoing slab and the resistance to relative motion of slab and mantle dominate the force balance, with drag beneath continental lithosphere and pull toward trenches on overthrusting plates small but significant. Harper [1978], with a substantially different formulation of the forward problem including asthenospheric counterflow, obtained a solution in which subduction zone pull, weighted for convergence rate and subducted plate age, and continental 'push' due to differential heating are the major significant driving forces.

These same relationships between absolute or relative motions and driving force models can be tested for the plate system in geologic times different from the present. Global absolute motion models for the early Tertiary [Solomon et al., 1977a; Jurdy, 1978] suggest that the negative correlation at present between plate speed and continental area and the positive correlation between plate speed and percentage of subducted boundary may not be generally valid. That dominantly continental plates do not always move slowly as at present has

also been demonstrated from the rapid pre-Cenozoic velocities of several continental masses with respect to the paleomagnetic pole [Gordon et al., 1978b]. Whether hot spots can be demonstrated to define a stable reference frame over periods of tens of millions of years depends critically on past plate reconstructions [Burke et al., 1973; Molnar and Francheteau, 1975; Solomon et al., 1977a]; absolute motions for the Pacific plate derived from a driving force model with ridge and trench forces and resistive drag are consistent with a fixed Hawaiian hot spot [Gordon et al., 1978a].

In summary, the efforts at testing models for plate forces against relative and absolute plate motions lend confidence to the abstraction of the driving mechanism into boundary forces and basal drag stress, but leave without definitive answers the relative importance of most of the forces in question. Testing these same types of force models against the intraplate stress field should help narrow the suite of possible driving forces.

TECHNIQUES FOR DETERMINING INTRAPLATE STRESS

There are a variety of independent methods for inferring the local state of stress within a plate, including the mechanisms of intraplate earthquakes, direct in situ measurement, and making use of recent geological features sensitive to ambient stress. For most of these techniques, the directions of the principal stresses may be recovered more reliably than the principal stress magnitudes. The principal stress directions form the primary basis for describing the intraplate stress field with which calculated stresses from driving force models will be compared.

Earthquake Source Mechanisms

The source mechanism of an earthquake contains information about the orientation of the principal stresses at the source. A major advantage of midplate earthquake mechanisms for inferring intraplate stress directions is that a medium to large earthquake is responding to the average state of stress in a volume perhaps several tens of kilometers in dimension. If an earthquake is idealized as brittle fracture along a fresh, frictionless fault, the maximum (P) and minimum (T) compressive principal stress axes will bisect the angles between the two nodal planes and will be orthogonal to the null axis. Because the seismic wave radiation pattern is fundamentally a measure of strain release rather than ambient stress and because the assumptions linking the fault orientation to principal stress directions are not likely to be generally valid, the error in assuming that the principal stress axes

bisect the focal planes may be as large as ±45° [McKenzie, 1969b].

If a large intraplate region is characterized by consistent fault plane solutions, the uncertainties may be considerably smaller than the maximum of ±45°, however. There are probably many pre-existing faults with a distribution of orientations in any large area. The inferred principal stress directions for earthquakes on pre-existing faults should still reflect the ambient stress field for regions with a distribution of such faults, since the earthquake will presumably occur on that plane which minimizes the resistance to failure. It is reasonable, therefore, to assume that the effect of pre-existing faults may be neglected for large areas with consistent earthquake mechanisms.

An isolated earthquake, of course, even if the inferred principal stresses are correct, may not reflect the regional stress field. The local stress field that caused the earthquake may be caused by heterogeneities in topography or loading history.

Most intraplate earthquakes have hypocentral depths of less than 20 or 30 km. While 30 km is deeper than most other stress measurement techniques can sample, stresses inferred from intraplate earthquakes still may not represent the state of stress across the entire thickness of the plate. At trenches,

for instance, the large bending moments associated with the downgoing slab may locally produce marked changes between the state of stress at the top and bottom of the plate [Engdahl and Scholz, 1977; Chapple and Forsyth, 1979]. For intraplate regions away from topographic loads such as Hawaii, the bending moments are probably negligible [Turcotte, 1974], and it will be assumed that well-characterized fault plane solutions represent the stress throughout the plate thickness.

Fault plane solutions provide information only about the orientation, and not the magnitude, of the stresses at the source. Other seismic parameters such as apparent stress and stress drop may contain some information about the magnitude of deviatoric stresses, but these quantities are only lower bounds. On the basis of available stress drop and apparent stress data for intraplate earthquakes, the typical shear stress in the lithosphere is at least 100 bars [Kanamori and Anderson, 1975; Richardson and Solomon, 1977].

In Situ Methods

There are two major types of in situ techniques used to estimate stress. The first, strain relief, uses the relaxation of a surface after stress has been removed to calculate the original strain [e.g., Leeman, 1971]. With additional information about the elastic properties of the sample, the stress can be determined. The second technique, hydrofracture, measures stress directly by applying pressure to a closed section of a borehole until failure occurs [Haimson and Fairhurst, 1967, 1970]. The methods for in situ measurement

of stress, including their relative advantages and disadvantages, have recently been reviewed by McGarr and Gay [1978].

Both types of in situ measurements can yield the magnitude and direction of the principal stresses. Hydrofracture has advantages over strain relief methods in that elastic properties do not have to be measured and in that the technique can be applied at great depth. In the Michigan basin, for instance, hydrofracture has been used to depths exceeding 5 km [Haimson, 1978]. Thus the hydrofracture technique is much less sensitive to the local topography that may mask tectonic stress near surface. It should be noted, however, that 5 km is still relatively shallow compared to the thickness of the lithosphere and such measurements need not represent a vertical average of the state of stress across the entire plate. One disadvantage of hydrofracture compared to strain relief methods is that data interpretation for the former technique is based on the premise that one of the principal stress directions is vertical, an assumption that may not always hold at depth despite the boundary condition at the free surface.

Interpretations of both strain relief and hydrofracture data require considerable care. Stresses due to local topography and residual stresses preserved in a medium after the original stress has been removed may mask regional stresses, particularly for the strain relief data which typically are taken near the Earth's surface or in mineshafts. Another source of uncertainty arises when both of the horizontal principal stresses are approximately equal. In this case, the azimuth of either stress axis is not well constrained.

Geological Information

There are a variety of geological features, ranging in dimensions from mineralogical grains to large structures on the tens of kilometers scale, which are strongly controlled by deviatoric stress and which therefore provide information on either the orientation or the magnitude of stresses acting at the time that the feature formed.

Information on stress orientation may be obtained from the strikes of large-scale faults, folds and rifts [e.g., Ahorner, 1975; Johnson and Page, 1976], from the orientation of dikes and of flank volcanic eruption features [e.g., Pollard and Muller, 1976; Nakamura et al., 1977], and from the orientation of joints, cracks, and stylolites [e.g., Greiner, 1978; Kohlbeck and Scheidegger, 1977].

Linear island chains have also been interpreted as tensional cracks extending through the lithosphere [Turcotte and Oxburgh, 1973], and thus indicative of principal horizontal stresses on a regional scale. Island chains with clear age progressions along the length of the chain, such as the Hawaiian -Emperor chain, have more commonly been regarded as the volcanic products of "hot spots" more or less fixed with respect to the deep mantle [Wilson, 1963; Morgan, 1972]. Some island chains, such as the Line Islands in the Pacific, however, do not show an age

progression along the length of the chain
Jarrard and Clague, 1977], so that a sing
seems an unlikely explanation. Regardless
Islands, they are at least 80 million
not likely to be closely related to the c
pattern.

Information on the magnitudes of shea
lithospheric mantle have recently been ob
microstructure of mantle-derived xenolith
from the density of dislocations in olivi
[Goetze and Kohlstedt, 1973] and from the
xenolith subgrains and recrystalized grai
1977; Mercier, 1978]. Used in connection
geobarometer, such techniques offer the p
profiles of differential stress versus de
differences so estimated range from a few
hundreds of bars, though the time period
stresses are representative and the rela
stresses to the eruption process that
to the surface are not well established.

There are clearly many uncertainties
of stress measurements. Measurements ha
relevance for regional stresses when the
large areas and where they are corrobor
independent techniques. In such cases,
sources of stress is probably small. F
are several large regions on the earth
techniques present a consistent pictur

principal stresses in the lithosphere. The data for most of these regions, described in detail in the next section, are consistent with the inference that these stresses are primarily the result of plate tectonic forces.

REGIONAL DESCRIPTION OF THE INTRAPLATE STRESS FIELD

Using the above techniques for inferring the directions of principal stresses in the lithosphere, we may summarize the observed intraplate stress field by region. The data used for this summary are listed in Table 1.

African Plate

Eastern and southern Africa are two regions where the state of stress in the lithosphere has been well studied. Geologic evidence, earthquake mechanisms, and in-situ measurements suggest different, but consistent patterns for the stresses in these two areas (Figure 1).

The tectonics of East Africa are dominated by the east African rift system (Figure 1), which extends from a few degrees north to at least 15° or 20°S [Fairhead and Girdler, 1971; Scholz et al., 1976]. Normal faulting mechanisms for earthquakes in the area confirm that the rift valley is an active extensional feature, with least compressive principal stress trending approximately E-W [Sykes, 1967; Maasha and Molnar, 1972]. One earthquake located near the eastern section of the rift southeast of Lake Victoria at 4°S, 35°E shows mainly strike-slip faulting with maximum compression trending nearly E-W [Fairhead and Girdler, 1971]. This earthquake, the only known strike-slip event associated with the rift system, is located near a normal fault [Fairhead and Girdler, 1971], and would be consistent with motion on a

left lateral transform fault between rift centers. (Note that Maasha and Molnar [1972] give a different, predominantly thrust, mechanism for this event, however.)

The western branch of the northern rift system appears to be much older, with faulting and grabens that are at least Jurassic in age [McConnell, 1967]. This branch clearly predates the opening of the Red Sea and the Gulf of Aden, suggesting that at least the western branch is not a newly forming plate boundary [Girdler and Styles, 1974, 1978]. The western branch is still active, however, with normal faulting earthquakes indicating minimum compressive principal stress trending nearly E-W [Sykes, 1967; Banghar and Sykes, 1969].

In the southern section of the rift system, the eastern and western branches merge and there is a general decrease in the extent of extension, with the rift valley becoming narrower and the walls lower. Normal faulting earthquakes, consistent with extension trending E-W, occur both within the rift and to the west in Zambia [Sykes, 1967; Fairhead and Girdler, 1971; Maasha and Molnar, 1972], though at least two of the largest of these events may be associated with the loading by Lake Kariba [Sykes, 1967]. By 20°S, the surface expression of the rift system dies out. A microearthquake study in Botswana between 18° and 21°S indicates that the rift system may be in the early stages of propagating further southward [Scholz et al., 1976].

While the rift system is clearly the product of regional extension, the question arises as to whether or not the rift should be classified as an intraplate phenomenon. If the rift system is the continental expression of a spreading center extending from the Afar triangle southward into Africa, then the state of stress in the region may not be related to forces acting on distant plate boundaries. Chase [1978a] and others have successfully interpreted differences in spreading rates between the Red Sea and the Gulf of Aden in terms of separation of African and Somalian plates along the East African rift system. Interpretation of the extensional nature of the rift system in terms of intraplate stresses is therefore questionable.

The only large earthquake in eastern Africa located well off the rift system has a strike-slip mechanism [Sykes and Sbar, 1974] with the P-axis trending NW-SE (Figure 1). The orientation of the P-axis implies horizontal compression roughly normal to the trend of the rift system and suggests that the state of stress may be very different in areas of east Africa away from the rift.

Southern Africa has a different tectonic setting than east Africa. South of 20°S observations of stress indicate that maximum compression trends E-W to NW-SE. These observations include earthquake mechanisms and in-situ measurements.

An earthquake on 29 September 1969 located at 33° S, 19°E, near Ceres, South Africa, had a strike-slip mechanism with maximum compressive principal stress inferred to be nearly E-W [Fairhead and Girdler, 1971; Maasha and Molnar, 1972]. Aftershocks for this event trended WNW-ESE in

agreement with the fault plane orientation.

In-situ measurements of stress in southern Africa have been made primarily using strain-relief methods, generally in mines [Gay, 1975, 1977]. As noted above, for such measurements it is not always possible to remove the effects of ore veins and of nearby cavities and tunnels. Nonetheless, the measured principal stresses show generally consistent orientations among measurements at a single site and between nearby sites [Gay, 1977]. The directions of maximum horizontal compression at six sites listed by Gay [1977] are shown in Figure 1. The magnitudes of the deviatoric stresses for these sites are up to several hundred bars [Gay, 1977].

In the western part of the African plate, the mechanisms of two oceanic intraplate earthquakes [Sykes and Sbar, 1974; Richardson and Solomon, 1977] and an in-situ strain-relief measurement [Hast, 1969] indicate a NW-SE trend for the maximum compressive stress (Figure 1). Sykes [1978] gives a thrust mechanism for the earthquake of 23 September 1974 in west Africa; the P axis trends roughly NE-SW, but is not well constrained.

Indian Plate

The Indian plate and relevant continental boundaries are shown in Figure 2. Stress directions inferred from

focal mechanisms for six earthquakes are shown for continental India. Five of these solutions are from Chandra [1977] and give dominantly thrust faulting; strike-slip mechanisms are possible for two of the events, but the inferred P axis is not a strong function of the uncertainties in the nodal plane solutions. On 10 December 1967 a large earthquake occurred near the Koyna Dam at 17.5°N, 73.8°E. The inferred P-axis trends NNW-SSE [Singh et al., 1975; Langston, 1976]. This event occurred in a relatively aseismic area of the Deccan Traps and the P-axis is fairly consistent with other events in India. Thus, although the earthquake may have resulted from the filling of the reservoir, perhaps through an increase in pore pressure and a reduction in effective stress, the stress directions inferred from the fault plane solution may still reflect the prevailing regional stress field.

In the Indian Ocean basin, much of the seismicity far from plate boundaries occurs in the general vicinity of the Ninetyeast ridge, probably an ancient transform fault [Sclater and Fisher, 1974]. Two recent large events near the ridge (Figure 2), on 25 May 1964 and 10 October 1970, have strike-slip focal mechanisms with the P-axis trending NW-SE to NNW-SSE, respectively [Sykes, 1970; Fitch, 1972]. Thrust fault earthquakes occurred to the west of the ridge, on 25 June 1974, and to the east of the ridge, on 26 June 1971. The P-axis for both events trends NW-SE [Sykes and Sbar, 1974; Stein

and Okal, 1978]. The style of faulting in the Indian Ocean appears to vary from strike-slip along the Ninetyeast ridge to generally thrust on either side of the ridge [Stein and Okal, 1978]. The orientation of the P-axis for all of the events, however, trends approximately NW-SE. The seismogenic intraplate stress for all these events may thus be similar, with the variation in style arising from the availability of a zone of lithospheric weakness, the Ninetyeast ridge, along which failure may occur. Since the Ninetyeast ridge is a major topographic high, the stress due to the topography, even though generally compensated [Bowin, 1973], may be an important contributor to the regional stress field. That the inferred axis of greatest compressive stress is not orthogonal to the ridge, however, is a strong argument against topographic loads dominating other sources of regional stress.

A variety of stress sensitive measurements indicate a consistent, but different, stress field for Australia. Fault plane solutions exist for five earthquakes in Australia between 1968 and 1973 [Fitch et al., 1973; Stewart and Denham, 1974; Mills and Fitch, 1977]. All events have either thrust or strike-slip mechanisms with the direction of maximum compressive horizontal stress nearly E-W in southern Australia and ENE-WSW to N-S in northern Australia (Figure 2). The P-axes all have very small plunge angles, indicating that the maximum compressive principal stress is nearly horizontal.

Strain-relief in-situ measurements of stress have been

made in Australia and Tasmania [Stephenson and Murray, 1970; Mathews and Edwards, 1969; Endersbee and Hofto, 1963]. The maximum compressive stresses average about 200 bars, with directions that strike E-W in the north and more NW-SE in the south (Figure 2), and are only roughly consistent with the general trends indicated by the fault plane solutions.

Most of the Indian plate far from plate boundaries is characterized by a state of compressive stress. On the Indian continent, south of the Himalayas, the axis of maximum compression is nearly horizontal and trends basically N-S. The Indian Ocean basin appears to be consistent with a more NW-SE trending maximum compression axis and may represent a transition from the nearly N-S trend in India to the nearly E-W to ENE-WSW trending axis of maximum compression inferred from most fault plane solutions and in-situ measurements in Australia.

Eurasian plate

The state of stress in western Europe has been well studied. There are numerous fault plane solutions, in situ strain measurements, and a variety of geological indicators of past and recent states of stress. A summary of the data for western Europe is shown in Figure 3.

Fault plane solutions have been determined for a large number of primarily strike-slip earthquakes in western Europe and have been summarized by Ahorner [1975]. Principal stress orientations inferred from these focal mechanism data, restricted to earthquakes with published fault plane solutions, are plotted in Figure 3. The directions for the maximum compressive stress, with few exceptions, trend NW-SE. The earthquakes represented include events between 1933 and 1971 over a region nearly 500 kilometers on a side, incorporating parts of the Rhine graben and of the Alps. The consistency of the directions argues for a large scale source of the stress. Most of the inconsistent data are either pre-1964, and hence predate the World Wide Standard Seismograph Network, or are located in the geologically complicated Alps.

In-situ measurements of stress have been made in western Europe by many workers and have recently been summarized by Ranalli and Chandler [1975] and Greiner and Illies [1977]. The magnitudes of the non-lithostatic stresses are generally on the order of tens of bars. These measurements are typically made using a strain-relief technique either near the earth's surface or in tunnels or mines. Although such measurements, taken singly, are suspect for reasons already mentioned, the consistency of the orientations of the maximum compressive stress as shown in Figure 3 (open circles) and the agreement with the inferred stress directions from mechanism studies are

remarkable.

Other indicators of stress, based on the orientation of such geological features as joints, slickensides and horizontal stylolites [Greiner, 1975; Scheidegger, 1977a,b], and shown in Figure 3 as open triangles, are also consistent with NW-SE maximum compressive principal stress.

The combination of fault plane solutions, in-situ measurements, and the orientation of stylolites and major geologic features are all consistent with a regional stress pattern for western Europe north of the Alps characterized by a compressive principal stress which is horizontal and has a NW-SE trend.

There are now focal mechanisms for many earthquakes in Asia. Each data point shown in Figure 4 represents the average of at least four closely spaced events with consistent mechanisms in various seismically active areas of Eurasia [Molnar et al., 1973; Tapponnier and Molnar, 1977]. Molnar et al. [1973] concluded that an "approximately N-S to NE-SW trending principal compressive stress appears to be transmitted across a large area north and east of the Himalayas". The Baikal rift zone, shown in Figure 4, is similar to the East African rift system with evidence of

extensional tectonics [Artemjev and Artyushkov, 1971]. As with the East African rift system, it is difficult to determine whether such extensional tectonics represent the formation of a new plate boundary or are truly intraplate in nature.

The earthquake mechanism data for the Eurasian plate east of Europe are presented for completeness, without meaning to imply that the solutions can be interpreted as strictly intraplate tectonics. Most of the earthquakes occur along major faults defining broad zones of extensive deformation and folding between relatively stable blocks [Molnar et al., 1973]. An approach which is based on treating these blocks as micro-plates separated by broad boundary zones is misleading because often such boundaries fail to completely enclose the stable blocks or die out without reaching a micro-plate triple junction [Tapponnier and Molnar, 1977]. The N-S trending compression to the north of the Himalayas has been explained in terms of the collision of India with Eurasia [Tapponnier and Molnar, 1976, 1977]. Both the Baikal extension and the lack of comparable deformation in India can also be fit within this theory. The major disruption of the Eurasian plate by the collision with India suggests that the stresses associated with this collision process have been generally larger than is typical of intraplate stresses at present.

Continental Americas

In South America there have been about a dozen intraplate earthquakes for which focal mechanism studies have been made. The inferred P-axis for four shallow thrust earthquakes and for five shallow strike-slip earthquakes located between 200 and 800 km east of the South American-Nazca plate boundary [Stauder, 1975] are shown in Figure 5. These mechanisms indicate that the maximum compressive stress is horizontal and oriented nearly E-W at the western edge of the South American plate between 2° and 14°S.

Farther eastward in central and eastern Brazil there have been several earthquakes that have focal mechanisms consistent with NW-SE horizontal maximum compression [Mendiguren and Richter, 1978]. Because these events either were small or occurred before the establishment of the WWSSN, not all of the focal planes or inferred pre-stress axes can be well constrained. Nonetheless, if the mechanisms are considered together, a consistent NW-SE trend for the P axis is a reasonable interpretation.

Intraplate stress data are abundant for the North American plate (Figure 6). Perhaps this richness contributes to the inferred complexity of the North American intraplate stress field. Much of continental North America east of the Rocky Mountains and north of the Gulf of Mexico is characterized by a horizontal maximum compressive principal stress with an E-W to ENE-WSW trend

[Sbar and Sykes, 1973, 1977; Haimson, 1977]. While there are exceptions, the bulk of the evidence, using a variety of techniques, strongly suggests a consistent regional pattern. The inferred stresses are of probable tectonic origin, since local effects of topography and glacial history are unlikely to produce such a generally uniform trend. It is also unlikely that the compressive stresses result from erosion as proposed by Voight and St. Pierre [1974] since focal mechanism solutions are almost identical for depths from 1 to about 25 km [Sbar and Sykes, 1977].

The techniques used in North American to infer the state of stress at depths from the surface to several kilometers include fault plane solutions, hydrofracture and strain-relief in-situ measurements, and such recent geologic features as post-glacial buckles or pop-ups. The magnitudes of the maximum horizontal compressive principal stress are on the order of a few hundred bars, with values varying from about 10 to 600 bars [Sbar and Sykes, 1973].

Fault plane solutions exist for a large number of earthquakes in North America away from plate boundaries. The inferred stress patterns east and west of the Rocky Mountains represent different tectonic regimes. North America west of the Rocky Mountains and east of the San Andreas fault is characterized by regional extension in the Basin and Range Province and normal faulting earthquakes along the Intermountain Seismic Belt [Smith and Sbar, 1974]. The origin of these extensional features is uncertain, but may well be related to ancient and recent changes in plate boundary types along western North America [Atwater, 1970; Burchfiel and Davis, 1975]. The orientation of the T-axis

for three normal faulting earthquakes along the Intermountain Seismic Belt that are typical of the several in the area are shown in Figure 7 [Sbar and Sykes, 1973; Smith and Sbar, 1974].

Beginning in the Colorado Plateau and extending eastward across North America to the Appalachian Mountains, fault plane solutions generally indicate thrust or strike-slip faulting with maximum compression trending E-W to NE-SW (Figure 6). The data presented in the figure have been selected from summaries by Sbar and Sykes [1973], Raleigh [1974], Hashizume [1977], and McGarr and Gay [1978], and do not represent all the focal mechanisms that have been published. Normal faulting earthquakes on continental shelves [Hashizume, 1973; Sykes and Sbar, 1974] have been excluded because the stresses involved in such events may be generated at least in part by thermal contraction of the continental margin [Sleep, 1971] or by sediment loading [Walcott, 1972], and hence may not be related to a regional stress field. Fault plane solutions for four small strike-slip earthquakes (M_S = 5.1-5.7) in a swarm in the Sverdrup Basin in Canada at 77° N, 106° W, not shown in Figure 6 because they lie off the map, indicate NE-SW maximum compression [Hasegawa, 1977]. Additional thrust-faulting solutions for North American events north of 60° N were reported by Sykes and Sbar [1974] and Hashizume [1974]. Finally, whenever several earthquakes in the same locality have similar mechanisms, only a representative solution is shown.

Although most of the earthquakes indicate E-W to NE-SW compression, there are exceptions. A well studied normal fault earthquake occurred on 21 October 1965 in southeastern Missouri at 37°N, 91°W [Mitchell, 1973; Street et al., 1974; Patton, 1976]. The T-axis trends NW-SE as shown in Figure 6. The event is located in an area of relatively high seismic activity for an intraplate region. The mechanisms for small earthquakes in this area show changes in fault types and trends of inferred stresses over distances of a few hundred kilometers and may well be affected by the local structure of the Mississippi Embayment and the Ozark Uplift [Street et al., 1974; Herrman and Canas, 1978], though the better determined mechanisms in the Missouri seismic zone indicate mostly E-W to NE-SW horizontal compression [Herrmann, 1979]. A similar rapid change in type of faulting is seen in the Appalachians, which appear to mark the eastern edge of the E-W to NE-SW trend of maximum compressive stress for most of eastern North America [Sbar and Sykes, 1977]. The eastern Missouri and Appalachian earthquakes indicate the complexity of the intraplate stress field in North America and the need to consider the effects of local geological structures in interpreting focal mechanisms in terms of regional tectonic stress.

Numerous in-situ stress and strain measurements have been made in North America. The in-situ data represented in Figure 6 have been selected from summaries by Sbar and Sykes [1973], Raleigh [1974], Ranalli and Chandler [1975], Haimson [1977], and McGarr and Gay [1978].

Post-glacial buckles or pop-ups are geologic evidence of the recent state of stress. Such buckles have been observed in New York, New England, Ohio, and eastern Canada [Sbar and Sykes, 1973]. Often they are associated with quarrying where the lithostatic load has been recently removed. Many of the features trend NW-SE, indicating an axis of maximum compressive stress striking approximately NE-SW [Sbar and Sykes, 1973].

The E-W to NE-SW trend in the maximum compressive stress indicated by in-situ measurements and recent geological features over a broad region between the Rockies and the Appalachians is consistent with the results from focal mechanism studies. This corroboration lends support to the interpretation of a systematic regional stress pattern, presumably of tectonic origin. The fact that in-situ stress data are consistent with other measures of stress is particularly encouraging because in-situ measurements can be made at will in regions of interest , and thus offer the potential to greatly extend our knowledge of the intraplate stress field without awaiting the occurrence of rare and unpredictable intraplate earthquakes.

Oceanic Regions

For oceanic regions, information about the intraplate stress field is limited primarily to earthquake focal mechanisms. The number of stress orientation data for oceanic regions is thus much smaller than for the continents. Further, it is generally impossible to corroborate

the stress directions inferred from oceanic earthquake mechanisms using in-situ measurement techniques. Stress directions inferred from a single isolated earthquake must always be suspect in their significance for the regional stress field, particularly in areas of active volcanism or of probable large bending stresses associated with the flexural response of the oceanic lithosphere to topographic loads.

There are a number of fault plane solutions for earthquakes in the Pacific plate. Several events are so small that well constrained fault plane solutions could not be obtained [Sykes and Sbar, 1974]. The limited first motion data indicate thrust faulting, with the P axis poorly defined (Figure 7). Two events on 24 September 1966 and 28 April 1968 at 12° N, 131° W and 45° N, 175° E, respectively, indicate thrust faulting with the maximum compressive stress nearly horizontal and trending NE-SW [Sykes and Sbar, 1974].

Focal mechanisms have been determined for several earthquakes beneath the island of Hawaii, including the large events on 23 April 1973 and 29 November 1975 [Unger et al., 1973; Ando, 1976]. The 1973 earthquake had a predominantly strike-slip mechanism with the P-axis trending NE-SW while the 1975 earthquake mechanism indicated a low-angle normal fault. Hawaii is not typical of a stable interior region of an oceanic plate. The stress field may be dominated by large bending stresses

associated with the load of the Hawaiian chain on the Pacific plate [Walcott, 1970; Watts and Cochran, 1974; Rogers and Endo, 1977] as well as stresses within the volcanic edifices [Fiske and Jackson, 1970]. Further, the events may be related to stresses associated with magma ascent beneath the active Hawaii volcanoes. The mechanisms of Hawaiian earthquakes need bear no relationship to the Pacific intraplate stress field.

Most of the Pacific plate far from plate margins and active seamount/island chains is characterized by thrust-type earthquakes where focal mechanisms can be well constrained. Limited data suggest that the maximum compressive stress may trend generally NE-SW.

The Nazca plate has had at least three intraplate earthquakes. The focal mechanism for an event on 25 November 1965 at 17°S, 100°W was obtained by Mendiguren [1971] using P-wave first motions and surface wave radiation. The P-axis is nearly horizontal and trends E-W (Figure 7). Two other nearby events that occurred in 1944 have mechanisms that are compatible with the solution for the 1965 earthquake, but the focal planes could not be further constrained [Mendiguren, 1971].

The fault plane solution for an oceanic earthquake that occurred in the Antarctic plate at 40°S, 105°W, on 9 May 1971, indicates a thrust mechanism [Forsyth, 1973] with a horizontal P-axis trending ESE-WNW

(Figure 7). Also shown in Figure 7 are oceanic thrust earthquakes in the Atlantic near the mid-Atlantic ridge at 44°N, 31°W, and two near the Caribbean plate at

approximately 20°N, 60°W [Sykes and Sbar, 1974].

Not included as oceanic intraplate events in our compilation are either earthquakes in generally young lithosphere [Sykes and Sbar, 1974; Stein, 1978] or earthquakes near trenches presumably related to bending of the plate as part of the subduction process [Hanks, 1971; Chapple and Forsyth, 1979]. Stable oceanic lithosphere older than 15 or 20 m.y. is generally characterized by a nearly horizontal maximum compressive stress [Sykes and Sbar, 1974], with a direction that appears to have a regional consistency (Figure 7). Stein [1979] has noted that many large oceanic intraplate earthquakes occurred on prominent bathymetric features indicative of zones of lithospheric weakness. While such zones of weakness may result in a large uncertainty in the specific local directions of principal stresses, the sense of faulting is still indicative of the general directions of the principal stresses, and the consistency of inferred stress directions from several events on different bathymetric features over a broad area is still strong support for a regional stress field of tectonic origin.

Summary

A summary of the global intraplate stress orientation data is shown in Figure 7. The basic data set shown is also documented in Table 1. The data shown represent a summary of the more complete regional summaries presented in Figures 1-6. Some of the complexity of the intraplate

stress field illustrated in those figures cannot be properly portrayed in a global view. Only representative data are shown for some areas where the data concentration is high and the neighboring data are consistent.

Although the global intraplate stress field is complicated, several large-scale patterns can be seen. Much of stable North America is characterized by an E-W to NE-SW trend for the maximum compressive stress. South American lithosphere beneath the Andes and perhaps farther east in the stable interior has horizontal compressive stresses trending E-W to NW-SE. Western Europe north of the Alps is characterized by a NW-SE trending maximum horizontal compression, while Asia has the maximum horizontal compressive stress trending more nearly N-S, especially near the Himalayan front. The Indian plate has a horizontal maximum compressive stress direction that varies from nearly N-S in continental India to roughly E-W to NE-SW in Australia. Horizontal stresses are variable in Africa, but tend to be compressive with an E-W to NW-SE trend in the south and west and extensional with an E-W trend in east Africa. Oceanic lithosphere older than 15 to 20 m.y. is generally characterized by a compressive state of stress.

The consistency, or lack thereof, of the intraplate stress field depends on several factors. Each of the techniques used for inferring stress has uncertainties that are often large or unknown. This is further complicated by the fact that measurements are often taken very near the earth's surface, or in mines and tunnels where the effects of nearby structures may be large. The geologic structure at

the measurement site may control the state of stress. Thus it is not surprising that the inferred intraplate stress field is complicated. Perhaps more surprising is the fact that general trends for the orientations of principal stresses can often be found that are reasonably consistent over regional dimensions. We show below that these regionally consistent intraplate stress orientations can be quite plausibly explained in terms of plate tectonic driving forces.

NUMERICAL MODELING OF GLOBAL INTRAPLATE STRESS

To compare the global intraplate stress fields predicted by various models of the driving mechanism with the observed intraplate stresses summarized above, a technique for modeling intraplate stress is necessary. Our first approach to this problem was based on the solution of a finite-difference approximation to the membrane equations for a thin, spherical shell [Solomon et al., 1975, 1977b; Richardson et al., 1976]. Because of the coarse grid used in the finite-difference analysis (10° x 10° in latitude and longitude), and because of some problems with the numerical solution of the equilibrium equations, a new finite-element analysis is used in this paper to calculate global intraplate stress. The finite-element technique has previously been applied to the problem of intralithospheric stress in a single plate by Richardson [1978].

The finite element method used in this paper has several advantages over the finite difference technique used in our earlier work. Irregular boundaries are easily modeled with finite element techniques by varying the size and orientation of the elements, and nodal forces equivalent to surface tractions and line forces acting on each element are particularly easy to specify without introducing a minor imbalance in the torque acting on the lithosphere. Further, the finite element procedure does not require the arbitrary adjustments to the grid near the coordinate poles to avoid the $1/\sin\phi$ singularity (where ϕ is colatitude) that was an artifact of the finite difference coordinate system [Richardson et al., 1976].

Finite Element Technique

If the lithosphere is approximated by a linear elastic shell in the membrane state of stress, the equilibrium condition between internal deformation and external loads follows from the variational principle of virtual work and leads to the standard matrix equation for finite elements [Bathe and Wilson, 1976, p. 74].

$$[K]\ [U] = [F] \qquad (1)$$

where [U] is the matrix containing the unknown nodal displacements, [K] is the stiffness matrix which depends on the geometry and elastic properties of the structure, and [F] is the matrix containing all loads acting on the structure.

When the dimensions of the stiffness matrix are very large, the Irons wave-front solution technique may be applied [Irons, 1970; Orringer, 1974]. This technique, based on Gauss elimination and back substitution, avoids prohibitively large in-core computer storage requirements by utilizing external storage space. This technique was applied to the models of the Nazca plate by Richardson [1978], although the total number of degrees of freedom for those models was only about 250.

The earth's lithosphere is divided into 5246 triangular plane stress elements as shown in Figures 8-11, where Figures 8 and 9 show the mid-latitude regions and Figures 10 and 11 show the north and south polar caps, respectively. Away from plate boundaries, each triangular element has dimensions of 5x5x7 degrees. Nodal spacing is approximately three degrees along plate boundaries. Twelve plates have been included and comparison with the finite difference grid used in Richardson et al. [1976] shows a definite improvement in the spatial resolution both of predicted stress within the plate and of plate boundary definition. Each element has three nodes, each of which has two in-plane degrees of freedom. These degrees of freedom correspond to the latitudinal and longitudinal components of displacement in the global coordinate system. There are 2625 nodes associated with the 5246 elements, giving a total of 5250 degrees of freedom.

Specification of Material Properties

Each element is assumed to have a thickness of 100 km. The elastic parameters of the elements away from plate boundaries

are assumed to be constant. Values for Young's modulus E and Poisson's ratio ν are taken as 7×10^{11} dyne/cm^2 and 0.25, respectively. The calculated stresses are independent of the specific choice for E as long as the Young's modulus is everywhere uniform. If the Young's modulus varies spatially, only the contrast, and not the actual values, will affect the calculated stresses. Variations in plate thickness can be modelled by decreasing Young's modulus by a factor proportional to the reduced plate thickness.

Normal and shear stresses are probably transmitted only inefficiently across a ridge compared to stable lithosphere because of the presence of relatively warm mantle material beneath the ridge. To model this effect, the Young's modulus for ridge elements is assumed to be 3.5×10^{10} dyne/cm^2, or a factor of twenty less than Young's modulus for stable lithosphere. For test cases, the calculated state of stress away from plate boundaries was not very sensitive to the choice of E for the ridge, as long as the contrast between various regions was less than about three orders of magnitude. For greater contrasts in E, the various regions were effectively isolated and numerical problems arose.

Convergent plate boundaries may also be regions where stresses are inefficiently transmitted from one plate to another. At subduction zones, some stress transmitted across the oceanic plate may deform the subducted slab rather than act on the neighboring plate. Also, inter-arc spreading and island arc volcanism indicate the presence of relatively hot material near the surface. At continental convergence zones, there may

be significant shear heating [Bird, 1976]. As a first order model of the elastic parameters at convergent plate boundaries, the Young's modulus is rather arbitrarily chosen equal to the value at ridges.

Transform faults must also act as weak regions because strain is concentrated in a narrow zone. This may be particularly true for transform faults along the major mid-ocean ridges. For these transforms, the lithosphere is usually young and therefore warmer than old lithosphere. In all of the models considered in this chapter, transform faults along the major mid-ocean ridges are assumed to have a Young's modulus equal to the value chosen for ridge elements. Transform faults in continental lithosphere, however, may be nearly as strong as stable plate regions. Deformation along the San Andreas fault appears to be strongly concentrated within a few tens of km of the fault [Savage and Burford , 1970]. Transform faults which are not dilated or compressed may behave similarly to plate interiors with respect to normal stress. Shear stresses clearly deform transform faults which therefore are weaker than plate interiors for such stresses. In a numerical formulation which does not include non-linear failure, this weakness might be modelled by assuming that the elastic constants are anisotropic along continental transform faults such that the values for Young's modulus and shear modulus parallel to the strike of the fault are less than the values perpendicular to the strike; future modeling should include some form of anisotropic elements. For models considered in this paper, continental transform fault boundary elements are assumed to have the same uniform

elastic constants as interior elements.

The plate boundary elements assumed to have a lower Young's modulus than typical plate interiors are illustrated in Figure 12.

Specification of Driving and Resistive Forces

The parameterization of various possible plate driving and resisting forces are as follows (see Figure 13): forces at spreading centers and subduction zones are generally assumed to act in the direction of relative plate motion and are proportional to the length of plate boundary. The relative plate velocities are taken from the RM2 model of Minster and Jordan [1978], except for the Philippine plate, where the Eurasian-Philippine angular velocity of Fitch [1972] has been used. Although more up-to-date information on the relative motion of the Philippine plate is now available [Chase, 1978a] the results of the global modeling are unlikely to change significantly for a change in the orientation of forces acting on the small Philippine plate.

Forces at plate boundaries might more properly be imposed perpendicular to the strike of the boundary. For most ridges and for some subduction zones, the difference between the direction defined by the perpendicular to strike and the direction of relative plate motion is small. For computational ease, it is much more convenient to specify the direction of forces along a plate boundary with a single rotation pole than to require knowledge of the strike of the boundary everywhere. Future modeling of subduction zone forces might take into account the age of subducted lithosphere, the curvature of

subduction zones, and the length of subducted slab. For the present modeling, it seems sufficient to assume that forces at subduction zones act in the direction of plate convergence, and that the magnitude of such forces may have a dependence on the rate of subduction.

Plate boundary forces are applied at nodal points immediately adjacent to and located symmetrically about the boundary. For computational reasons which may be justified physically, the forces actually applied at nodes on either side of the plate boundary act along great circles locally tangent to the small circle about the rotation pole rather than along the small circles themselves. With such a specification, symmetric forces acting on the boundary will create no net torque on the lithosphere. The difference between the directions inferred from great and small circle paths is less than a few degrees for all distances greater than 20 degrees from the pole of rotation. For distances less than 20 degrees, the difference increases. Forces defined by great circle directions will remain orthogonal to a plate boundary that lies on a meridian about the pole of rotation as the boundary approaches the pole. This specification should more closely approximate the directions of gravitational forces at a ridge, for instance, than would forces defined by small circles about the rotation pole.

The driving force F_R at ridges is taken always to be symmetric about the ridge boundary. Ridge forces adopted are shown in Figure 14. For most models, the net force F_T exerted on the surface plates by the subducted slab is assumed to act symmetrically

about the trench boundary (Figure 15). This condition may be relaxed, however, by specifying drag forces to balance the torque exerted by forces which are concentrated on the subducting plate, a feature of some alternative models. The magnitude of F_T may vary spatially to include a dependence on the rate of subduction. Continental convergence zone forces are shown in Figure 16.

Drag forces due to motion of the lithosphere with respect to the mantle may be specified for each element. The drag force F_D is assumed to be proportional to plate area and to the velocity of the plate with respect to the underlying mesosphere. The direction of the force is opposite to the 'absolute' plate velocity $\underset{\sim}{v}$ if the force resists plate motions, and given by

$$\underset{\sim\sim}{F_D} = -D\underset{\sim}{v} \qquad (2)$$

where D is a drag coefficient which may vary spatially between continental, young oceanic, and old oceanic lithosphere. Drag forces are not specified for plate boundary elements. At plate boundaries the motions between the plate and the mantle material below are probably very complicated. At least for ridges, the mantle material may have a relatively low viscosity and hence the drag forces there may be negligible.

No forces are explicitly applied along transform faults. If drag forces dominate the driving mechanism, shear stresses along transform faults will be high in the models as a consequence of the rapid variation in the direction of drag forces across

the transform, and so will be consistent with the inference that resistance on transforms is significant for plates driven by basal shear [Hanks, 1977].

MODELS OF INTRAPLATE STRESS

In this section various models of the driving mechanism are tested against the observed intraplate stress field using finite element analysis to calculate predicted stresses. The first class of models includes only symmetric forces acting on plate boundaries. In later models, drag forces on the base of the plates are included. A representative list of all models studied is given in Table 2. The various force parameters include F_R, the symmetric force exerted at ridges; F_T, the symmetric force exerted at trenches; F_S, the additional force exerted on the subducted plate at trenches; F_V, a velocity-dependent symmetric force at trenches (see below); F_C, the symmetric force at continental convergence zones; and D_c, D_o, D_y, the drag coefficients (equation 2) beneath continental, old oceanic, and young oceanic lithosphere, respectively. The forces F_R, F_T, F_S, F_V are positive if they drive plate motion, and F_C, D_c, D_o, D_y are positive if they resist plate motion.

Forces only at Plate Boundaries

The simplest models each include only one of the force parameters. While all of these models are too simple to match the inferred intraplate stress field, they each isolate the effect of one of the possible forces. Because we are concerned only with intraplate stress, a trade-off for symmetric forces exists between the magnitude of the applied forces and the stiffness of boundary elements.

For example, additional resistance at a trench boundary could be included by increasing the stiffness of the boundary or by decreasing the driving forces. If the strain on boundary elements was required to be proportional to the spreading (or subduction) rate, this trade-off would no longer apply.

The first such model, E1, includes only a horizontal pushing force F_R, equivalent to 100 bars compressive stress across a 100 km thick plate, at all spreading centers (Figure 14). The predicted deviatoric intraplate stress field for model E1 is shown in Figure 17. Though the calculated stresses here and throughout will be refered to as deviatoric stresses, they are strictly the differences between the horizontal and vertical stresses. In classical continuum mechanics, deviatoric stresses are measured with respect to the hydrostatic, rather than the vertical, stress. We shall nonetheless use the term deviatoric stress in this non-standard fashion to emphasize that a calculated tensile stress does not necessarily imply a net tensional state of stress in the earth.

Most of the earth's surface is predicted to be in a state of deviatoric compression for model E1. The typical magnitude of the calculated stresses is about 50 bars. Away from plate boundaries the stress field various smoothly. Near ridge boundaries the maximum compressive stress is generally aligned with the local direction of plate motion. Both of these features are as one would expect, and lend confidence to the numerical techniques that have been used.

Comparison with the observed intraplate stress field shown in Figure 7 shows moderate agreement in several regions. In eastern North America the predicted maximum compressive principal stresses trend N-S to NE-SW. In the western portion of the Nazca plate a state of deviatoric compressive stress is predicted, although the direction is poorly constrained because the two principal stresses are of nearly the same magnitude. The southern portion of the Indian plate shows a NW-SE to nearly E-W trend for the maximum compressive stress. The Pacific plate is generally in a state of compression.

A second simple model, E2, has only symmetric pulling forces F_T at trenches (Figure 15) equivalent to a deviatoric tensile stress of 100 bars across a 100 km thick plate. The predicted stress field for model E2 is shown in Figure 18. Most of the earth's surface is in a state of deviatoric tension, with typical values of about 50 bars in the middle of the plates. The predicted stresses for this model are inconsistent with the observed stress field. Although this is a very simple model, it indicates that slab pulling forces cannot completely dominate the intraplate stress field.

The net pulling force due to the slab is the difference between the gravitational force and the resisting forces acting on the slab as it moves with respect to the mantle. This net force may depend on the subduction rate. For subduction rates greater than about 9 cm/yr, the gravitational force on the slab may be nearly constant [Richter and McKenzie, 1979]. For lower subduction rates there is likely to be a lesser gravitational force due to the reduced thermal contrast between slab and mantle.

The viscous drag resisting motion of the slab may increase with velocity until, at some terminal velocity, the resisting and pulling forces approximately balance [Forsyth and Uyeda, 1975]. To model these ideas, a slab force F_V is assumed which increases linearly from zero with subduction rate v from v = 0 to 4 cm/yr, decreases linearly to zero from v = 4 to 12 cm/yr, and is zero at higher v. At v = 4 cm/yr, F_V is equivalent to a deviatoric tensile stress of 100 bars across a 100 km thick plate. The predicted stress field for a model (E3) with only F_V present is quite similar to that for E2, with generally extensional horizontal stresses, but with relatively higher stresses near some trenches (Tonga-Kermadec, Mariana, Kuril-Japan).

As noted above, convergence zone forces are probably different for zones of continental convergence such as the Himalayan and Alpine belts than for regions of oceanic lithosphere subduction. The force at continental convergence zones from the uplifted mountain belts should exert a compressive stress on the plates and thus yield a net resistance to convergence. As a first approximation, the force per unit length along those portions of the African-Eurasian and Indian-Eurasian plate boundaries undergoing continental collision are assumed to be equal and uniform, in spite of considerable structural complexities in both regions. The directions of these forces (Figure 16) are nearly perpendicular to the strike of the topography associated with the convergence zones. The calculated stresses for a model, E4, with only continental convergence zone forces are

shown in Figure 19, where F_C has been assumed to be equivalent to a deviatoric compressive stress of 100 bars. The largest stresses, about 50 bars, occur in the Eurasian and Indian plates near the Himalayas. As expected, the magnitude of the stresses decreases away from the plate boundaries. In North America, for example, the stresses are only a few bars.

Comparison between Figures 19 and 7 shows several interesting features. First, the directions of the calculated maximum compressive stresses in northern India and Asia are similar to those inferred from the focal mechanisms for these areas. Also, the predicted maximum compressive stress varies from N-S to NW-SE between northern and central portions of the Indian plate. In the northern portions of the Asian plate the component of deviatoric tension is consistent with Baikal rift tectonics. The calculated stresses in Asia for model E4 are qualitatively similar to the results obtained by Tapponnier and Molnar [1976, 1977] from a slip-line analysis which treated India as a rigid indentor impinging upon Asia. The calculated maximum compressive deviatoric stress in Europe for model E4 trends NW-SE, also in agreement with the data for this area.

For models considered later in this chapter, forces associated with continental convergence zones appear to be important for intraplate stresses in regions adjacent to such zones, but have little effect at great distances.

For this simple class of models with only plate boundary forces, it is not possible to consider forces which are concentrated on one side of subduction zones. Below we consider

models including a force F_S at trenches which acts only on the subducted plate. Such a force exerts a net torque on the lithosphere, which must be balanced by drag forces to satisfy mechanical equilibrium.

A linear combination of models is possible because the deformation of an elastic lithosphere is linear in the applied forces. To consider the effects of both ridge and convergence zone forces, the results from models E1-E4 are linearly superposed in models E5 through E16 (Table 2).

The results of comparing predicted and observed stress for these models with only plate boundary forces may be briefly summarized. Models that produce a reasonable fit to the observed data (e.g., E15, E16) all include substantial ridge pushing forces. For models with boundary forces only, an upper limit of about 3:1 for F_T/F_R may be set. For higher ratios of F_T/F_R, the predicted horizontal stresses are dominantly extensional and fit the observations poorly (Table 2). If F_V (rate-dependent slab forces) replaces F_T, the bound F_V/F_R is slightly higher, about 5:1. Forces at continental convergence zones bordering Eurasia are important for the intraplate stress field in nearby regions, but have insufficient effect in other parts of the lithosphere to increase the upper bounds established for the ratios F_T/F_R and F_V/F_R.

The boundary forces considered above, with the exception of continental convergence forces, are assumed to drive, rather than resist, plate motions. Although the net torque exerted on the lithosphere is zero for all of the boundary force models considered thus far, forces acting to resist plate motions have

not been explicitly included. The next set of models will consider the role of drag forces acting on the base of the lithosphere.

Viscous Drag Forces

Drag forces on the base of the lithosphere depend on the velocity of the plate with respect to the mantle and on the mantle viscosity. As discussed above, the motion of the plates with respect to the mantle is poorly known. For the first set of drag models considered, a linear drag law of the form given in equation (2) will be assumed. The absolute velocities are determined from the condition that the drag forces exert no net torque on the lithosphere [Solomon and Sleep, 1974]. The drag coefficient D is positive if F_D resists plate motions.

Model E17 is characterized by drag forces of the form given in equation (2), where the drag coefficient is taken to be everywhere uniform. The calculated absolute plate velocity field for the Pacific plate is given by an angular velocity of 7.0×10^{-7} deg/yr about a pole at 62.4°S, 111.1°E, in good agreement with other similar models [Solomon et al., 1975]. Absolute motions for the other plates may be calculated from the plate velocities relative to the Pacific plate [Minster and Jordan, 1978]. We should note that model E17 can never be a physically realizable model by itself, since viscous shear at the base of the plates is acting to resist motion induced by other forces not explicitly included. We present results for models with only drag forces to isolate the effects of various forces which are incorporated in later, more complete models.

The calculated stresses for model E17 are shown in Figure 20. The largest deviatoric stresses are tensile in the western Pacific and Asia and compressional in the eastern Pacific and the Nazca plate. The stresses are small in eastern North America and Europe. The calculated stresses are in poor agreement with the observed stress field in the western Pacific, Asia, and the Indian plate.

The drag coefficient may be enhanced beneath continents relative to oceans [Jordan, 1975] or beneath old oceanic lithosphere relative to younger regions [Schubert et al., 1976]. Model E18, with drag only beneath continental lithosphere, and model E19, with drag forces only beneath oceanic lithosphere older than 80 m.y., were constructed to explore the effects of various parameterizations of the drag coefficient. From the comparison of predicted and observed stresses for models E17-E19 and their combinations, we may make the following conclusions. If only drag forces act on the plates (an unreasonable assumption), the drag coefficient beneath oceanic lithosphere must be non-zero if compressive stresses are required for oceanic regions. The calculated stresses are similar in direction for uniform drag and old oceanic drag force models. The drag coefficient beneath continents may be higher than beneath oceans by a factor of up to 10 without significantly affecting the continental stresses.

A model in which drag forces drive rather than resist plate motions can be constructed from model E17 by assuming that the drag forces act in the direction of absolute plate motions. For such a case, the sense of stress at each point

in Figure 20 is reversed and the magnitude of the stress is unchanged. Such a model (E20) predicts deviatoric compression in Eurasia, the western Pacific and Indian plates and deviatoric tension in the eastern Pacific, Nazca and South American plates.

Models with only drag forces cannot be expected to match the observed intraplate stresses very well, since the contribution of plate boundary forces due to ridges, subduction zones, and continental convergence zones have been neglected. In the next class of models, both plate boundary and drag forces are included with the aims both of establishing limits on the various contributions to the driving mechanism and of finding a best model.

Combined Boundary and Drag Forces

Models E21-E23 are designed to test whether the limit of about 3:1 for F_T/F_R established for the boundary force models may be increased by adding resistive drag forces. Stresses for model E21, in which a small amount of drag has been added to model E7 are very similar to those for model E7, with small differences confined primarily to the Pacific plate. The effect of increasing the drag coefficient in model E22 is to increase the magnitude of the calculated deviatoric tensile stresses in Asia and the western Pacific and of the compressive deviatoric stresses for the eastern Pacific and Nazca plates. The stresses in North America and Europe are not changed appreciably. Calculated stresses for model E23, with a large drag coefficient, include dominantly deviatoric tension in the western Pacific, Asia, and southern Indian plates. The predicted stresses are

compressive in the Nazca plate, and agree with the earthquake data for this plate. The maximum compressive stress is small and oriented NW-SE in eastern North America.

Models E21-E23 indicate that adding uniform drag forces does not increase the upper bound of about 3:1 for F_T/F_R. The only areas where adding drag forces improves the fit to the data are the western Pacific and Nazca plates.

Concentrating the drag coefficient by a factor of six beneath continents produces stresses very similar to those for model E21, where the drag coefficient was assumed to be uniform, with the main difference being that the compressive component of the stresses is slightly increased for continents and slightly decreased for oceanic lithosphere for model E24 compared to model E21. The fit to the observed data is only marginally changed. Even if the drag coefficient beneath continents is enhanced by a factor of 11 compared to oceanic lithosphere (model E25), there are only minor changes in the stress field (e.g., in South America and the Pacific) compared to E24.

The fit to the observed stresses in Europe, Asia, and India can be improved over models E21-E25 by including forces at continental convergence zones (model E26). The fit to the observed data is essentially unchanged away from the continental convergence zones.

Models E21-E26 (see Table 2) indicate that resistive drag forces acting on the base of the plate cannot significantly improve the fit to the observed intraplate stress data for

the limiting case of slab to ridge forces. The drag coefficient beneath the continents may be larger by a factor of ten with little effect as long as drag forces do not dominate the intraplate stress field.

In the previous models, drag forces were assumed to resist plate motions. A simple model (E27) in which drag forces drive plate motions with resistance to plate motion provided by compressive forces at continental convergence zones and at trenches predicts stresses as shown in Figure 21 (Table 2). Drag is assumed to be in the direction of local absolute plate velocity ($D<0$) in equation (2). The fit to the data is poor for the eastern Pacific, Nazca, and South American plates. The calculated stresses in eastern North America are acceptable, but the orientations of the maximum compressive stresses in Europe and Asia are inconsistent with the data. The calculated stresses for model E27, in general, are at best in only moderate agreement with the data.

The effect of increasing the drag coefficient for models in which drag drives plate motions (E28) is to predict larger deviatoric tension in the eastern Pacific, Nazca, and South American plates. Increasing the drag coefficient will further degrade the fit between calculated and observed stresses in these regions.

It is unfair to conclude that viscous drag does not drive the plates from simple models such as E27-E28. However, for the assumptions made about the forces acting on the plate boundaries and about the relationship between drag forces and the velocities of plates with respect to the mantle, models with resistive drag forces are in better agreement with the

observed intraplate stresses than are models with plate-driving drag forces.

It is probably an oversimplification to assume that drag forces either uniformly resist or drive plate motions. An alternative approach, taken by Richardson [1978] and Davies [1978], is to suppose that drag balances the net torque on each plate due to boundary forces. The resulting drag will vary from plate to plate and will not bear a simple relationship to relative plate motions in contrast to the drag derived from absolute plate motion models consistent with known relative velocities. It is straightforward with such an approach to consider subduction zone forces that act only on the subducted plate.

A model of driving forces (E29) with symmetric forces at ridges and continental convergence zones and with subduction zone forces acting only on the subducted plate is considered as a test of the Davies [1978] concept. The basal shear or viscous drag on each plate arises from the rotation of the plate with respect to the underlying mantle (which may be moving). The basal shear necessary to balance the torque on each plate is given in Table 3. Note that the poles for drag to balance boundary forces do not always correspond closely to hot-spot poles [e.g., Minster and Jordan, 1978].

Davies [1978] assumed that kilobars of shear stress act on transform faults [c.f., Hanks, 1977] and used the results of Chapple and Tullis [1977] to estimate slab forces. Because of the large resistive forces assumed at trenches, Davies concluded

that plates without significant subducted slabs such as South America and Eurasia were driven from below by drag forces. For model E29, no forces have been specified on transform faults or on the non-subducting plate at subduction zones. Thus, for example, no drag forces are specified on the Caribbean plate Though a direct comparison of the Davies [1978] model with model E29 is therefore not strictly possible, model E29 represents a first attempt to model subduction-zone forces that act only on the subducted plate.

The stresses for model E29 are shown in Figure 22. For several areas the predicted stresses agree very well with the data. In the North American and Nazca plates, the orientation of the maximum compressive stress is well matched by the model. The fit is almost as good in Europe and in Asia north of the Himalayas. In the Indian plate, compressive stresses trend NW-SE in continental India, in agreement with the data, but the fit is poorer in Australia. In South America, the maximum compressive stress trends E-W, in only moderate agreement with the data. In the Pacific and the eastern part of the African plate the agreement with the data is poor. On the whole, the model provides a better fit to continental than oceanic data, and suggests that any force pulling the overthrust plate toward the trench is probably lower in magnitude than the net pull on the subducted plate.

The last three models represent an attempt to find a best model, rather than limiting models, of the driving mechanism. Models E30-E32 have symmetric forces at ridges and continental convergence zones equivalent to a deviatoric compressive stress

of 100 bars (200 bars for continental convergence zones in E32) across a 100 km thick lithosphere, symmetric forces at subduction zones equivalent to a deviatoric tensile stress of 100 bars, and drag forces on the base of the lithosphere with a drag coefficient that is concentrated by a factor of four (E30) to six (E31-E32) beneath continents (Table 2). The predicted directions of principal stresses for model E31 are shown in Figure 23;stresses for models E30 and E32 are generally similar. The model stresses are in good agreement with the data for eastern North America, Europe, Asia near the Himalayas,and the Indian plate. The fit to the data is good in South America, especially away from the trench, and in western Africa and is acceptable in most of the Pacific plate. The orientation of the calculated maximum compressive stress in the Nazca plate for model E31 is only in moderate agreement with the orientation inferred from the single fault plane solution available [Mendiguren, 1971]. The fit to the data in the northern Pacific, eastern Asia, and east Africa is rather poor. The fit to the data in the northern Pacific and eastern Asia could probably be improved if subduction zone or drag forces were decreased along the western Pacific plate margin or if slab forces were concentrated on the subducted plate. No attempt, however, has been made to vary plate boundary forces locally to match inferred stresses. If such an approach were adopted, most observed stresses could probably be matched but the solution for the driving mechanism would be unjustifiably arbitrary and non-unique. The approach used in this paper has

been to treat each potential driving and resisting force acting on the plates by class, and make estimates of the importance of each type of force. Thus, while models E30-E32 are good models in terms of the fit between calculated and observed stresses, the actual driving mechanisms for plate tectonics are not tightly constrained to the particular forces that have been assumed for these models. The role of modeling intraplate stresses is best suited to testing the relative importance of various forces acting on the plates, rather than determining the exact balance of forces that make up the driving mechanism.

SUMMARY AND CONCLUSIONS

With a variety of techniques it appears to be possible to measure reliably the orientations of principal stresses within the plates. Over large regions of stable plate interiors the directions of principal stresses as inferred from intraplate earthquake mechanisms, in situ measurements, and recent stress-sensitive geological features show consistent trends indicative of a regional stress field. In areas far from recent deglaciation, large-scale topographic loading and erosion, or thermal activity, such regional stresses may be reasonably ascribed to the tectonic driving and resistive forces associated with the motions of the plates. This paper tests models of those forces by calculating the intraplate stress predicted from each model and comparing the predicted and observed orientations of principal stresses.

The calculated intraplate stress field is very sensitive to forces applied at plate boundaries and on the base of the plates. The predicted stresses are in best agreement with the observed intraplate stress orientations when pushing forces at ridges are included and when the net pulling force of subducted lithosphere is less than a few times larger than other forces acting on the plates. Resistive forces associated with trench thrust faults and motion of the slab with respect to the mantle must nearly balance the negative buoyancy of the relatively cool, dense slab [Smith and Toksöz, 1972; Forsyth and Uyeda, 1975]. The upper limit on net slab forces may be extended by less than a factor of two if slab forces are assumed to depend on the subduction

rate such that the force acting on the fastest moving plates (e.g., the Pacific and Nazca plates) is reduced.

Forces resisting further convergence at continental collision zones along the Eurasian plate are important for intraplate stresses, and improve the fit to the data, in Europe, Asia, and the Indian plate. The upper bound on the ratio of net slab force to other forces is not affected by the inclusion of continental convergence zone forces.

Resistive viscous drag forces acting on the base of the plate improve the fit to the intraplate stress field for the Nazca and South American plates as long as some drag acts beneath oceanic lithosphere. The intraplate stress field is not very sensitive to an increased drag coefficient beneath old oceanic lithosphere compared to young oceanic or continental lithosphere. Increasing the drag coefficient beneath continents by a factor of five or ten changes the calculated stresses only slightly and has little effect on the overall fit of calculated stresses to observed stresses as long as some resistive drag acts beneath oceanic lithosphere.

Models in which drag forces drive rather than resist plate motions are in poor agreement with the data. This poor agreement may depend on the oversimplified model of the adopted interaction between the plate and the asthenosphere. The actual flow pattern in the mantle, including possible multiple scales of convection [Richter and Parsons, 1975] , and the resulting drag forces acting on the base of the plates, may be considerably more complicated than has been assumed in these models.

An alternative approach to modeling drag is to require

drag forces to balance the torques due to boundary forces for each plate [Davies, 1978; Richardson, 1978]. The drag forces thus depend on the assumed boundary forces. The calculated stresses for one choice of boundary forces (model E29), with symmetric forces at ridges and continental convergence zones and forces exerted only on the subducted plate at subduction zones, are in good agreement with the data for the Nazca and several continental plates but in poor agreement with the data for oceanic plates near subduction zones.

The calculated stresses for several regions suggest limitations of the modeling and indicate improvements that might be included in future work. Most models failed to predict extensional deviatoric stresses in east Africa. Africa is surrounded by ridge and continental convergence plate boundaries which have been assumed in this paper to compress the plates. The absolute velocity of the African plate is small compared to most plates, and drag forces have been assumed to be proportional to velocity. Increasing the drag coefficient sufficiently to affect African intraplate stresses degrades the fit to the data in most other regions. If the assumed form of boundary and drag forces is correct, then some

other forces must dominate the tectonics of east Africa. Forces associated with northward motion of Africa on an ellipsoidal earth during the past hundred million years may produce the extensional tectonics of east Africa [Oxburgh and Turcotte, 1974]. Alternatively, the east African rift may be a plate boundary between the African and Somalian plates, rather than an intraplate feature [Chase, 1978a]. Future modeling of the intraplate stress field might treat the rift system as a spreading plate boundary.

Some models predict deviatoric tension in the Nazca plate while predicting stresses elsewhere in reasonable agreement with existing data. It may be that the inactive Galapagos Rise, ignored in this modeling, may contribute to the state of compression inferred from the thrust earthquakes in the Nazca plate [c.f., Richardson, 1978]. Alternatively, the slab forces acting along the Peru-Chile trench may be less than have been assumed. Support for such a view may be found in the pronounced gap in intraslab seismicity between 200 and 500 km depth beneath South America [Isacks and Molnar, 1971]. The portion of the slab able to pull on the Nazca plate may thus be confined to depths above 200 km, and the net pull may be less than has been assumed in the simple models of slab forces used here.

For most models, the calculated stresses for South America and eastern Asia have a large component of deviatoric tension that is not supported by the data. This may result from the assumption for these models that slab forces act symmetrically about the trench axis. A model with slab forces only on the subducted plate produced stresses for South

America and eastern Asia in much better agreement with the data [c.f., Mendiguren and Richter, 1978]. The assumption of symmetric subduction zone forces is undoubtedly an oversimplification and methods for balancing the torque due to asymmetric slab forces other than simple drag forces acting on each plate should be explored.

The Andes may represent another source for compressive stresses in South America. In much the same manner that the Himalayas and Alps may stress the plates, the horizontal density variation associated with the Andes may produce compressive stresses in South America. Future modeling might include the effects of major mountain ranges and perhaps the effects of horizontal density variations associated with continental margins [Artyushkov, 1973].

The number of parameters associated with driving mechanism models is already fairly large (e.g., Table 2). It is likely that if even more parameters were considered, such as subduction zone forces that varied from region to region, the fit to the data could be improved. The models are already non-unique, and the philosophy behind the modeling in this paper has been to describe the dominant features of the driving mechanism that are functions of boundary type with as few free parameters as possible.

In future modeling of this kind it would be worthwhile to compute plate velocities in addition to intraplate stresses. Conceptually, this calculation is straightforward because the viscous equation for stress

$$\sigma_{ij} = \lambda v_{i,i}\delta_{ij} + \eta\left(\frac{\partial v_i}{\partial x_j} + \frac{\partial v_j}{\partial x_i}\right)$$

where v_i is the ith component of velocity and λ and η are the bulk and shear viscosities, is homologous to the elastic equation for stress. Thus, an ordinary finite element routine can be used if displacements are interpreted as velocities and elastic constants are interpreted as the homologous viscous constants. A finite bulk viscosity must be assumed, because in two dimensions there is a net dilatation or compression of the plates at plate boundaries. With a set of viscous constants for different kinds of plate boundaries, driving forces would be fit to observed plate velocites as well as intraplate stresses. The drag forces, if any, then would be automatically self-consistent with the plate velocities in a successful model.

There may be some numerical difficulties with such an approach. It would be desirable to impose a large viscosity contrast between plate boundaries and plates so that plate velocities would be well defined within plates. This contrast, however, will cause the velocity to be nearly constant within the plates. Round-off errors in computing the horizontal derivatives of velocity and hence stresses may thus cause numerical problems. A small amount of strain within plates will probably have to be tolerated in such models. An alternative numerical approach would be to include forces due to drag at each element which were proportional to the calculated displacement. This approach would require extensive modification of standard finite element routines.

The main contribution of this work about the question of the driving mechanism for plate tectonics is the demonstration that observed intraplate stress directions can be explained in terms of the forces acting on the edge and along the base of the lithospheric plates. Comparison of observed intraplate stresses with calculated stresses for various models of the driving mechanism is an effective test of the relative importance of plate driving and resisting forces. The modeling can be extended in the future to include distributed forces due to topographic features such as continents, thermal forces associated with regions of anomalously thin or thick lithosphere, and explicit shear resistance along transform faults. The role of drag forces can be further tested for specific and realizable flow patterns in the mantle. Additional data on the intraplate stress field, particularly for oceanic regions, should help to define regional patterns that are now poorly known. Of special importance for further constraining models of the plate tectonic driving mechanism is the reliable determination of the magnitudes of principal lithospheric stresses on a regional scale.

Acknowledgements. We thank Tom Jordan and Peter Molnar for providing results and data prior to publication. We are also grateful to Mike Fehler for assistance in plotting the figures and to Eric Bergman, Brad Hager, Robert Herrmann, and Lynn Sykes for constructive comments on the manuscript. This research was supported by the Division of Earth Sciences, National Science Foundation, NSF Grants EAR74-21894 and EAR78-12936 and by the National Aeronautics and Space Administration, Grant NSG-7329. One of us (S.C.S.) also acknowledges the support of an Alfred P. Sloan Research Fellowship.

REFERENCES

Abe, K., Lithospheric normal faulting beneath the Aleutian trench, Phys. Earth Planet. Int., 5, 190-198, 1972.

Aggarwal, Y.P., Scaling laws for global plate motions: Consequences for the driving mechanism, interplate stresses and mantle viscosity (abstract), Eos Trans. Amer. Geophys. Un., 59, 1202, 1978.

Ahorner, L., Present-day stress field and seismotectonic movements along major fault zones in Central Europe, Tectonophysics, 29, 233-249, 1975.

Ahorner, L., H. Murawski, and G. Schneider, Seismotektonische traverse von der Nordsee bis zum Appennin, Geol. Rundsch., 61, 915-942, 1972.

Ahorner, L. and G. Schneider, Herdmechanismen von Erdbeben im Oberrhein-Graben und in seinen Randgebirgen, in J.H. Illies and K. Fuchs (editors), Approaches to Taphrogenesis, Schweizerbant, Stuttgart, 104-117, 1974.

Ando, M., A source model of the M=7.2 Kalapana earthquake of November 29, 1975 (abstract), EOS, Trans. Am. Geophys. Un., 57, 954, 1976.

Artemjev, M.E., and E.V. Artyushkov, Structure and isostasy in the Baikal Rift and the mechanism of rifting, J. Geophys. Res., 76, 1197-1211, 1971.

Artyushkov, E.V., Stresses in the lithosphere caused by crustal thickness inhomogeneities, J. Geophys. Res., 78, 7675-7708, 1973.

Atwater, T., Implications of plate tectonics for the Cenozoic tectonic evolution of western North America, Geol. Soc.

Am. Bull., 81, 3513-3536, 1970.

Banghar, A.R., and L.R. Sykes, Focal mechanisms of earthquakes in the Indian Ocean and adjacent regions, J. Geophys. Res., 74, 632-649, 1969.

Bathe, K-J. and E.L. Wilson, Numerical Methods in Finite Element Analysis, Prentice-Hall, Englewood Cliffs, 1976.

Bender, P.L. and E.C. Silverberg, Present tectonic-plate motions from lunar ranging, Tectonophysics, 29, 1-7, 1975.

Bird, G.P., Thermal and mechanical evolution of continental convergence zones: Zagros and Himalayas, Ph.D. Thesis, Massachusetts Institute of Technology, Cambridge, 1976.

Bowin, C., Origin of the Ninety East ridge from studies near the equator, J. Geophys. Res., 78, 6029-6043, 1973.

Brace, W.F., and J.B. Byerlee, California earthquakes: why only shallow focus?, Science, 168, 1573-1575, 1970.

Brune, J.N., T.L. Henyey, and R.F. Roy, Heat flow, stress and rate of slip along the San Andreas fault, California, J. Geophys. Res., 74, 3821-3827, 1969.

Burchfiel, B.C. and G.A. Davis, Nature and controls of Cordilleran orogenesis, western United States: extensions of an earlier synthesis, Am. Jour. Sci., 275-A, 363-396, 1975.

Burke, K., W.S.F. Kidd, and J.T. Wilson, Relative and latitudinal motion of Atlantic hot spots, Nature, 245, 133-137, 1973.

Capozza, M., S. Martinetti, and R. Ribacchi, Results of stress measurements of rock masses by means of borehole devices, Proc. Intl. Symp. on Determination of Stresses in Rock Masses, 540-549, 1971.

Chandra, U., Earthquakes of peninsular India - a seismo-tectonic study, Bull. Seis. Soc. Am., 67, 1387-1413, 1977.

Chapple, W. M., and D.W. Forsyth, Earthquakes and bending of plates at trenches, J. Geophys. Res., in press, 1979.

Chapple, W.M. and T.E. Tullis, Evaluation of the forces that drive the plates, J. Geophys. Res., 82, 1969-1984, 1977.

Chase, C.G., Plate kinematics: the Americas, East Africa, and the rest of the world, Earth Planet. Sci. Lett., 37, 355-368, 1978a.

Chase, C.G., Extension behind island arcs and motions relative to hot spots, J. Geophys. Res., 83, 5385-5387, 1978b.

Chase, C.G., Asthenospheric counterflow: a kinematic model, Geophys. J.R. Astron. Soc., in press, 1979.

Clague, D.A., and R.D. Jarrard, Tertiary Pacific plate motion deduced from the Hawaiian-Emperor chain, Geol. Soc. Am. Bull., 84, 1135-1154, 1973.

Coates, R.J., T.A. Clark, C.C. Counselman, III, I.I. Shapiro, H.F. Hinteregger, A.E. Rogers, and A.R. Whitney, Very long baseline interferometry for centimeter accuracy geodetic measurements, Tectonophysics, 29, 9-18, 1975.

Davies, G.F., The roles of boundary friction, basal shear stress, and deep mantle convection in plate tectonics, Geophys. Res. Lett., 5, 161-164, 1978.

DeBremaecker, J.-C., Is the oceanic lithosphere elastic or viscous?, J. Geophys. Res., 82, 2001-2004, 1977.

Endersbee, L.A. and E.D. Hofto, Civil engineering design and studies in rock mechanics for Poatina underground power station,Tasmania, J. Inst. Eng. Aust., 35, 187-206, 1963.

Engdahl, E.R. and C.H. Scholz, A double Benioff zone beneath the central Aleutians: an unbending of the lithosphere, Geophys. Res. Lett., 4, 473-476, 1977.

Fairhead, J.D. and R.W. Girdler, The seismicity of Africa, Geophys. J. Roy. Astron. Soc., 24, 271 -301, 1971.

Fiske, R.S., and E.D. Jackson, Orientation and growth of Hawaiian volcanic rifts: regional structure versus gravitational stresses, Proc. Roy. Soc. London, A329, 299-326, 1972.

Fitch, T.J., Plate convergence, transcurrent faults, and internal deformation adjacent to southeast Asia and the western Pacific, J. Geophys. Res., 77, 4432-4460, 1972.

Fitch, T.J., M.H. Worthington, and I.B. Everingham, Mechanisms of Australian earthquakes and contemporary stresses in the Indian Ocean plate, Earth Planet. Sci. Lett., 18, 345-356, 1973.

Forsyth, D.W., Compressive stress between two mid-ocean ridges, Nature, 243, 78-79, 1973 .

Forsyth, D.W. and S.Uyeda, On the relative importance of driving forces of plate motion, Geophys. J. Roy. Astron. Soc., 43, 163-200, 1975.

Frank, F.C., Plate tectonics, the analogy with glacier flow and isostasy, in Flow and Fracture of Rocks, Amer. Geophys. Un. Geophys. Mon. 16, 285-292, 1972.

Fraser, C.D. and B.E. Pettitt, Results of a field test to determine the type of orientation of a hydraulically induced formation feature, J. Petrol. Tech., 14, 463-466, 1962.

Gay, N.C., In-situ stress measurements in southern Africa, Tectonophysics, 29, 447-459, 1975.

Gay, N.C., Principal horizontal stresses in southern Africa, Pure Appl. Geophys., 115, 3-10, 1977.

Girdler, R.W. and P. Styles, Two stage Red Sea floor spreading, Nature, 247, 7-11, 1974.

Girdler, R.W. and P. Styles, Sea floor spreading in the western Gulf of Aden, Nature, 271, 615-617, 1978.

Goetze, C. and D.L. Kohlstedt, Laboratory study of dislocation climb and diffusion in olivine, J. Geophys. Res., 78, 5961-5971, 1973.

Gordon, R.G., A. Cox and C.E. Harter, Absolute motion of an individual plate estimated from its ridge and trench boundaries, Nature, 274, 752-755, 1978a.

Gordon, R.G., M.O. McWilliams, and A. Cox, Pre-Tertiary velocities of continental plates: a lower bound from paleomagnetic data (abstract), Eos Trans. Amer. Geophys. Un., 59, 1202, 1978b.

Greiner, G., In-situ stress measurements in southwest Germany, Tectonophysics, 29, 265-274, 1975.

Greiner, G. and J.H. Illies, Central Europe: active or residual tectonic stresses, Pure Appl. Geophys., 115, 11-26, 1977.

Hager, B.H., Oceanic plate motions driven by lithospheric thickening and subducted slabs, Nature, 276, 156-159, 1978.

Hager, B.H. and R.J. O'Connell, Kinematic models of large scale flow in the Earth's mantle, J. Geophys. Res., in press, 1979.

Haimson, B.C., Crustal stress in the continental United States as derived from hydrofracturing tests, in The Earth's Crust, Am. Geophys. Un. Geophys. Mon. 20, 576-592, 1977.

Haimson, B., Crustal stress in the Michigan basin, J. Geophys. Res., 83, 5857-5863, 1978.

Haimson, B. and C. Fairhurst, Initiation and extension of hydraulic fractures in rock, Soc. Petr. Engr. J., 71, 310-318, 1967.

Haimson, B. and C. Fairhurst, In-situ stress determinations at great depth by means of hydraulic fracturing, in Rock Mechanics - Theory and Practice, W.H. Somerton (editor), Proc. Eleventh Symp. on Rock Mechanics, AIME, New York, 559-584, 1970.

Hales, A.L., Gravitational sliding and continental drift, Earth Planet. Sci. Lett., 6, 31-34, 1969.

Hanks, T.C., The Kuril Trench-Hokkaido Rise system: large shallow earthquakes and simple models of deformation, Geophys. J. Roy. Astron. Soc., 23, 173-189, 1971.

Hanks, R.C., Earthquake stress drops, ambient tectonic stresses and stresses that drive plate motions, Pure Appl. Geophys., 115, 441-458, 1977.

Harper, J.F., On the driving forces of plate tectonics, Geophys. J. Roy. Astron. Soc., 40, 465-474, 1975.

Harper, J.F., Asthenosphere flow and plate motions, Geophys J. Roy. Astron. Soc., 55, 87-110, 1978.

Hasegawa, H.S., Focal parameters of four Sverdrup Basin, Arctic Canada, earthquakes in November and December, 1972, Canad. Jour. Earth Sci., 14, 2481-2494, 1977.

Hashizume,M., Two earthquakes on Baffin Island and their tectonic implications, J. Geophys. Res., 78, 6069-6081, 1973.

Hashizume,M., Surface wave study of earthquakes near northwestern Hudson Bay, Canada, J. Geophys. Res., 79, 5458-5468, 1974.

Hashizume, M., Surface-wave study of the Labrador Sea earthquake December, 1971, Geophys. J. Roy. Astron. Soc., 51, 149-168, 1977.

Hast, N., The measurement of rock pressure in mines, Sv. Geol. Undersokn., 52, 183 pp., 1958.

Hast, N., The state of stress in the upper part of the earth's crust, Tectonophysics, 8, 169-211, 1969.

Hast, N., Global measurements of absolute stress, Phil. Trans. Roy. Soc. Lond. A-274, 409-419, 1973.

Haxby, W.F. and D.L. Turcotte, Stresses induced by the addition or removal of overburden and associated thermal effects, Geology, 4, 181-184, 1976.

Herget, G., Ground stress determinations in Canada, Rock Mechanics, 6, 53-64, 1974.

Herrmann, R.B., Surface wave focal mechanisms for eastern North American earthquakes with tectonic implications, J. Geophys. Res., in press, 1979.

Herrmann, R.B., and J.-A Canas, Focal mechanism studies in the New Madrid seismic zone, Bull. Seismol. Soc. Amer., 68, 1095-1102, 1978.

Holmes, A., A review of the continental drift hypothesis, Mining Mag., 40, 205-209, 286-288, 340-347, 1929.

Hooker, V.E. and C.F. Johnson, Near-surface horizontal stresses, including the effects of rock anisotropy, U.S. Bur. Mines Rept. Inv. 7224, 29 pp., 1969.

Irons, B.M., A frontal solution program for finite element analysis, Intl. J. Num. Method. Eng., 2, 5-32, 1970.

Isacks, B. and P. Molnar, Distribution of stresses in the descending lithosphere from a global survey of focal mechanism solutions of mantle earthquakes, Rev. Geophys. Space Phys., 9, 103-174, 1971.

Jarrard, R.D. and D.A. Clague, Implications of Pacific Island seamount ages for the origin of volcanic chains, Rev. Geophys. Space Phys., 15, 57-76, 1977.

Jordan, T.H., The continental tectosphere, Rev. Geophys. Space Phys., 13, 1-12, 1975.

Jurdy, D.M., An alternative model for early Tertiary absolute plate motions, Geology, 6, 469-472, 1978.

Jurdy, D.M., and R. Van der Voo, A method for the separation of true polar wander and continental drift, including results for the last 55 m.y., J. Geophys. Res., 79, 2945-2952, 1974.

Kanamori, H., Seismological evidence for a lithospheric normal faulting - the Sanriku earthquake of 1933, Phys. Earth Planet Int., 4, 289-300, 1971.

Kanamori, H. and D.L. Anderson, Theoretical basis of some empirical relations in seismology, Bull. Seis. Soc. Am., 65, 1073-1095, 1975.

Kaula, W.M., Absolute plate motions by boundary velocity minimizations, J. Geophys. Res., 80, 244-248, 1975.

Kohlbeck, F. and A.E. Scheidegger, On the theory of the evolution of joint orientation measurements, Rock Mechanics, 9, 9-25, 1977.

Lachenbruch, A.H., A simple mechanical model for oceanic spreading centers, J. Geophys. Res., 78, 3395-3417, 1973.

Lachenbruch, A.H. and G.A. Thompson, Oceanic ridges and transform faults: their intersection angles and resistance to plate motions, Earth Planet. Sci. Lett., 15, 116-122, 1972.

Langston, C.A., A body wave inversion of the Koyna, India, earthquake of December 10, 1967, and some implications for body wave focal mechanisms, J. Geophys. Res., 81, 2517-2529, 1976.

Leeman, E.R., The CSIR "doorstopper" and triaxial stress measuring instruments, Rock Mechanics, 3, 25-50, 1971.

Lliboutry, L., Plate movement relative to rigid lower mantle, Nature, 250, 298-300, 1974.

Maasha, N. and P. Molnar, Earthquake fault parameters and tectonics in Africa, J. Geophys. Res., 77, 5731-5743, 1972.

Mathews, K.E. and D.B. Edwards, Rock mechanics practice at Mount Isa Mines, Limited Australia, in Mining and Technology, Proc. Commonwealth Mining and Metallurgy Congress 9th, VI, Inst. Mining and Metallurgy, London, 321-388, 1970.

McConnell, R.B., The East African rift system, Nature, 215, 578-581, 1967.

McElhinny, M.W., Mantle plumes, paleomagnetism and polar wandering, Nature, 241, 523-524, 1973.

McGarr, A. and N.C. Gay, State of stress in the earth's crust, Ann. Rev. Earth Planet. Sci., 6, 405-436, 1978.

McKenzie, D.P., Speculations on the consequences and causes of plate motions, Geophys. J. Roy. Astron. Soc., 18, 1-32, 1969a.

McKenzie, D.P., The relationship between fault plane solutions for earthquakes and the directions of the principal stresses, Bull. Seis. Soc. Am., 59, 591-601, 1969b.

McKenzie, D.P., Plate tectonics, in The Nature of the Solid Earth, E.C. Robertson (editor), McGraw-Hill, 323-360, 1972.

McKenzie, D.P. and N. Weiss, Speculation on the thermal and tectonic history of the earth, Geophys. J. Roy. Astron. Soc., 42, 131-174, 1975.

Mendiguren, J.A., Focal mechanism of a shock in the middle of the Nazca plate, J. Geophys. Res., 76, 3861-3879, 1971.

Mendiguren, J.A., and F.M. Richter, On the origin of compressional intraplate stresses in South America, Phys. Earth Planet. Inter., 16, 318-326, 1978.

Mercier, J.-C.C., Application of the olivine geopiezometers to mantle dynamics (abstract), EOS, Trans. Am. Geophys. Un., 59, 375, 1978.

Mercier, J.-C.C., D.A. Anderson, and N.L. Carter, Stress in the lithosphere: inferences from steady state flow of rocks, Pure Appl. Geophys., 115, 199-226, 1977.

Mills, J.M. and T.J. Fitch, Thrust faulting and crust-upper mantle structure in east Australia, Geophys. J. Roy. Astron. Soc., 48, 351-384, 1977.

Minster, J.B., T.H. Jordan, P. Molnar, and E. Haines, Numerical modeling of instantaneous plate tectonics, Geophys. J. Roy. Astron. Soc., 36, 541-576, 1974.

Minster, J.B. and T.H. Jordan, Present-day plate motions, J. Geophys. Res., 83, 5331-5354, 1978.

Mitchell, B.J., Radiation and attenuation of Rayleigh waves from southeastern Missouri earthquake of October 21, 1965, J. Geophys. Res., 78, 886-899, 1973.

Molnar, P., T.J. Fitch, and F.T. Wu, Fault plane solutions of shallow earthquakes and contemporary tectonics in Asia, Earth Planet Sci. Lett., 19, 101-112, 1973.

Molnar, P., and J. Francheteau, The relative motion of 'hot spots' in the Atlantic and Indian Oceans during the Cenozoic, Geophys. J. Roy. Astron. Soc., 43, 763-774, 1975.

Morgan, W.J., Deep mantle convection plumes and plate motions, Bull. Amer. Assoc. Petrol. Geol., 56, 203-213, 1972.

Nakamura, N., K.H. Jacob, and J.N. Davies, Volcanoes as possible indicators of tectonic stress orientation: Aleutians and Alaska, Pure Appl. Geophys., 115, 87-112, 1977.

Orringer, O., FRAP (FRontal Analysis Program), Aeroelastic and Structures Laboratory, Massachusetts Institute of Technology, Cambridge, 1974.

Oxburgh, E.R. and D.L. Turcotte, Membrane tectonics and the East African rift, Earth Planet. Sci. Lett., 22, 133-140, 1974.

Patton, H., A note on the source mechanism of the southeastern Missouri earthquake of October 21, 1965, J. Geophys. Res., 81, 1483-1486, 1976.

Pavoni, N. and E. Peterschmitt, Das Erdbeben von Juerre vom 21 Juni 1971 und seine Beziehugen zur Tektonik des Faltenjura, in Approaches to Taphrogenesis, J.H. Illies and K. Fuchs (editors), Schweizerbart, Stuttgart, 322-329, 1974.

Pollard, D.D. and O.H. Muller, The effect of gradients in

regional stress and magma pressure on the form of sheet intrusions in cross section, J. Geophys. Res., 81, 975-984, 1976.

Raleigh, C.B., Crustal stress and global tectonics, in Advances in Rock Mechanics, Proc. 3rd Congress, International Society of Rock Mechanics, IA, 593-597, 1974.

Raleigh, C.B., J.H. Healy, and J.D. Bredehoeft, Faulting and crustal stress at Rangely, Colorado, in Flow and Fracture of Rocks, Am. Geophys. Un. Geophys. Mon. 16, 275-284, 1972.

Ranalli, G. and T.E. Chandler, The stress field in the upper crust as determined from in-situ measurements, Geol. Rundsch., 64, 653-674, 1975.

Richardson, R.M., Finite element modeling of stress in the Nazca plate: driving forces and plate boundary earthquakes, Tectonophysics, 50, 223-248, 1978.

Richardson, R.M., S.C. Solomon, and N.H. Sleep, Intraplate stress as an indicator of plate tectonic driving forces, J. Geophys. Res., 81, 1847-1856, 1976.

Richardson, R.M. and S.C. Solomon, Apparent stress and stress drop for intraplate earthquakes, Pure Appl. Geophys., 115, 317-331, 1977.

Richter, F.M., Dynamical models for sea-floor spreading, Rev. Geophys. Space Phys., 11, 223-287, 1973.

Richter, F.M., On the driving mechanism of plate tectonics, Tectonophysics, 38, 61-88, 1977.

Richter, F.M. and D.M. McKenzie, Simple plate models of mantle convection, J. Geophys. Res., in press, 1979.

Richter, F.M. and B. Parsons, On the interaction of two scales

of convection in the mantle, J. Geophys. Res., 80, 2529-2541, 1975.

Roegiers, J., The development and evaluation of a field method for in-situ stress determination using hydraulic fracturing, Ph.D. thesis, Univ. Minnesota, Minneapolis, 1974.

Rogers, D.B., and E.T. Endo, Focal mechanisms for upper mantle earthquakes and flexure of the lithosphere near Hawaii (abstract), Eos Trans Amer. Geophys. Un., 58, 1231, 1977.

Savage, J.C. and R.O. Burford, Accumulation of tectonic strain in California, Bull. Seism. Soc. Am., 60, 1877-1901, 1970.

Sbar, M.L. and L.R. Sykes, Contemporary compressive stress and seismicity in eastern North America: an example of intraplate tectonics, Bull. Geol. Soc. Am., 84, 1861-1882, 1973.

Sbar, M.L. and L.R. Sykes, Seismicity and lithospheric stress in New York and adjacent areas, J. Geophys. Res., 82, 5771-5786, 1977.

Scheidegger, A.E., Geotectonic stress-determinations in Austria, Intl. Symp. Field Measurements in Rock Mechanics, 197-208, 1977a.

Scheidegger, A.E., Field measurements of joints and their significance for the determination of rock stresses in Switzerland, Geographica Helvetica (in German), 3, 121-134, 1977b.

Schneider, G., R. Schick, and H. Berckhemer, Fault-plane solutions of earthquakes in Baden-Württemberg, Z. Geophys., 32, 383-393, 1966.

Scholz, C.H., T.A. Koczynski, and D.G. Hutchins, Evidence for

incipient rifting in southern Africa, Geophys. J. Roy. Astron. Soc., 44, 135-144, 1976.

Schubert, G., C. Froidevaux, and D.A. Yuen, Oceanic lithosphere and asthenosphere: thermal and mechanical studies, J. Geophys. Res., 81, 3525-3540, 1976.

Sclater, J.G., R.N. Anderson, and M.L. Bell, Elevations of ridges and evolution of the central eastern Pacific, J. Geophys. Res., 76, 7888-7915, 1971.

Sclater, J.G. and R.L. Fisher, The evolution of the east central Indian Ocean, Bull. Geol. Soc. Am., 85, 683-702, 1974.

Singh, D.D., B.K. Rastogi, and H.K. Gupta, Surface-wave radiation pattern and source parameters of Koyna earthquake of December 10, 1967, Bull. Seismol. Soc. Am., 65, 711-731, 1975.

Sleep, N.H., Thermal effects of the formation of Atlantic continental margins by continental breakup, Geophys. J. Roy. Astron. Soc., 24, 325-350, 1971.

Sleep, N.H., and S. Biehler, Topography and tectonics at the intersections of fracture zones and central rifts, J. Geophys. Res., 75, 2748-2752, 1970.

Smith, A.T. and M.N. Toksöz, Stress distribution beneath island arcs, Geophys. J. Roy. Astron. Soc., 29, 289-318, 1972.

Smith, R.B. and M.L. Sbar, Contemporary tectonics and seismicity of the western United States with emphasis on the Intermountain Seismic Belt, Geol. Soc. Am. Bull., 85, 1205-1218, 1974.

Solomon, S.C. and K.T. Paw U, Elevation of the olivine-spinel transition in subducted lithosphere: seismic evidence, Phys. Earth Planet Int., 11, 97-108. 1975.

Solomon, S.C. and N.H. Sleep, Some simple physical models for absolute plate motions, J. Geophys. Res., 79, 2557-2567, 1974.

Solomon, S.C., N.H. Sleep, and R.M. Richardson, On the forces driving plate tectonics: inferences from absolute plate velocities and intraplate stress, Geophys. J. Roy. Astron. Soc., 42, 769-801, 1975.

Solomon, S.C., N.H. Sleep and D.M. Jurdy, Mechanical models for absolute plate motions in the early Tertiary, J. Geophys. Res., 36, 203-212, 1977a.

Solomon, S.C., N.H. Sleep, and R.M. Richardson, Implications of absolute plate motions and intraplate stress for mantle rheology, Tectonophysics, 37, 219-231, 1977b.

Stauder, W., Subduction of the Nazca plate under Peru as evidenced by focal mechanisms and by seismicity, J. Geophys. Res., 80, 1053-1064, 1975.

Stauder, W. and O.W. Nuttli, Seismic studies: south central Illinois earthquake of November 9, 1968, Bull. Seis. Soc. Am., 60, 973-981, 1970.

Stein, S., An earthquake swarm on the Chagos-Laccadive ridge and its tectonic implications, Geophys.J.Roy. Astron. Soc., 55, 577-588, 1978.

Stein, S., Intraplate seismicity on bathymetric features: the 1968 Emperor trough earthquake, J. Geophys. Res., in press, 1979.

Stein, S. and E.A. Okal, Seismicity and tectonics of the Ninety-east ridge area: evidence for internal deformation

of the Indian plate, J. Geophys. Res., 83, 2233-2245, 1978.

Stephenson, B.R. and K.J. Murray, Application of the strain rosette relief method to measure principal stresses throughout a mine, Intl. J. Rock Mech. Min. Sci., 7, 1-22, 1970.

Stesky, R.M., W.F. Brace, D.K. Riley, and P. -Y.F. Robin, Friction in faulted rock at high temperature and pressure, Tectonophysics, 23, 177-203, 1974.

Stewart, I.C.F., and D. Denham, Simpson Desert earthquake, central Australia, August 1972, Geophys. J. Roy. Astron. Soc., 39, 335-341, 1974.

Stocker, R.L. and M.F. Ashby, On the rheology of the upper mantle, Rev. Geophys. Space Phys., 11, 391-426, 1973.

Street, R.L., R.B. Herrmann and O.W. Nuttli, Earthquake mechanism in the central United States, Science, 184, 1285-1289, 1974.

Strubhar, M.K., J.L. Fitch, and E.E. Glenn, Jr., Multiple vertical fractures from an inclined wellbore - a field experiment, J. Petrol. Tech., 27, 614-647, 1975.

Swolfs, H.S., Jr., J. Handin, and H.R. Pratt, Field measurements of residual strain in granitic rock masses, Proc. Intl. Soc. Rock Mech., Congr. 3, 2A, 563-568, 1974.

Sykes, L.R., Mechanism of earthquakes and the nature of faulting on the mid-ocean ridges, J. Geophys. Res., 72, 2131-2153, 1967.

Sykes, L.R., Intraplate seismicity, reactivation of preexistin zones of weakness, alkaline magmatism, and other tectonism postdating continental fragmentation, Rev. Geophys. Space Phys., 16, 621-688, 1978.

Sykes, L.R., Seismicity of the Indian Ocean and a possible nascent island arc between Ceylon and Australia, J. Geophys.

Res., 75, 5041-5055, 1970.

Sykes, L.R. and M.L. Sbar, Focal mechanism solution of intra-plate earthquakes and stresses in the lithosphere, in Geodynamics of Iceland and the North Atlantic Area, L. Kristjansson (editor), 207-224, 1974.

Tapponnier, P. and P. Molnar, Slip-line field theory and large scale continental tectonics, Nature, 264, 319-324, 1976.

Tapponnier, P. and P. Molnar, Active faulting and tectonics in China, J. Geophys. Res., 82, 2905-2930, 1977.

Tapponnier, P. and P. Molnar, Active faulting and Cenozoic tectonics of the Tien Shan, Mongolia, and Baykal regions, J. Geophys. Res., in press,1979.

Tullis, T.E., Reflections on measurement of residual stress in rock, Tectonophysics, 115, 57-68, 1977.

Turcotte, D.L., Membrane tectonics, Geophys. J. Roy. Astron. Soc., 36, 33-42, 1974.

Turcotte, D.L. and E.R. Oxburgh, Mid-plate tectonics, Nature, 244, 337-339, 1973.

Turcotte, D.L. and G.C. Schubert, Structure of the olivine-spinel phase boundary in the descending lithosphere, J. Geophys. Res., 76, 7980-7987, 1971.

Unger, J.D., R.Y. Koyanagi, and P.L. Ward, An important Hawaiian earthquake (abstract), EOS, Trans. Am. Geophys. Un., 54, 1136, 1973.

van Andel, T.H., Cenozoic migration of the Pacific plate, northward shift of the axis of deposition, and paleobathymetry of the central equatorial Pacific, Geology, 2, 507-510, 1974.

Voight, B., and B.H.P. St. Pierre, Stress history and rock stress, Proc. Third Congr. Intl. Soc. Rock Mech., 2, 580-582, 1974.

von Schonfeldt, H.A., An experimental study of open-hole hydraulic fracturing as a stress measurement method with particular emphasis on field tests, Ph.D. thesis, Univ. Minnesota, Minneapolis, 1970.

Wagner, D., Statistical decision theory applied to the focal mechanisms of Peruvian earthquakes, Ph.D. thesis, St. Louis Univ., St. Louis, 176 pp. 1972.

Walcott, R.I., Flexure of the lithosphere at Hawaii, Tectonophysics, 9, 435-446, 1970.

Walcott, R.I., Gravity flexure, and the growh of sedimentary basins at a continental edge, Geol. Soc. Amer. Bull., 83, 1845-1848, 1972.

Watts, A.B. and J.R. Cochran, Gravity anomalies and flexure of the lithosphere along the Hawaiian-Emperor seamount chain, Geophys. J. Roy. Astron. Soc., 38, 119-141, 1974.

Wetmiller, R.J., The Quebec-Maine border earthquake, 15 June 1973, Canad. J. Earth Sci., 12, 1917-1928, 1975.

Wilson, J.T., A possible origin of the Hawaiian Islands, Canad. J. Physics, 41, 863-870, 1963.

Winterer, E.L., Bathymetry and regional tectonic setting of the Line Islands Chain, Deep Sea Drilling Project, Initial Report, 33, 731-747, 1976.

Zoback, M.D. and J.H. Healy, In-situ stress measurements near Charleston, South Carolina (abstract), EOS, Trans. Am. Geophys. Un., 58, 493, 1977.

Table 1 Summary of Global Intraplate Stress Data

Number[1]	Date	Type[2]	m_b	Lat°N	Long°E	P-Axis/Pl[3]	T-Axis/Pl	Ref.
1	Aug69[4]	1		48.1	-114.8	56/72	273/13	ff
2	4Oct67	1	5.1	38.5	-112.1	237/58	57/40	ff
3	1969-1970[4]	1		40.1	-108.8	275/0	185/0	ff
4	2Oct71	1	5.0	64.4	- 86.6	235/20	54/70	o
5	24Nov69	1	5.0	60.6[5]	- 58.7	137/25	328/65	nn
6	7Dec71	1	5.4	55.1	- 54.4	247/5	144/75	p
7	1971[4]	1		43.9	- 74.5	71/18	250/73	cc
8	1969[4]	1		41.0	- 74.6	56/63	302/11	cc
9	17Dec64	1	5.6	44.5	- 31.3	296/21	166/60	nn
10		3		ca 43.8	ca- 88.5	65		n
11		3		ca 39.	ca- 89.5	60		n
12		3		ca 36.	ca- 98.	65		kk
13		3		ca 39.5	ca- 78.5	25		n
14		3		ca 33.	ca- 80.3	50		rr
15		3		ca 30.8	ca- 98.3	300		bb
16	25Nov65	1	5.75	-17.1	-100.2	276/0	10/74	v
17	9May71	1	6.2	-39.8	-104.8	106/15	286/75	j
18	10May63	1		- 2.2	- 77.6	250/6	341/16	qq
19	9Feb67	1	6.3	- 2.9	- 74.9	243/15	340/24	qq
20	3Nov63	1		- 3.5	- 77.8	79/8	239/81	qq
21	19Jun68	1	6.1	- 5.5	- 77.2	272/9	115/80	qq
22	20Mar72	1	6.1	- 6.8	- 76.8	262/20	76/70	gg
23	14Feb70	1	5.8	- 9.9	- 75.6	264/17	124/68	gg
24	24Jul69	1	5.9	-11.9	- 75.1	99/15	206/48	gg
25	10ct69	1	5.8	-11.9	- 75.1	91/15	198/48	gg
26	15Oct71	1	5.7	-14.1	- 73.3	268/2	177/24	gg
27	31 Jan55	1	6.75	-12.5	- 57.4	142/1	330/89	w
28	13Feb64	1	5.3	-18.1	- 56.8	211/7	301/62	w
29	1975-1976[4]	1	<3.8	-20.2	- 44.7	140/10		w
30		2		ca 62.8	ca 6.5	271		q
31		2		ca 59.9	ca 5.5	86		q
32		2		ca 58.1	ca 7.0	294		q

Table 1 continued

Number[1]	Date	Type[2]	m_b	Lat°N	Long°E	P-Axis/Pl[3]	T-Axis/Pl	Ref.
33		2		ca 52.6	ca - 8.6	344		q
34		2		ca 41.	ca - 8.	278		q
35	18Feb71	1	5.6	51.0	5.6	326/36	56/8	a
36	24Feb52	1	4.9[5]	49.3	8.4	127/0	37/46	c
37	21Jun71	1	5.7	46.3	5.7	315/32	54/14	z
38	5Feb68	1	5.7	46.5	5.7	134/7	314/83	z
39	18Jun68	1	4.7	45.7	8.0	186/9	88/16	b
40	15May51	1	5.0	45.2	9.5	107/33	202/2	b
41	18Oct36	1	5.6	46.0	12.0	162/24	64/18	b
42	27Oct64	1	5.4	47.9	16.0	237/4	329/26	b
43	1946-1965[4]	1		47.4	8.6	119/7	27/7	b
44	8Feb33	1	5.4	48.8	8.2	334/7	72/55	a
45	30Dec35	1	5.0[5]	48.6	8.2	318/20	70/41	c
46	4Sep59	1	4.1[5]	48.4	7.7	156/42	57/10	c
47	19Sep65	1	4.1[5]	48.0	8.3	187/32	86/18	c
48	28Apr61	1	4.9[5]	47.7	7.9	ca 145/10	ca 45/10	ee
49	25May65	1	2.7[5]	48.0	9.8	0/0	90/0	ee
50	22Jan70	1	4.5	48.4	9.0	153/14	63/0	b
51		2		ca 45.9	ca 6.9	40		r
52		2		ca 45.9	ca 8.5	333		d
53		2		46.1	8.8	140		m
54		2		46.1	10.3	165		m
55		2		47.1	8.3	104		m
56		2		49.5	6.4	126		m
57		2		49.2	8.0	75		m
58		2		49.0	8.7	140		m
59		2		47.6	13.1	160		m
60		2		49.7	8.7	125		m
61		2		48.2	9.0	141		m
62		2		47.8	7.6	165		m
63		4		ca 48.0	ca 9.	300		dd
64		4		ca 47.	ca 8.	125		l

Table 1 continued

Number[1]	Date	Type[2]	m_b	Lat°N	Long°E	P-Axis/Pl[3]	T-Axis/Pl	Ref.
65	20Oct72	1	5.7	20.6	- 29.7	117/2	207/2	aa
66	30Oct71	1	6.0	- 0.5	- 4.8	147/12	24/66	nn
67	9Oct66	1	5.1	12.6	30.8	301/36	42/15	nn
68	7May64	1	6.4	- 3.9	35.1	65/15	167/35	g
69	20Mar66	1	6.1	0.6	30.0	352/80	114/6	ll
70	23Sep63	1	5.8	- 16.7	28.7	138/75	283/10	ll
71	29Sep69	1	5.9	- 32.9	19.7	90/10	181/6	t
72		2		5.8	- 10.0	320		g
73		2		- 17.3	14.0	332 (ave. of 4)		k
74		2		- 20.3	30.0	20		k
75		2		- 30.0	22.2	342 (ave. of 2)		k
76	24Oct69	1	5.3	24.8	72.4	8/0	98/55	e
77	10Dec67	1	6.0	17.5	73.7	338/36	65/2	s
78	15Apr64	1	5.5	21.7	88.0	181/22	55/55	e
79	27Mar67	1	5.4	15.6	80.1	188/20	8/70	e
80	10Oct70	1	5.9	- 3.6	86.2	172/3	82/11	h
81	25May64	1	5.5	- 9.1	88.9	311/7	41/7	mm
82	26Jun71	1	5.8	- 5.2	96.9	320/18	206/51	nn
83	25Jun74	1	6.1	- 25.8	84.2	323/28	167/60	hh
84	14Oct68	1	6.0	- 31.7	117.0	271/13	20/50	i
85	10Mar70	1	5.7	- 31.0	116.5	282/16	23/39	i
86	24Mar70	1	6.2	- 21.9	126.6	235/0	114/61	i
87	28Aug72	1	5.6	- 25.0	136.4	181/1	237/39	jj
88	27May71	1	5.6	- 53.9	150.5	--[6]	--[6]	nn
89		2		- 20.7	139.5	81		u
90		2		- 31.5	146.0	97 (ave. of 2)		ii
91		2		- 42.0	146.8	335		f
92	28Apr68	1	5.5	44.8	174.5	70/5	174/56	nn
93	26Apr73	1	5.9	19.9	- 155.1	73/29	339/8	pp
94	24Sep66	1	5.3	12.0	- 130.8	225/1	161/42	nn
95	3May69	1	5.2	8.3	- 175.5	--[6]	--[6]	nn
96	13Apr67	1	5.2	- 7.0	- 151.0	--[6]	--[6]	nn
97	29Jul68	1	4.9	- 7.4	- 148.2	--[6]	--[6]	nn

TABLE 1 continued

Number [1]	Date	Type[2]	m_b	Lat°N	Long °E	P-Axis/Pl[3]	T-Axis/Pl	Ref.
98	27Jun57	1		56.3	117.0	107/73	341/17	y
99	5Jan68	1		56.5	121.2	252/58	2/12	y
100	14Sep58	1		56.7	121.0	275/40	125/6	y
101	29Aug59	1		52.7	107.0	228/70	323/2	y
102	18Jan67	1		56.7	120.9	239/20	335/15	y
103	14Jun71	1		56.2	123.6	183/58	3/32	y
104	4Dec57	1		45.3	99.2	50/5	310/55	y
105	23Jun58	1		48.7	102.8	66/5	333/34	y
106	5Jan67	1		48.2	102.9	237/4	147/0	y
107	20Jan67	1		48.1	103.0	68/0	337/64	y
108	4Jul74	1		45.1	94.0	33/0	123/0	y
109	29Aug63	1		39.6	74.2	0/15	180/75	y
110	11Feb69	1		41.4	79.2	182/3	279/57	y
111	14Sep69	1		39.6	74.9	157/12	276/78	y
112	5Jun70	1		42.5	78.8	0/15	180/75	y
113	29Jul70	1		39.9	77.8	145/15	278/62	y
114	23Mar71	1		41.5	79.3	141/9	28/72	y
115	15Jun71	1		41.5	79.4	164/10	344/80	y
116	29Sep74	1		40.4	78.0	210/20	84/60	y
117	26Dec51	1		40.0	95.4	207/16	297/4	oo
118	21May62	1		37.1	95.7	192/0	282/65	oo
119	19Apr63	1		35.5	96.4	54/7	147/22	oo
120	16Mar64	1		37.0	95.5	170/33	354/57	oo
121	24Mar71	1		35.5	98.2	230/9	126/38	oo
122	7Mar66	1		37.4	115.0	69/0	159/0	oo
123	22Mar66	1		37.5	115.0	65/0	155/0	oo
124	22Mar66	1		37.7	115.1	261/7	171/7	oo
125	27Mar67	1		38.6	116.6	67/7	157/7	oo
126	18Jul69	1		38.4	119.5	69/12	335/16	oo
127	5Feb66	1		26.2	103.2	123/0	33/7	oo
128	13Feb66	1		26.2	103.2	119/27	210/2	oo
129	4Jan70	1		24.1	102.5	346/4	76/4	oo

TABLE 1 continued

Number	Date	Type	m_b	Lat°N	Long°E	P-Axis/Pl[3]	T-Axis/Pl	Ref.
130	11May64	1		28.2	104.0	272/3	182/11	oo
131	9Mar73	1	5.5	-34.0	150.0	64/6	323/65	x
132	3Sep68	1	5.5	20.6	- 62.2	299/10	119/80	nn
133	23Oct64	1	6.4	19.8	- 56.0	164/3	258/54	nn

[1] Numbers refer to Figure 7.

[2] Type: 1 = fault plane solution; 2 = strain-relief in-situ measurement; 3 = hydrofracture in-situ measurement; and 4 = stress-sensitive geologic features.

[3] Azimuth and plunge of P-axis for fault plane solutions. Azimuth of maximum compressive stress for in-situ measurements and geologic features. Azimuth in degrees measured clockwise from north.

[4] Composite fault plane solution.

[5] Local magnitude M_L.

[6] Fault planes could not be constrained, but indicate a thrust mechanism.

References for Table 1

a Ahorner [1975]
b Ahorner et al. [1972]
c Ahorner and Schneider [1974]
d Capozza et al. [1971]
e Chandra [1977]
f Endersbee and Hofto [1963]
g Fairhead and Girdler [1971]
h Fitch [1972]
i Fitch et al. [1973]
j Forsyth [1973]
k Gay [1977]
l Greiner [1975]
m Greiner and Illies [1977]
n Haimson [1977]
o Hashizume [1974]
p Hashizume [1977]
q Hast [1969]
r Hast [1973]
s Langston [1977]
t Maasha and Molnar [1972]
u Mathews and Edwards [1970]
v Mendiguren [1971]
w Mendiguren and Richter [1978]
x Mills and Fitch [1977]
y Tapponnier and Molnar [1979]
z Pavoni and Peterschmidt [1974]
aa Richardson and Solomon [1977]
bb Roegiers [1974]
cc Sbar and Sykes [1977]
dd Scheidegger [1977b]
ee Schneider et al. [1966]
ff Smith and Sbar [1974]
gg Stauder [1975]
hh Stein and Okal [1978]
ii Stephenson and Murray [1970]
jj Stewart and Denham [1974]
kk Strubhar et al. [1975]
ll Sykes [1967]
mm Sykes [1970]
nn Sykes and Sbar [1974]
oo Tapponnier and Molnar [1977]
pp Unger et al. [1973]
qq Wagner [1972]
rr Zoback and Healy [1977]

TABLE 2 Driving Force Models:

Fit of Predicted to Observed Stress Directions

Model	Force Parameters[1]								Fit to Observed Stresses[2]								Figure
	F_R	F_T	F_V	F_C	F_S	D_C	D_O	D_Y	NAM	SAM	EUA	IND	AFR	PAC	NAZ	ANT	
E1	1	0	0	0	0	0	0	0	1	1	1	1	1	1	1	1	17
E2	0	1	0	0	0	0	0	0	0	0	0	0	1	0	0	0	18
E3	0	0	1	0	0	0	0	0	0	0	0	0	1	0	0	0	
E4[3]	0	0	0	1	0	0	0	0	-	-	1	2	1	-	-	-	19
E5	1	0.5	0	0	0	0	0	0	1	1	1	1	1	1	1	1	
E6	1	1	0	0	0	0	0	0	1	1	2	2	1	1	0	1	
E7	1	3	0	0	0	0	0	0	0	0	0	1	1	0	0	0	
E8	1	0	1	0	0	0	0	0	1	1	1	2	1	1	1	1	
E9	1	0	3	0	0	0	0	0	1	0	2	1	1	1	0	1	
E10	1	0	5	0	0	0	0	0	1	0	1	1	1	0	0	0	
E11	1	3	0	2	0	0	0	0	1	0	2	1	1	0	0	0	
E12	1	3	0	3	0	0	0	0	1	0	1	1	1	0	0	0	
E13	1	3	0	5	0	0	0	0	1	0	2	2	1	1	0	0	
E14	1	0	5	3	0	0	0	0	1	0	2	2	1	1	0	0	
E15	1	1	0	1	0	0	0	0	1	1	2	2	1	1	1	1	
E16	1	2	0	1	0	0	0	0	1	0	2	2	1	1	0	1	
E17	0	0	0	0	0	1	1	1	1	2	0	0	1	1	2	2	20

TABLE 2 continued

Model	Force Parameters[1]								Fit to Observed Stresses[2]								Figure
	F_R	F_T	F_V	F_C	F_S	D_C	D_O	D_Y	NAM	SAM	EUA	IND	AFR	PAC	NAZ	ANT	
E18	0	0	0	0	0	1	0	0	1	1	0	1	1	0	0	0	
E19	0	0	0	0	0	0	1	0	1	2	0	0	1	1	2	2	
E20	0	0	0	0	0	-1	-1	-1	0	0	1	1	0	1	0	0	
E21	1	3	0	0	0	.1	.1	.1	0	0	0	1	1	0	0	0	
E22	1	3	0	0	0	.3	.3	.3	1	0	0	1	1	0	0	1	
E23	1	3	0	0	0	.5	.5	.5	1	1	0	0	2	0	2	2	
E24	1	3	0	0	0	.6	.1	.1	1	0	0	1	1	0	0	0	
E25	1	3	0	0	0	1.1	.1	.1	1	1	0	1	1	0	0	0	
E26	1	3	0	2	0	1.1	.1	.1	1	1	1	2	1	0	0	1	
E27	0	-1	0	1	0	-.2	-.2	-.2	1	1	1	1	0	1	0	0	21
E28	0	-1	0	1	0	-.5	-.5	-.5	1	0	1	1	0	1	0	0	
E29[4]	1	0	0	2	1	-	-	-	2	1	1	1	1	0	2	1	22
E30	1	1	0	1	0	.4	.1	.1	2	1	1	2	1	1	1	1	
E31	1	1	0	1	0	.6	.1	.1	2	1	1	2	1	1	1	1	23
E32	1	1	0	2	0	.6	.1	.1	2	1	2	2	1	1	1	1	

[1] Units for F_R, F_V, F_C, and F_S are 1×10^{15} dyne cm^{-1}, which is equivalent to a stress of 100 bars across a 100 km thick plate. Units for D_C, D_O, and D_Y are 1×10^{6} dyne cm^{-2}, which is equivalent to a shear stress of 1 bar for an absolute plate velocity of 1 cm/yr.

[2] NAM is the North American plate; SAM, South American; EUA, Eurasian; IND, Indian; AFR, African; PAC, Pacific; NAZ, Nazca; and ANT, Antarctic. The numeral 2 indicates a fairly good visual fit to general pattern of the observed intraplate stress directions in Figure 7; 1, a reasonable fit to the sense, if not the exact orientation, of the data in Figure 7; and 0, a poor fit to both sense and orientation.

[3] Calculated stresses for NAM, SAM, PAC, NAZ, and ANT are so small with respect to EUA, IND, and AFR that the fit cannot be determined.

[4] Drag forces specified for each plate as listed in Table 3.

TABLE 3 Shear Stress on the Base

of the Plates for Model E29

Plate	Absolute Rotation Pole[1] Lat°N	Long°E	Shear Stress[2], bars
Pacific	-57.3	71.4	2.6
North American	-44.3	- 35.5	2.9
South American	-58.2	142.7	2.7
Eurasian	43.2	- 56.1	0.6
African	66.1	77.8	1.4
Indian	46.8	2.0	5.3
Antarctic	11.7	-148.1	2.8
Nazca	43.0	- 78.5	10.1
Cocos	38.4	170.8	47.0
Caribbean	--	--	0
Arabian	36.1	46.5	21.9
Philippine	-36.9	- 24.7	24.0

[1] Absolute rotation pole of plate (right-handed rule) with respect to presumedly fixed mantle.

[2] Basal shear stress $-D \cdot \underset{\sim}{\omega} \times \underset{\sim}{r}$ at 90° distance from the rotation pole, where $\underset{\sim}{\omega}$ is absolute angular velocity and $\underset{\sim}{r}$ is radius from the Earth's center.

FIGURE CAPTIONS

Figure 1. Intraplate stress orientation data for the African plate. Plate boundaries shown as heavy lines. Continental boundaries, taken as the thousand fathom bathymetric contour, shown as light lines. Filled circles, open circles, and open triangles, represent stress orientations from fault plane solutions, in-situ measurements, and geologic structures, respectively. The P-and T- axes for fault plane solutions point inward and outward, respectively. Both P- and T-axes are shown for strike-slip earthquakes, but only the P-axis for predominantly thrust earthquakes and the T-axis for predominantly normal faulting earthquakes are indicated. Filled circles without arrows denote thrust-fault earthquakes for which the orientation of the P-axis is poorly constrained. For in-situ data, the line gives the direction of the maximum horizontal compressive stress. Dashed lines indicate less reliable data. Data for fault plane solutions are from Sykes [1967], Fairhead and Girdler [1971], Maasha and Molnar [1972], Sykes and Sbar [1974], and Richardson and Solomon [1977]. Data for in-situ stress directions are from Gay [1977] and Hast [1969].

Figure 2. Intraplate stress orientation data for the Indian plate. All conventions as in Figure 1. Data for fault plane solutions are from Sykes [1970], Fitch [1972], Fitch et al. [1973], Stewart and Denham [1974], Sykes and Sbar [1974], Langston [1976], Chandra [1977], Mills and Fitch [1977] and Stein and Okal [1978]. Data for in-situ stress directions are from Endersbee and Hofto [1963],

Mathews and Edwards [1970], and Stephenson and Murray [1970].

Figure 3. Intraplate stress orientation data for Europe. All conventions as in Figure 1, except that the T-axes for those earthquakes with a significant strike-slip component are omitted for clarity. Data for fault plane solutions are from Schneider et al. [1966], Ahorner et al. [1972], Pavoni and Peterschmitt [1974], Ahorner and Schneider [1974] and Ahorner [1975]. Data for in-situ stress directions are from Hast [1958, 1969, 1973] , Capozza et al. [1971], Greiner and Illies [1977]. Data for geological indicators of stress are from Greiner [1975] and Scheidegger [1977a,b].

Figure 4. Selected intraplate stress orientations inferred from earthquake mechanisms in Asia. All conventions as in Figure 1. Each data point represents the average orientations of P- and T-axes inferred from the mechanisms of at least four closely-spaced earthquakes with consistent fault-plane solutions [Molnar et al., 1973; Tapponnier and Molnar, 1977; 1979]. Most of the earthquakes indicated are the product of extensive deformation of the Eurasian plate along well-developed faults in response to the collision of India with Asia [Molnar et al., 1973], and as such, cannot be strictly interpreted in terms of principal intraplate stress directions.

Figure 5. Intraplate stress orientations inferred from earthquake mechanisms in the South American plate. All conventions as in Figure 1. Because of the density of the data, only the P-axis is shown for events near the Nazca

plate boundary, although several of the mechanisms have a significant strike-slip component. Data from Wagner [1972], Stauder [1975], and Mendiguren and Richter [1978].

Figure 6. Selected intraplate stress orientation data for North America east of the Intermountain Seismic Belt. All conventions as in Figure 1. Data for fault plane solutions are from Stauder and Nuttli [1970], Smith and Sbar [1974], Sykes and Sbar [1974], Street et al. [1974], Wetmiller [1975], Hashizume [1977] and Sbar and Sykes [1977]. Data for in situ stress directions are from Fraser and Pettitt [1962], Hooker and Johnson [1969], von Schonfeldt [1970], Raleigh et al. [1972], Roegiers [1974], Herget [1974], Strubhar et al. [1975], Sbar and Sykes [1977], Haimson [1977] and Zoback and Healy [1977].

Figure 7. Global summary of intraplate stress orientation data. Numbers refer to Table 1. Other conventions as in Figure 1.

Figure 8. Finite element grid for mid-latitudes, part 1. Constant strain triangular elements have dimensions of 5x5x7 degrees for plate interiors and 3x3x4 degrees for plate boundaries. There are a total of 5246 elements for the entire grid.

Figure 9. Finite element grid for mid-latitudes, part 2. For other details, see Figure 8.

Figure 10. Finite element grid for the north polar region.

Figure 11. Finite element grid for the south polar region.

Figure 12. Location of plate boundary elements with lowered Young's modulus.

Figure 13. Schematic illustration of forces potentially important for the driving mechanism.

Figure 14. Forces at ridge boundaries. Forces are applied in the direction of the arrows.

Figure 15. Forces at subduction zone boundaries. Lines denote orientation of forces acting toward the trench axis from either side of the plate boundary.

Figure 16. Forces at continental convergence zones. Arrows denote orientation of forces.

Figure 17. Principal horizontal deviatoric stresses in the lithosphere for model E1 (Table 2). Principal stress axes without arrows and with arrows pointing outward denote deviatoric compression and tension, respectively. Relative magnitude of principal stresses is indicated by the length of stress axes.

Figure 18. Principal horizontal deviatoric stresses in the lithosphere predicted for model E2 (Table 2). For other details, see Figure 17.

Figure 19. Principal horizontal deviatoric stresses in the lithosphere for model E4 (Table 2). For other details, see Figure 17.

Figure 20. Principal horizontal deviatoric stresses in the lithosphere for model E17 (Table 2). For other details, see Figure 17.

Figure 21. Principal horizontal deviatoric stresses in the lithosphere for model E27 (Table 2). For other details, see Figure 17.

Figure 22. Principal horizontal deviatoric stresses in the lithosphere for model E29 (Table 2). For other details, see Figure 17.

Figure 23. Principal horizontal deviatoric stresses in the lithosphere for model E31 (Table 2). For other details, see Figure 17.

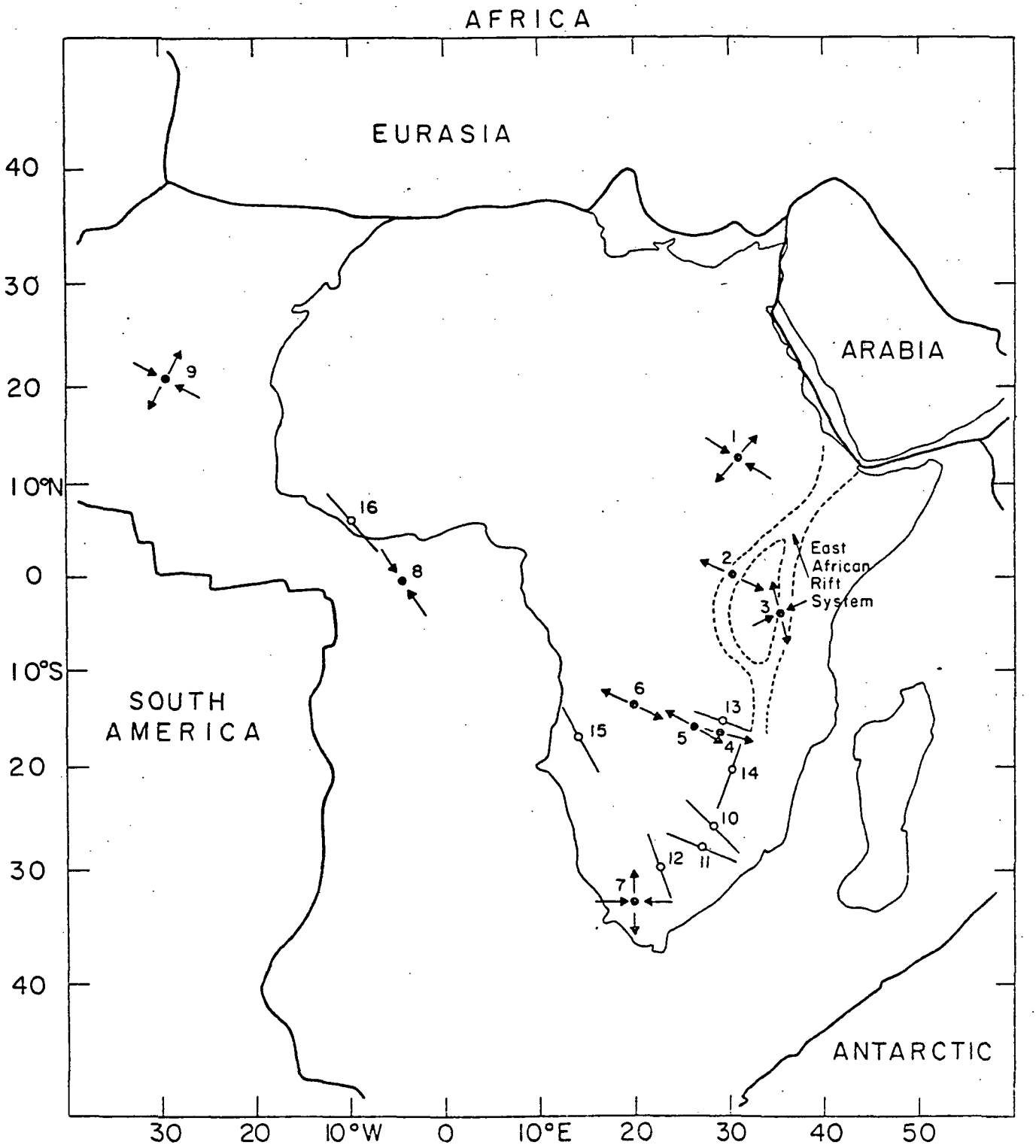
AFRICA
EURASIA
ARABIA
SOUTH AMERICA
ANTARCTIC
East African Rift System
40
30
20
10°N
0
10°S
20
30
40
30
20
10°W
0
10°E
20
30
40
50
1
2
3
4
5
6
7
8
9
10
11
12
13
14
15
16

Figure 1

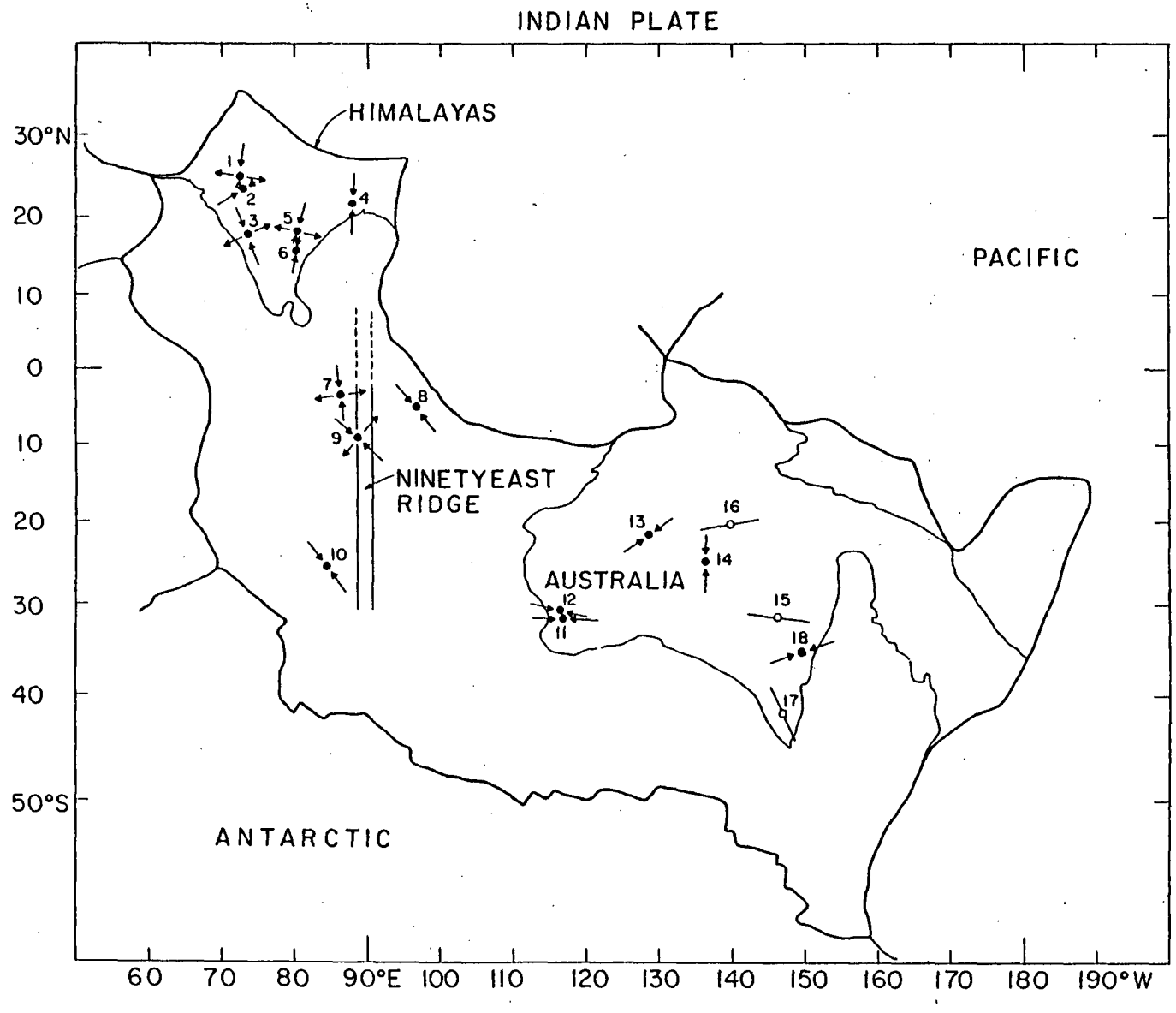
INDIAN PLATE
HIMALAYAS
PACIFIC
NINETYEAST RIDGE
AUSTRALIA
ANTARCTIC
30°N
20
10
0
10
20
30
40
50°S
60
70
80
90°E
100
110
120
130
140
150
160
170
180
190°W
1
2
3
4
5
6
7
8
9
10
11
12
13
14
15
16
17
18

Figure 2

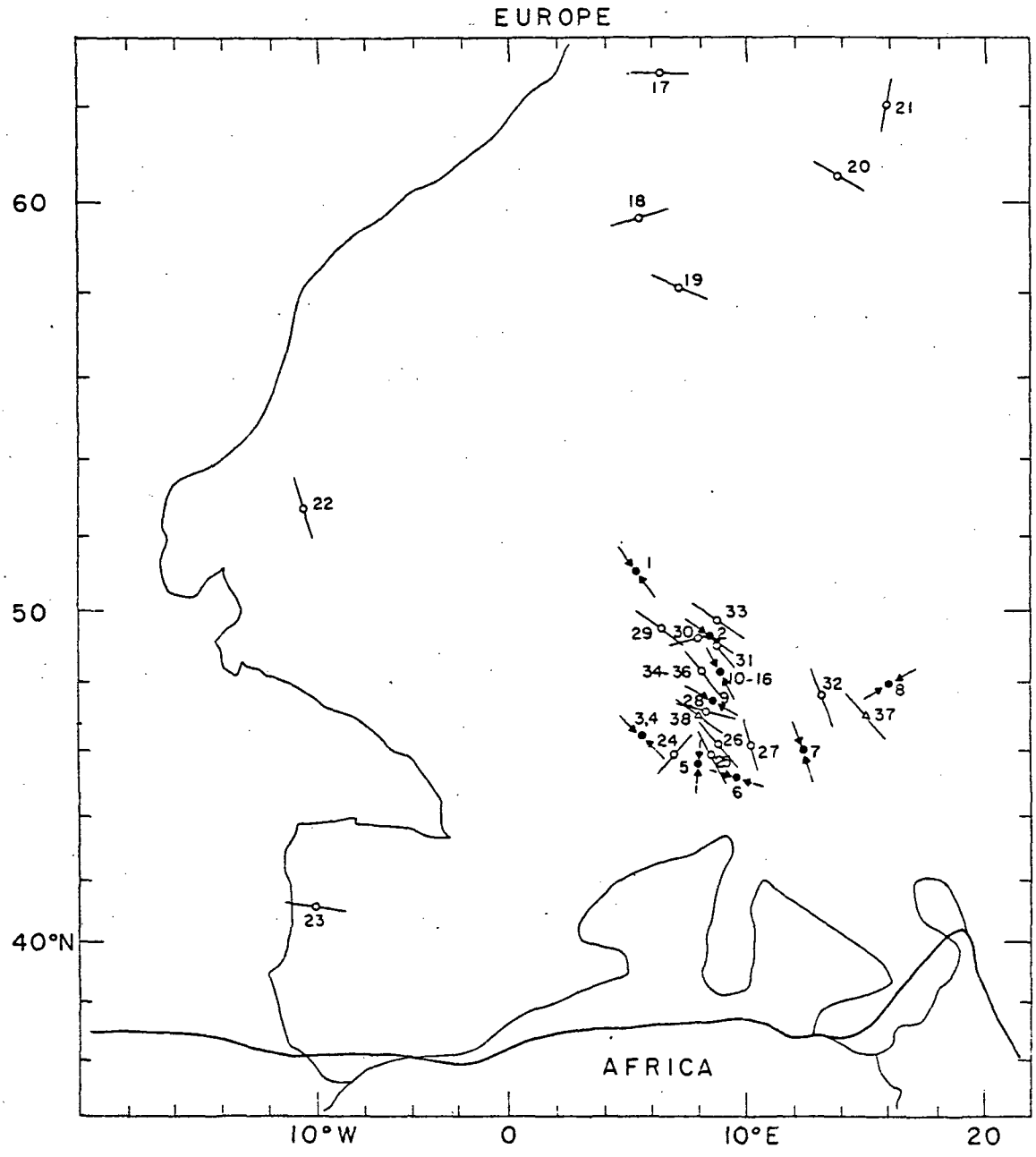
EUROPE
AFRICA
60
50
40°N
10°W
0
10°E
20
17
21
20
18
19
22
1
33
29
30
2
31
34-36
10-16
32
8
28
37
3,4
38
24
26
27
7
5
6
23

Figure 3

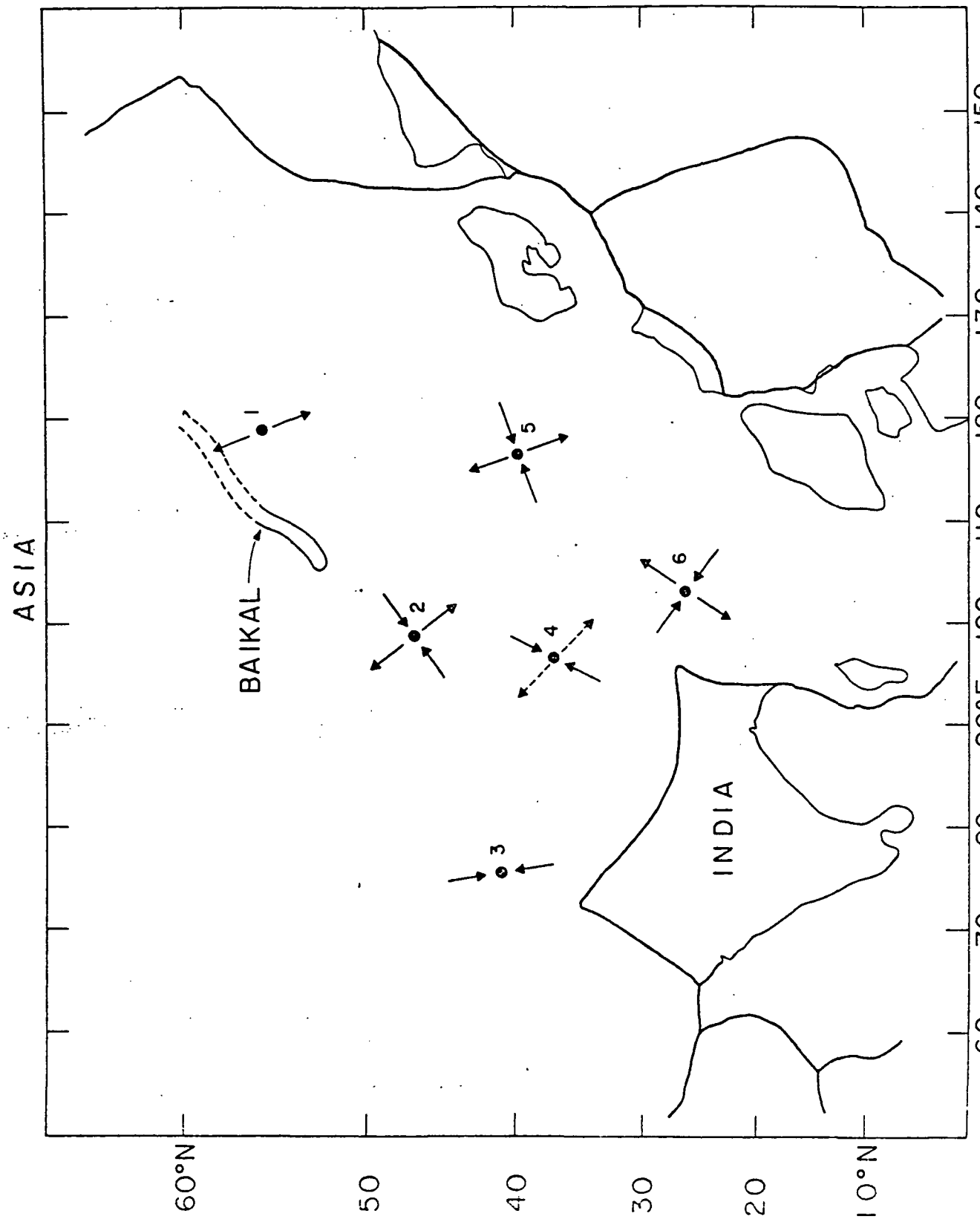
ASIA
BAIKAL
INDIA
1
2
3
4
5
6
60°N
50
40
30
20
10°N
60
70
80
90°E
100
110
120
130
140
150

Figure 4

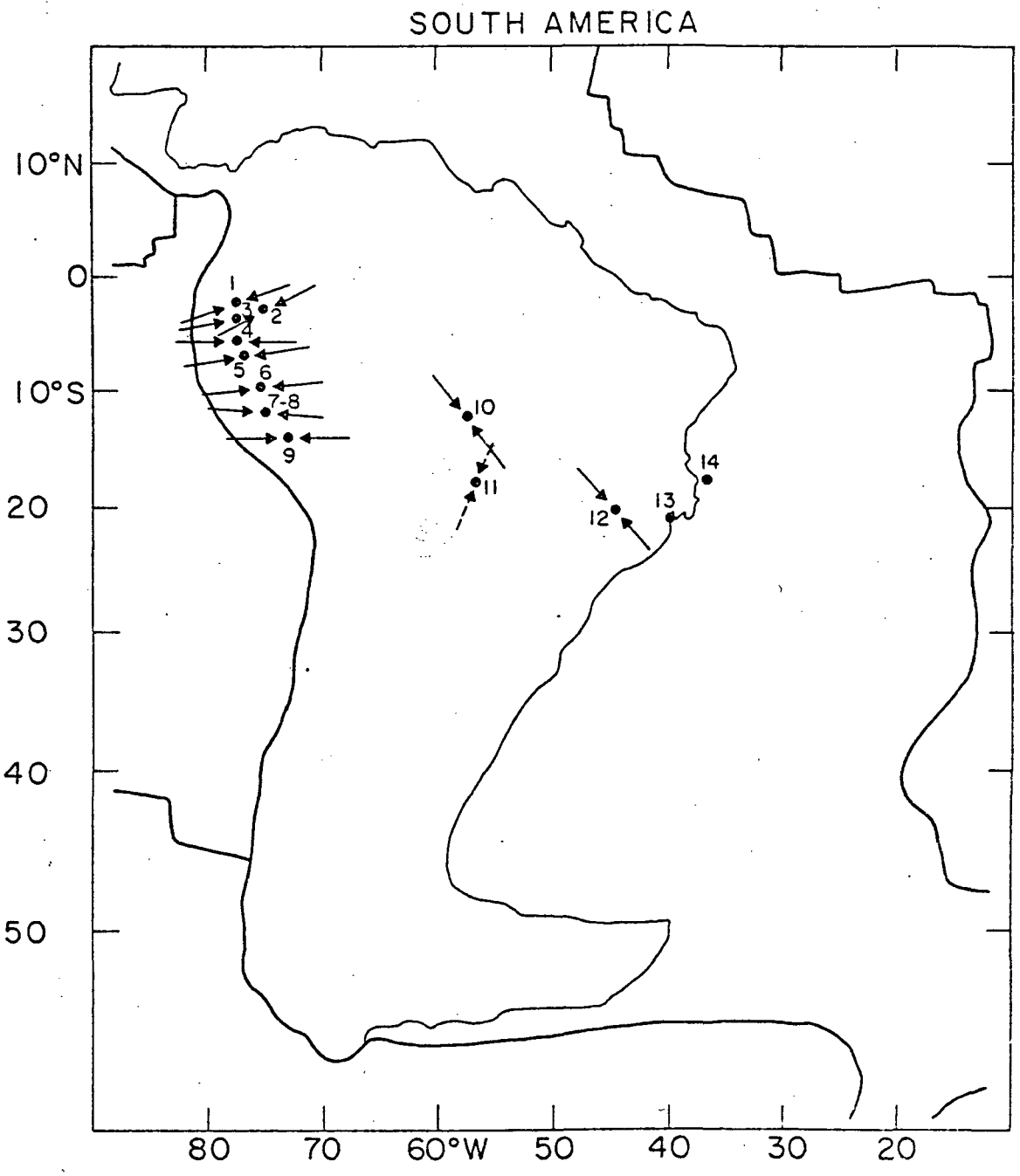
SOUTH AMERICA
10°N
0
10°S
20
30
40
50
80
70
60°W
50
40
30
20
1
2
3
4
5
6
7-8
9
10
11
12
13
14

Figure 5

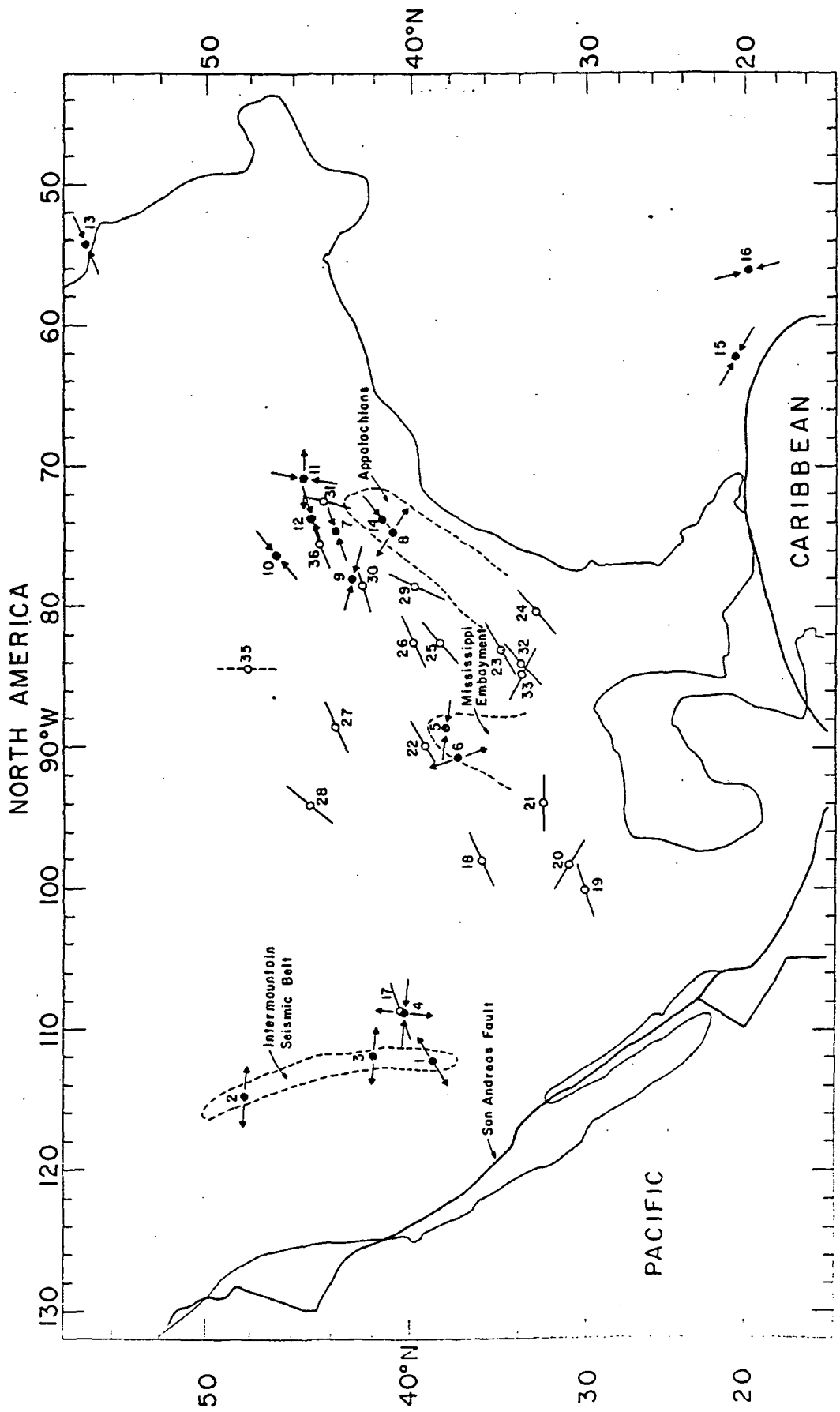
NORTH AMERICA
CARIBBEAN
PACIFIC
Appalachians
Mississippi Embayment
Intermountain Seismic Belt
San Andreas Fault
40°N
90°W

Figure 6

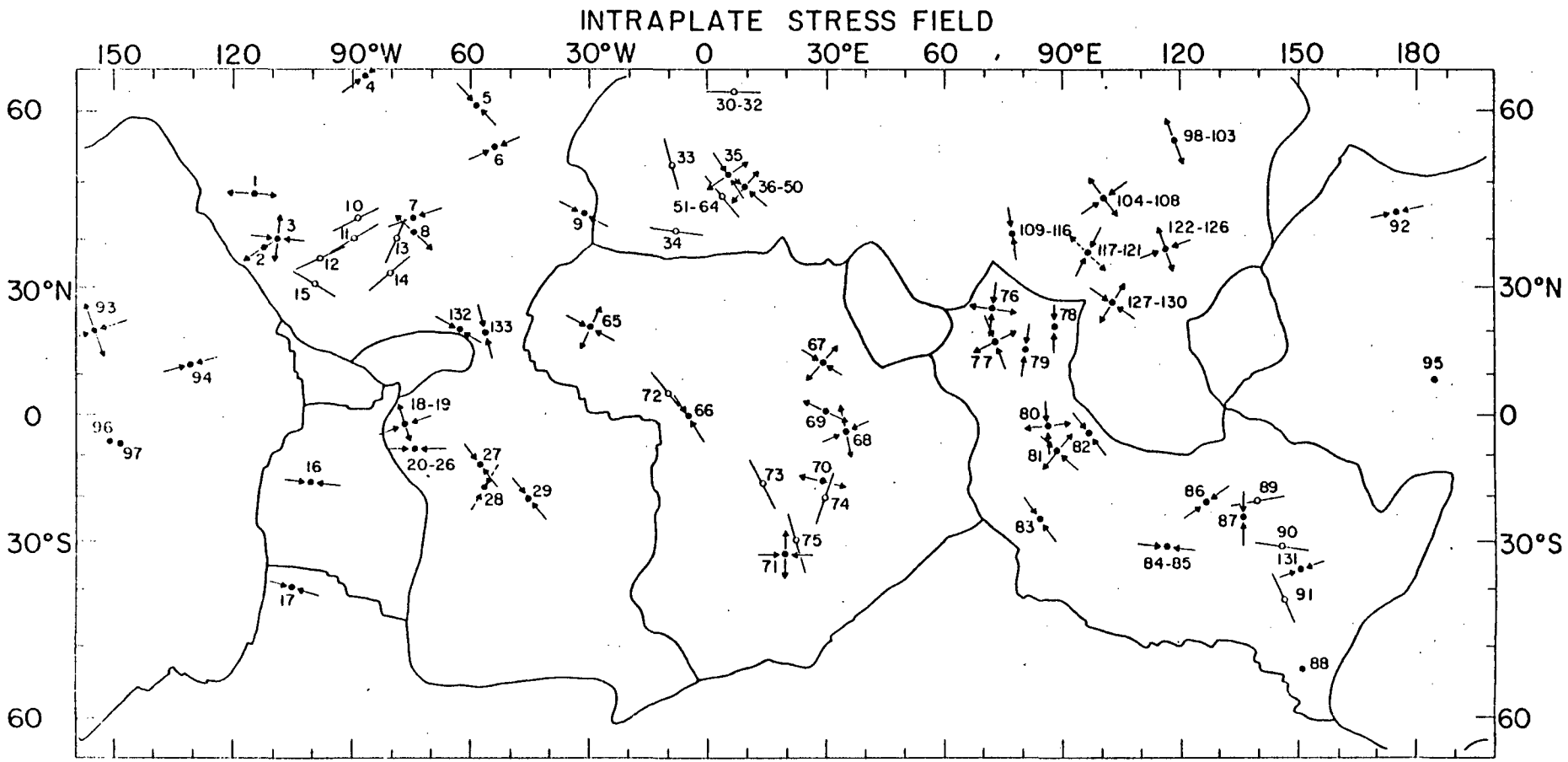
INTRAPLATE STRESS FIELD
150
120
90°W
60
30°W
0
30°E
60
90°E
120
150
180
60
30°N
0
30°S
60
1
2
3
4
5
6
7
8
9
10
11
12
13
14
15
16
17
18-19
20-26
27
28
29
30-32
33
34
35
36-50
51-64
65
66
67
68
69
70
71
72
73
74
75
76
77
78
79
80
81
82
83
84-85
86
87
89
90
91
92
93
94
95
96
97
98-103
104-108
109-116
117-121
122-126
127-130
131
132
133
88

Figure 7

FINITE ELEMENT GRID
MID LATITUDES: PART I

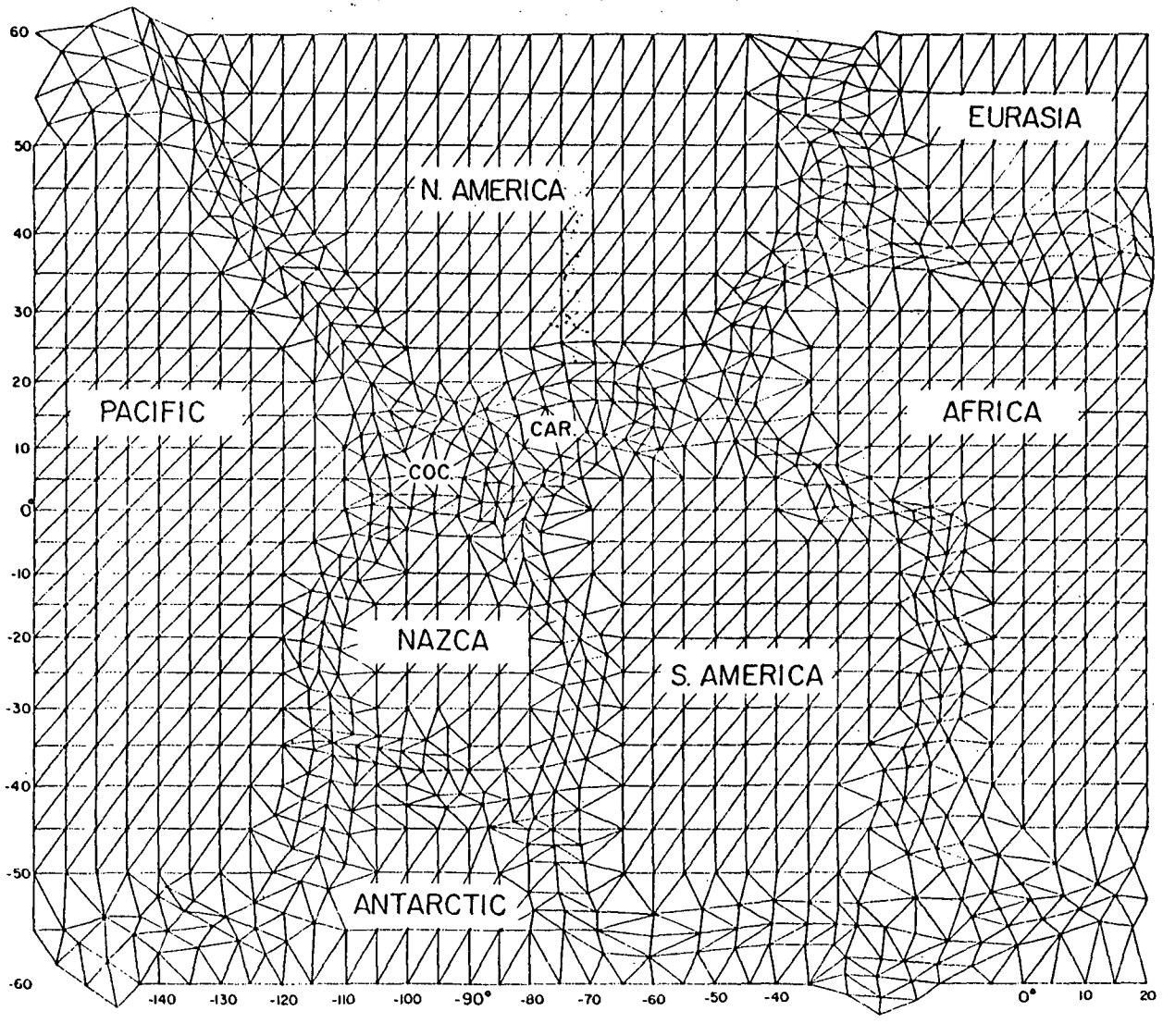

Figure 8

FINITE ELEMENT GRID
MID LATITUDES: PART 2

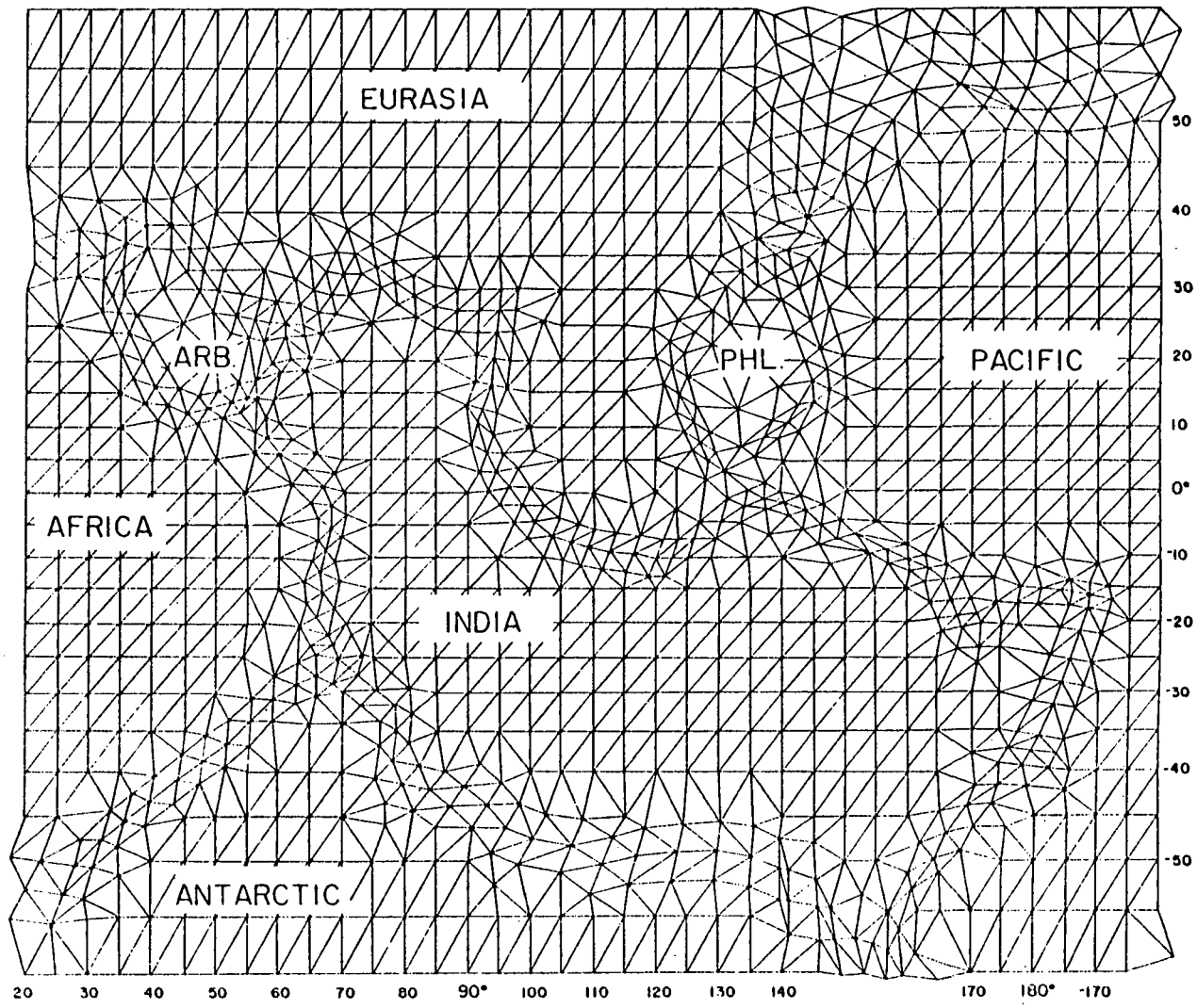

Figure 9

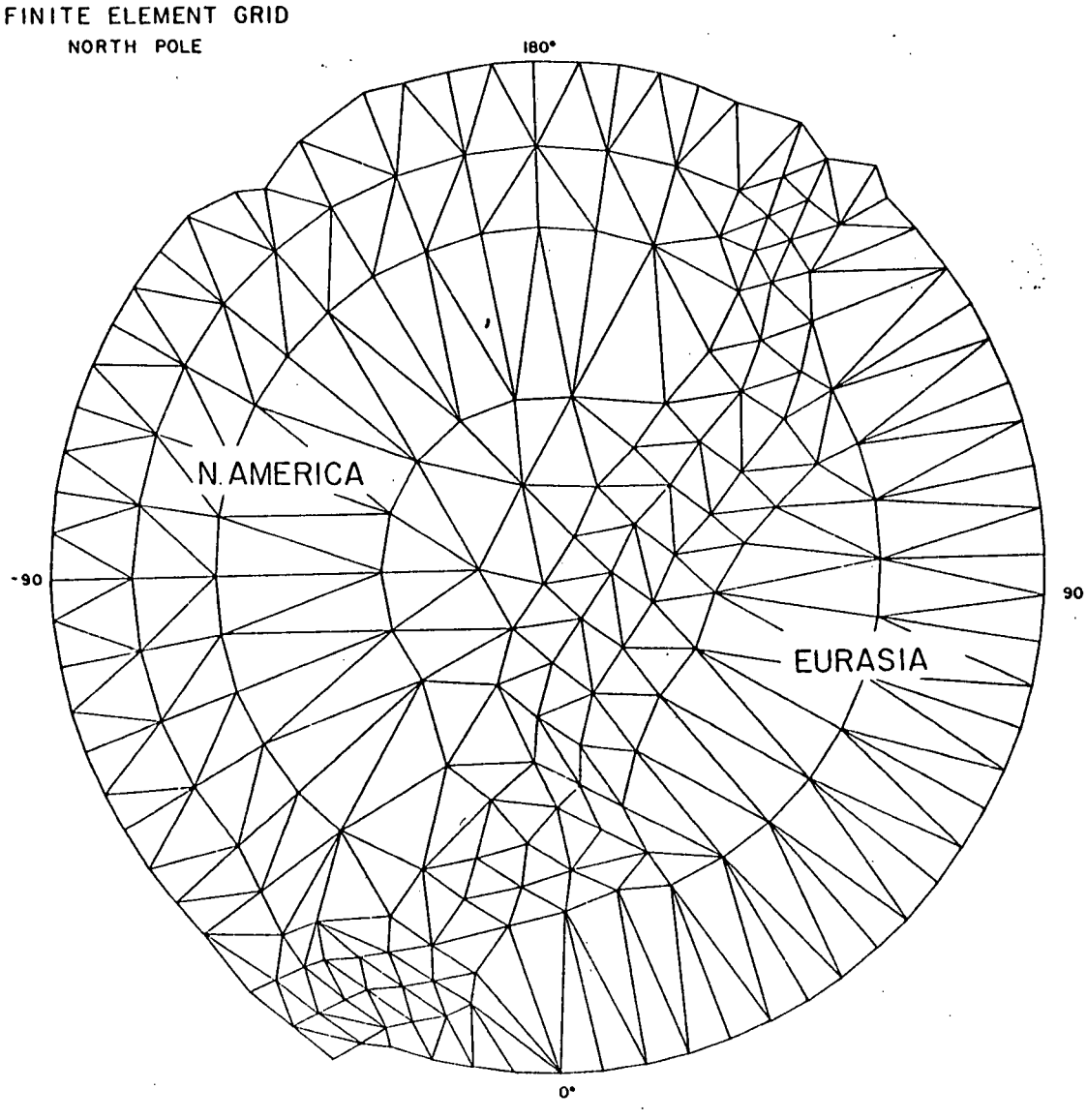

Figure 10

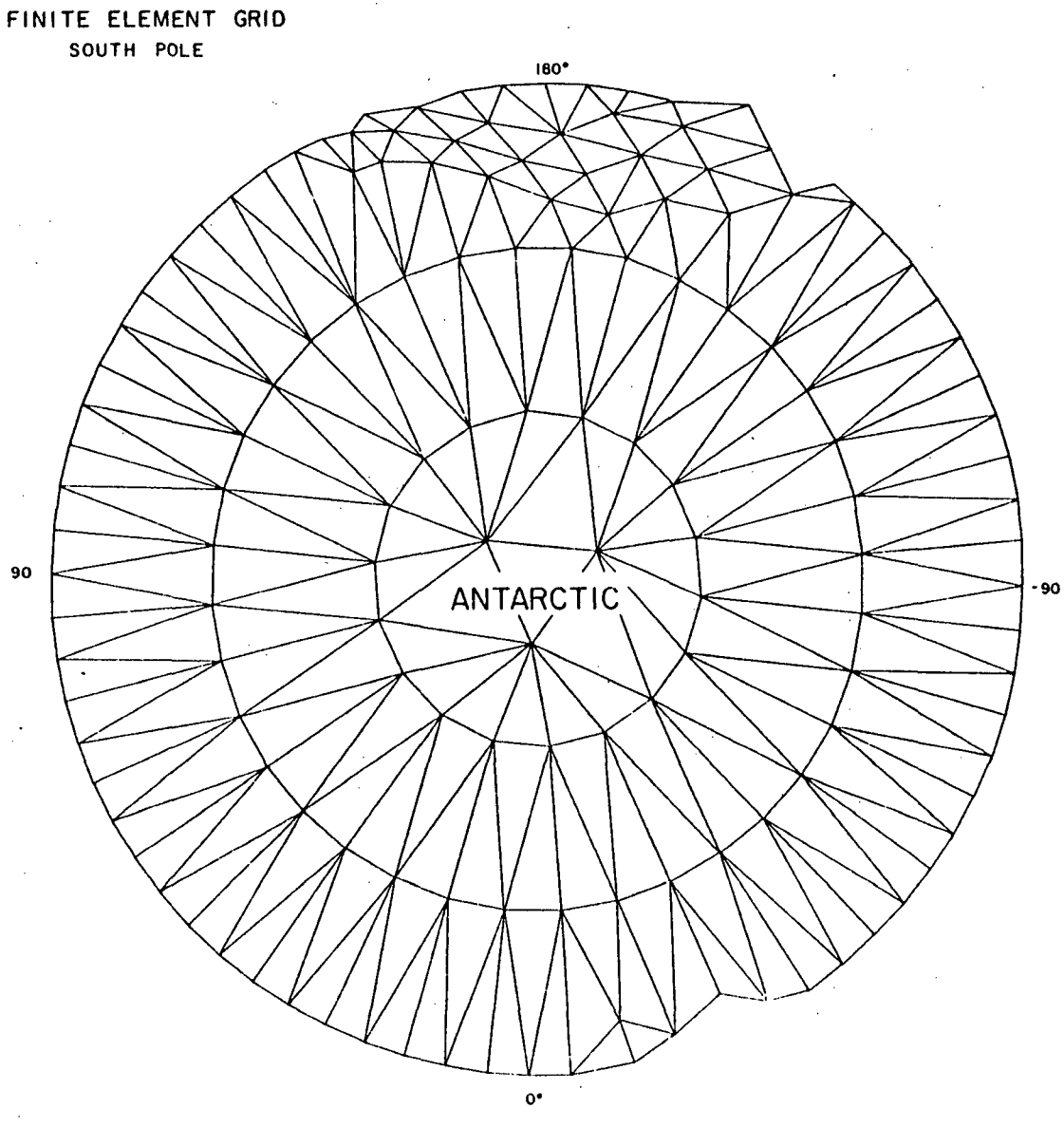

Figure 11

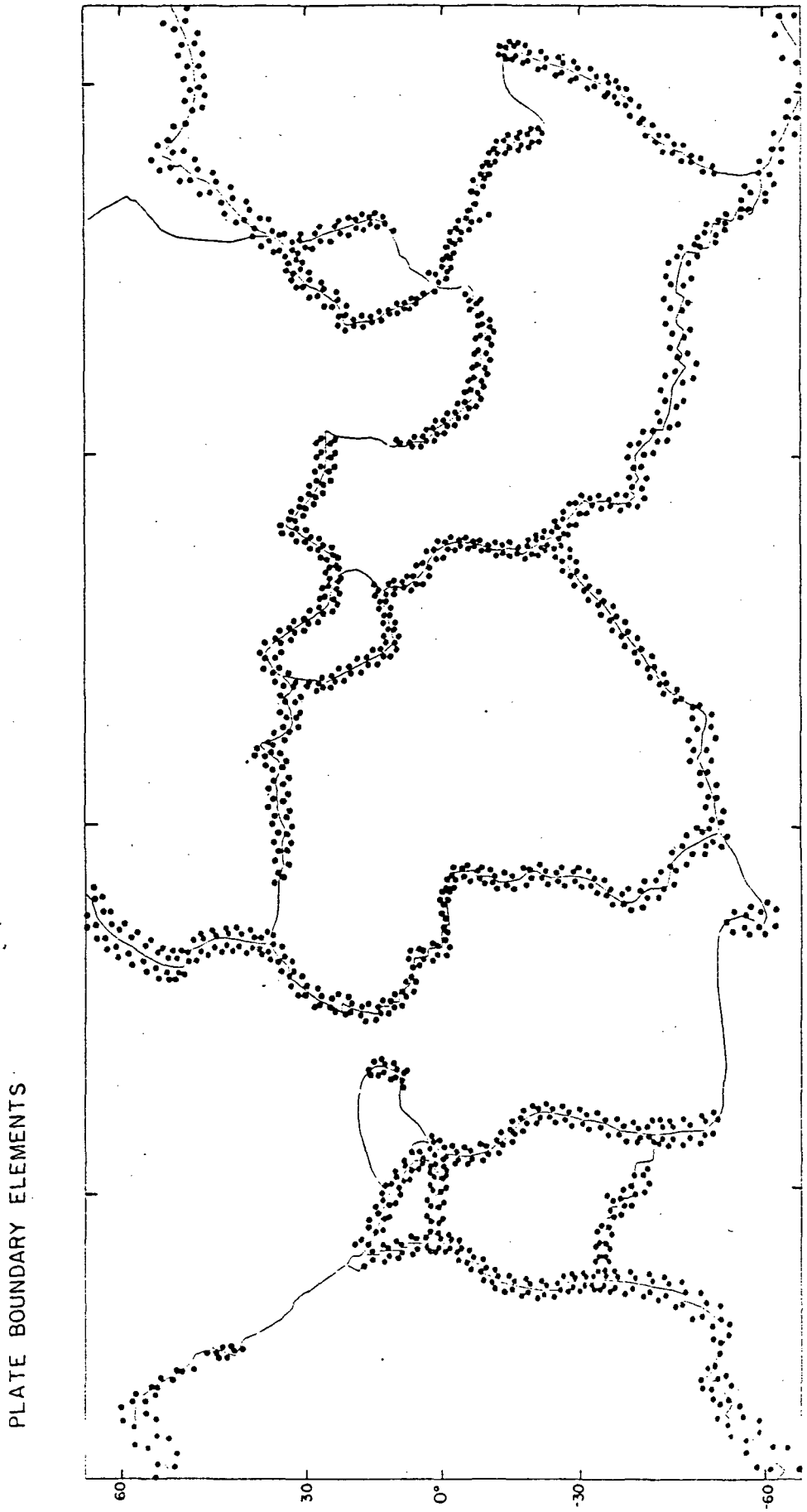

Figure 12

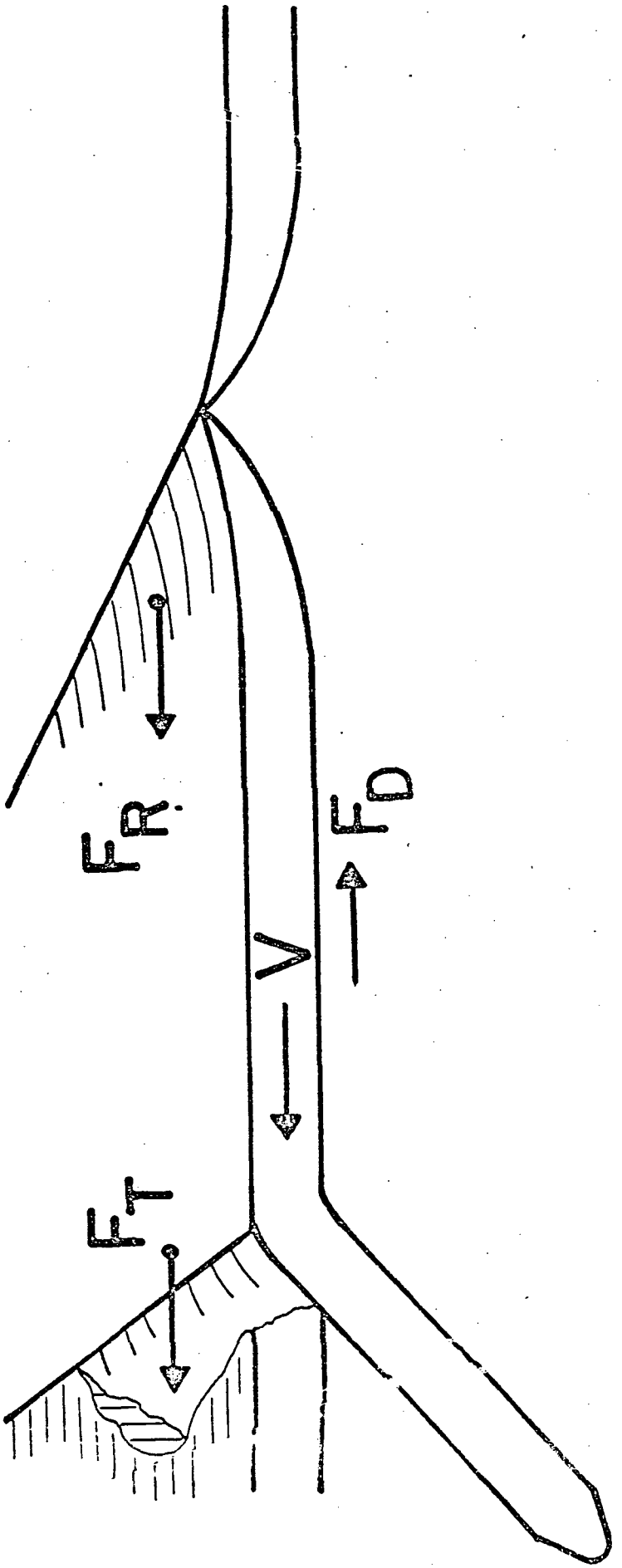

Figure 13

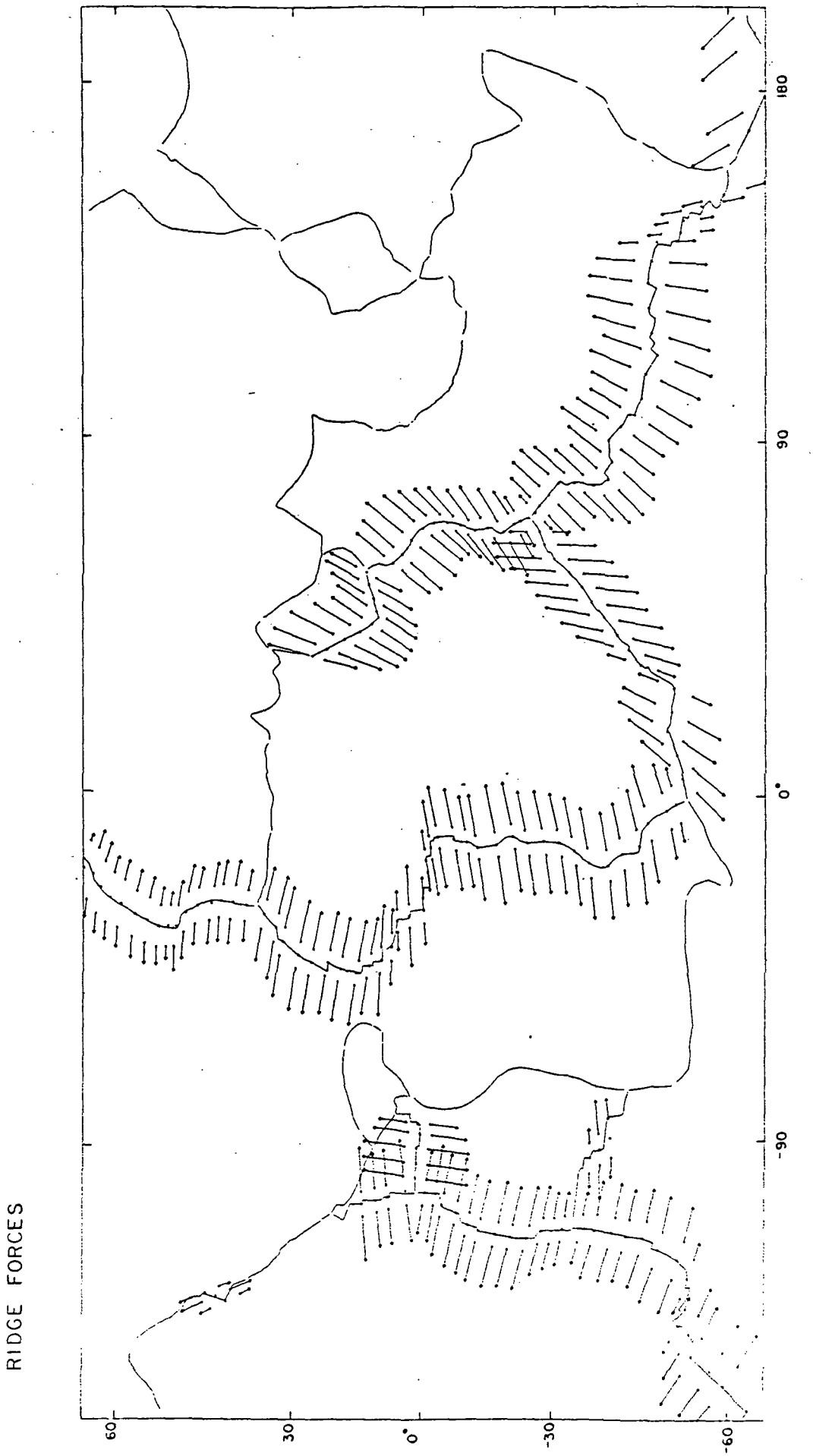

Figure 14

SUBDUCTION ZONE FORCES

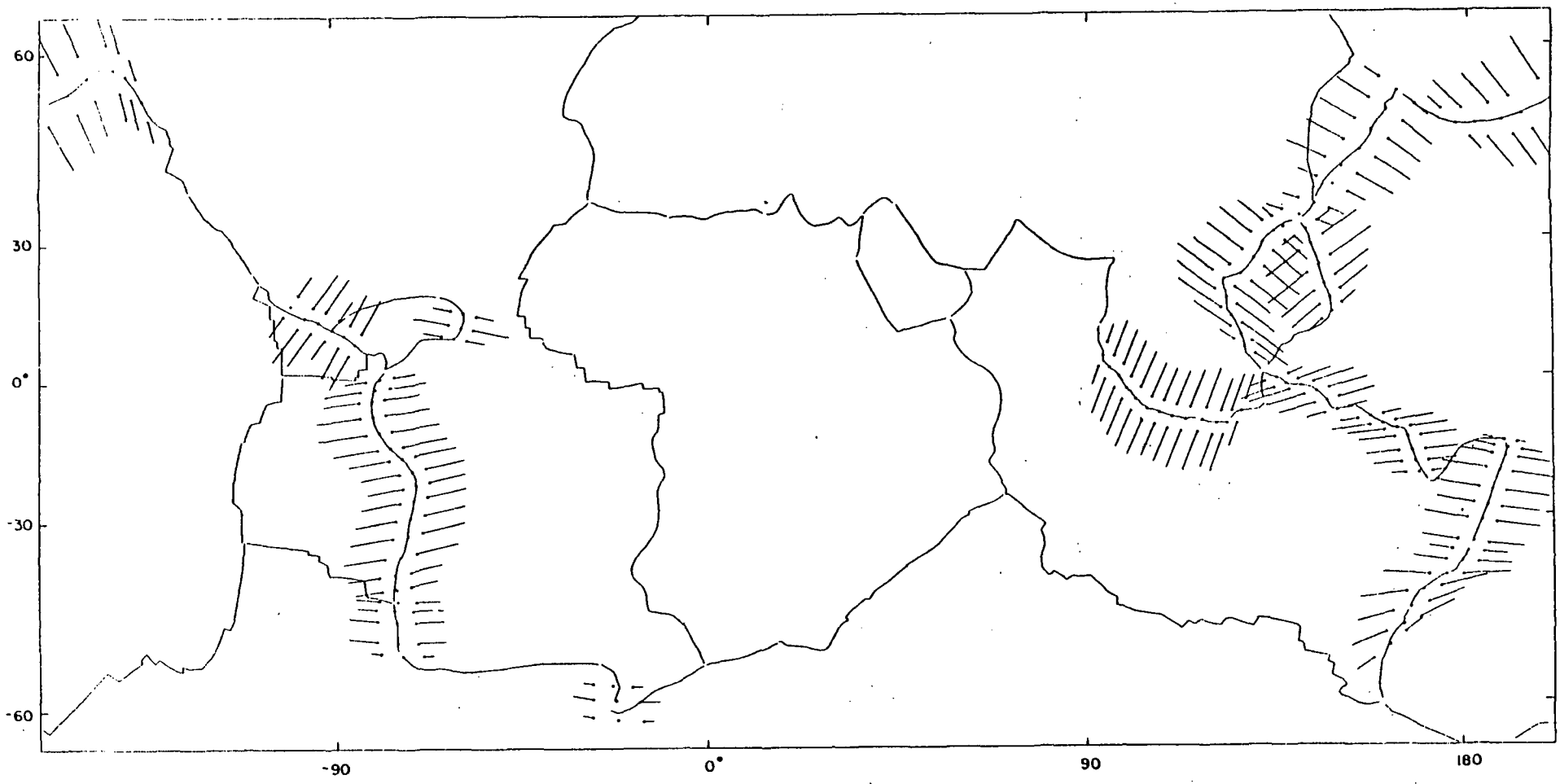

Figure 15

CONTINENTAL CONVERGENCE ZONE FORCES

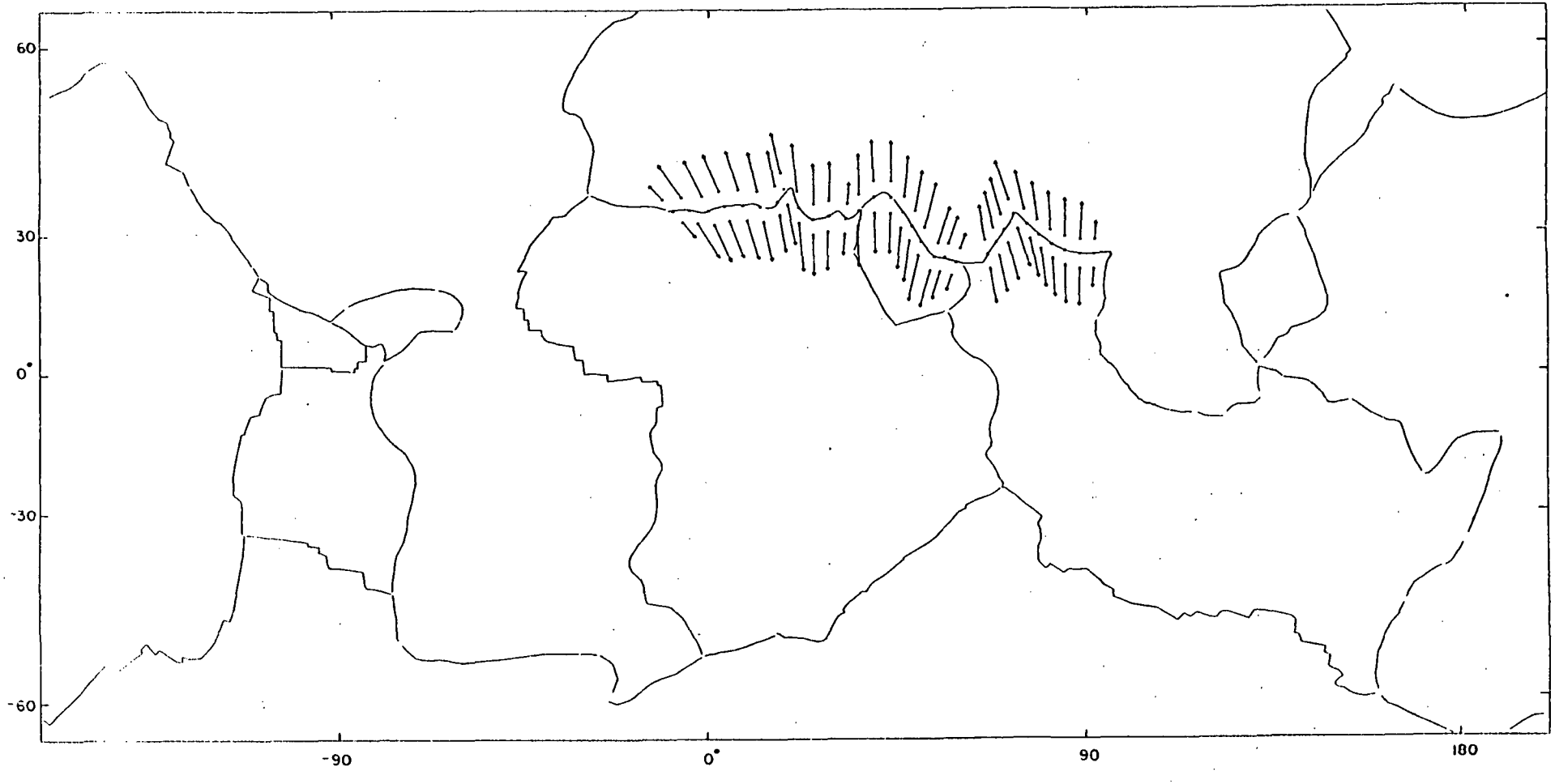

Figure 16

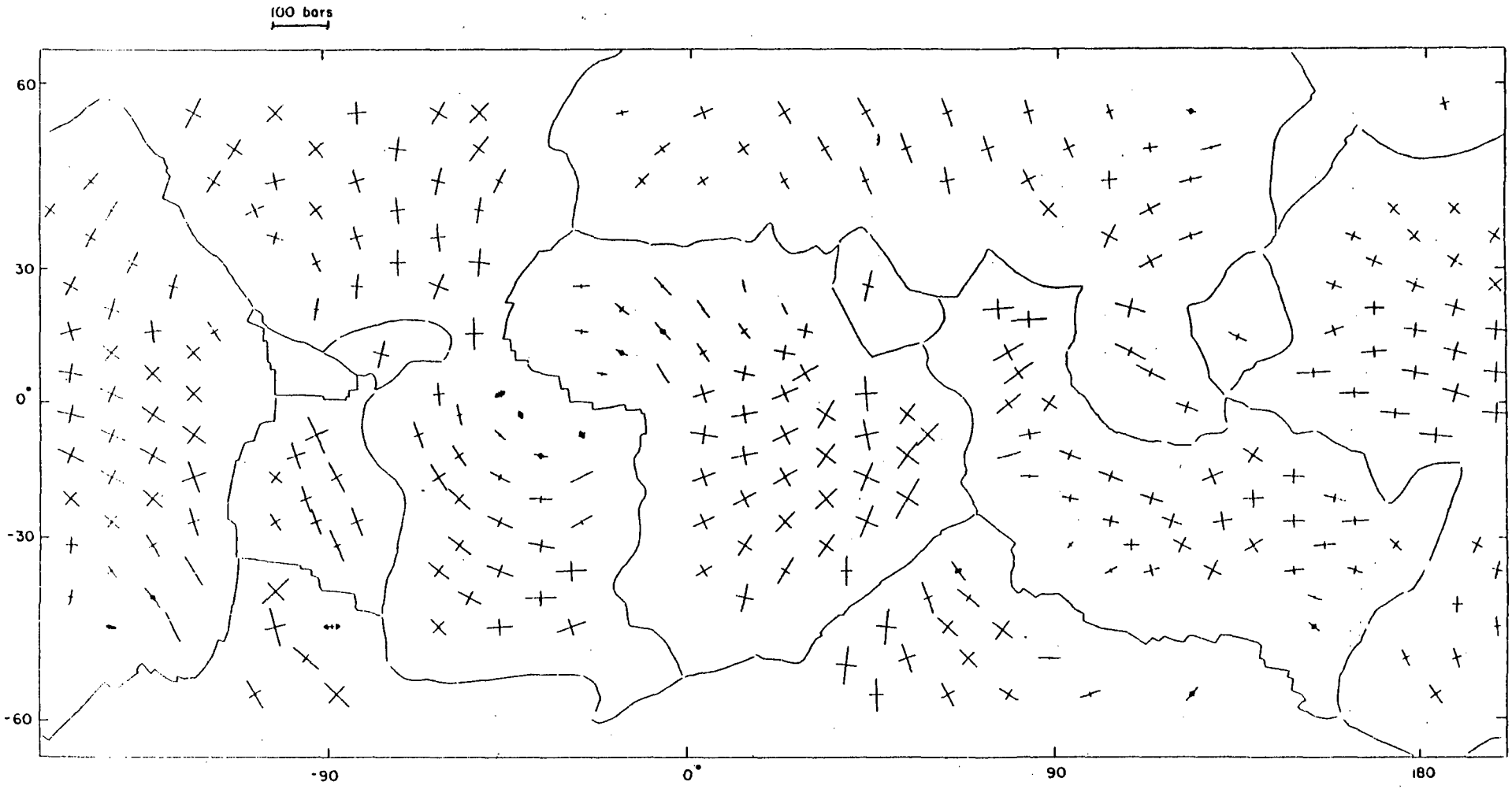

Figure 17

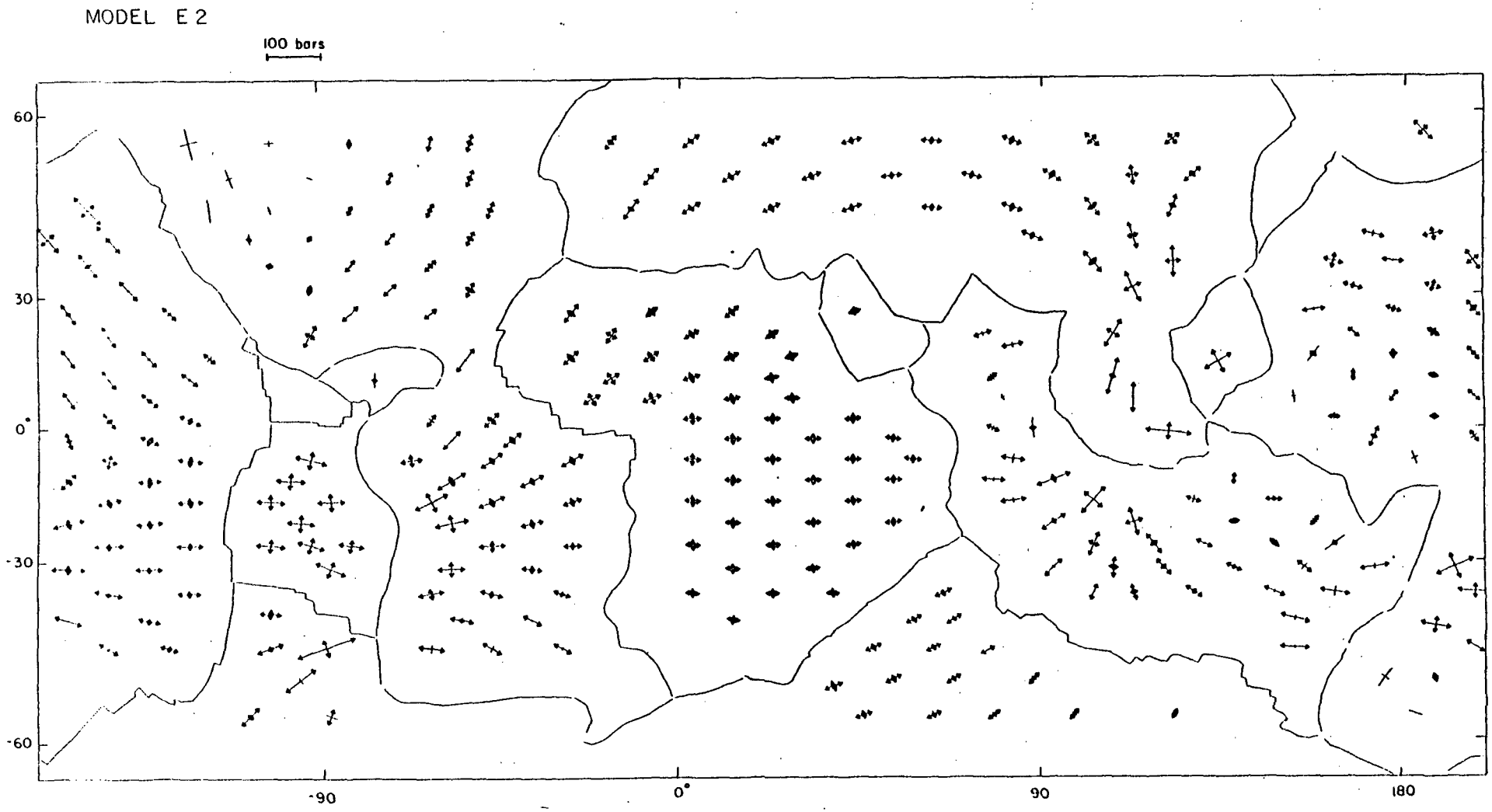

Figure 18

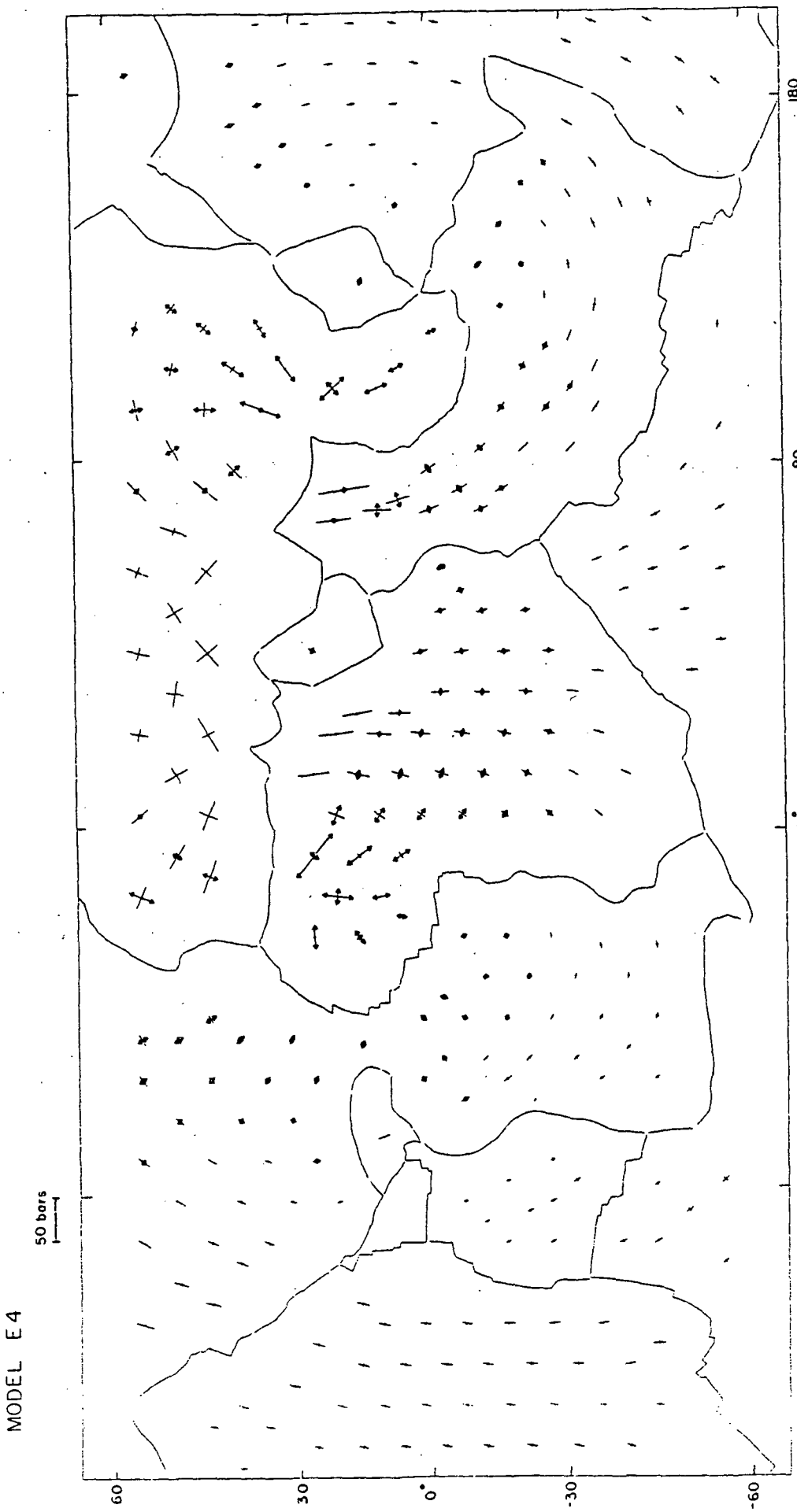

Figure 19

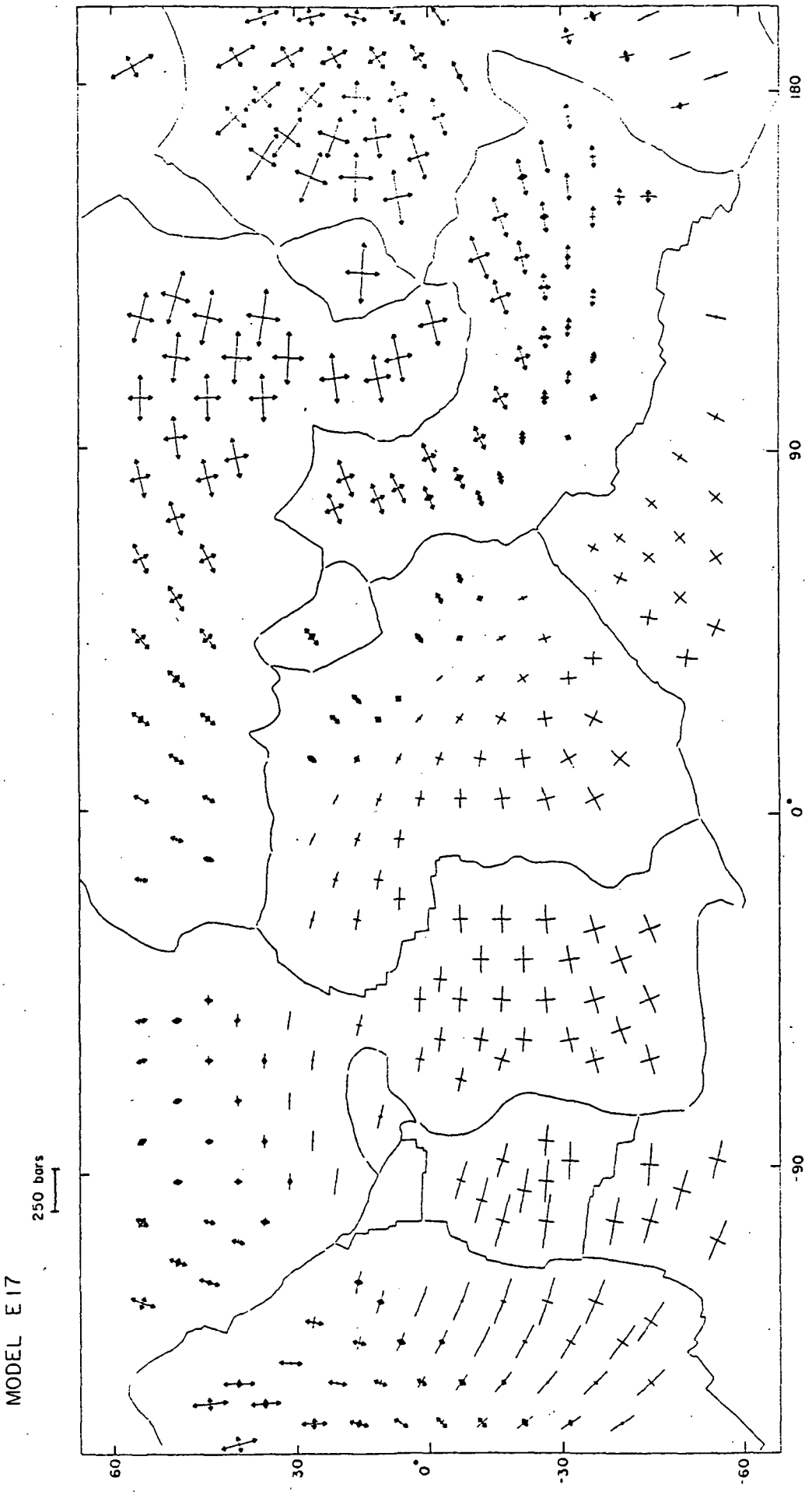

Figure 20

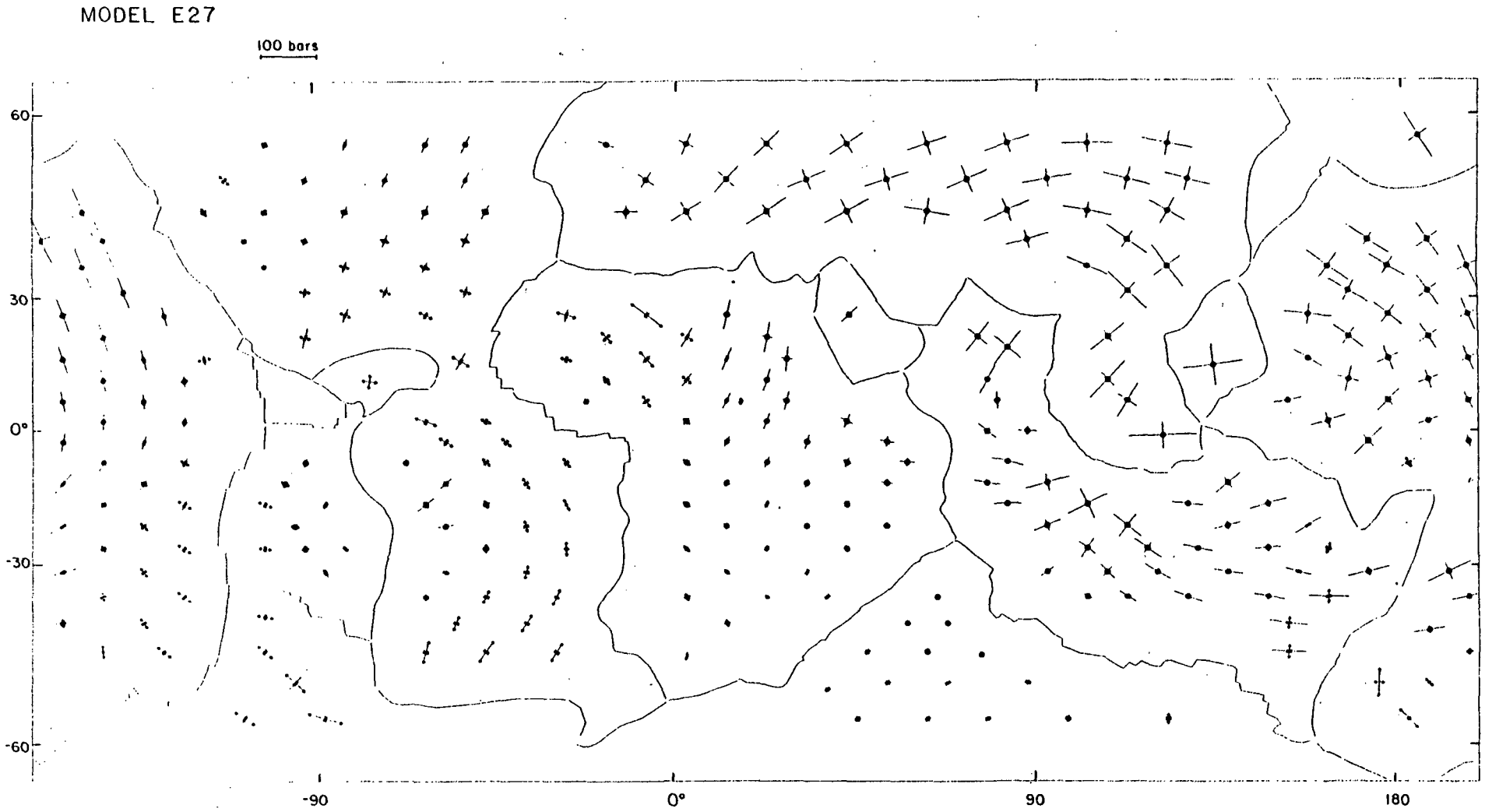

Figure 21

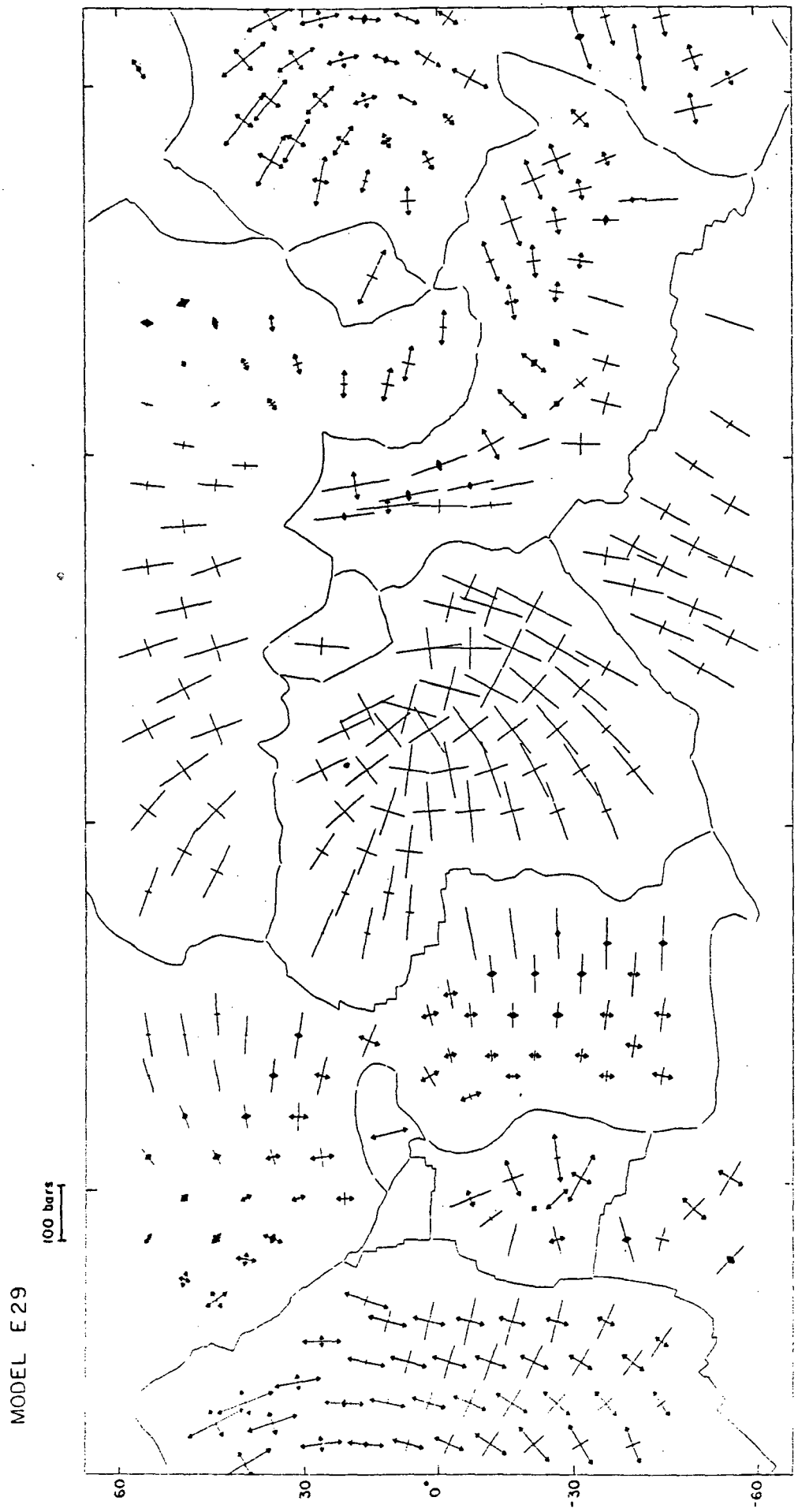

Figure 22

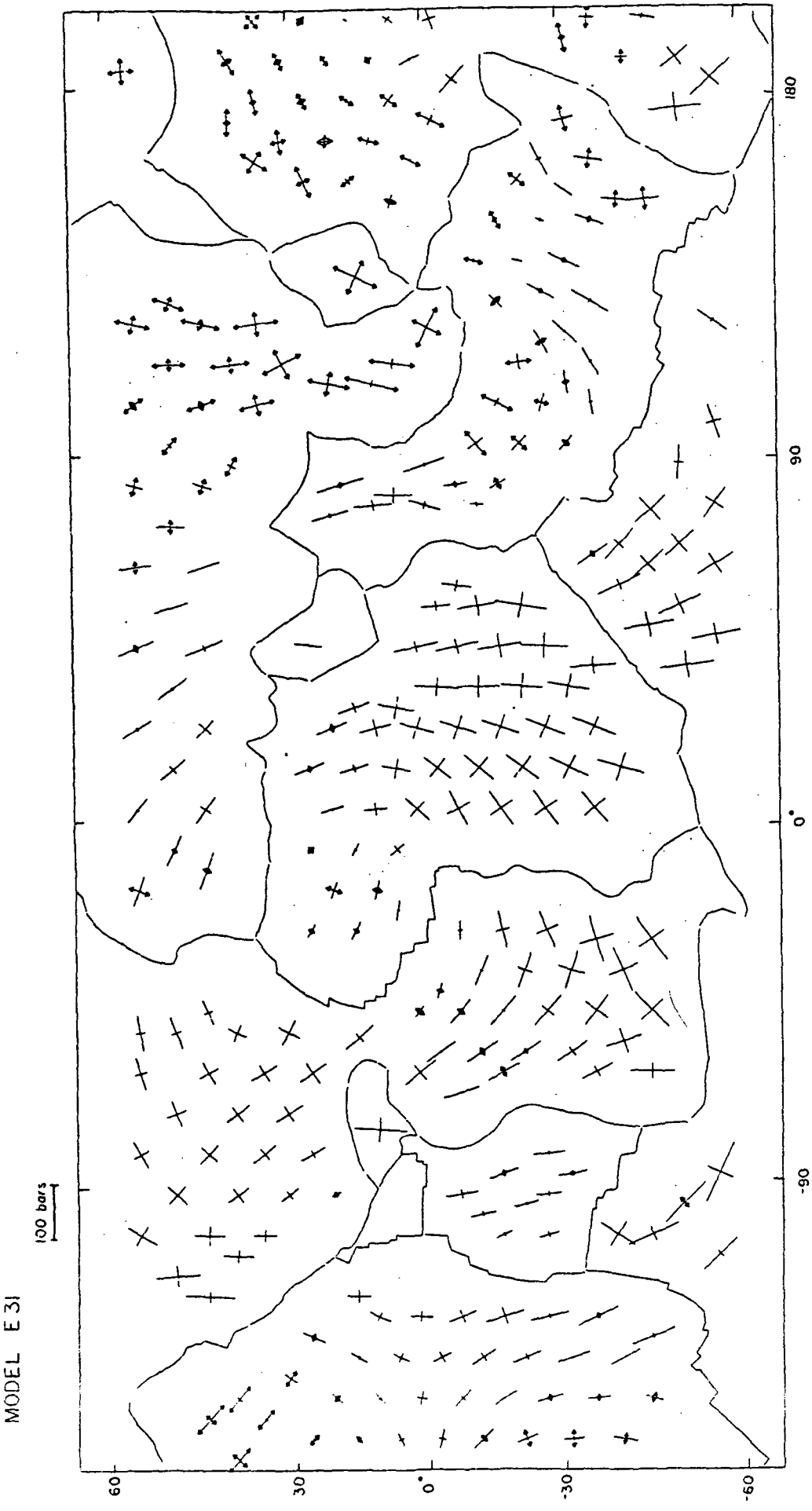

Figure 23

III. THREE DIMENSIONAL FINITE ELEMENT MODEL OF TIME DEPENDENT DEFORMATION AND STRESS IN THE LITHOSPHERE FOLLOWING EARTHQUAKE FAULTING

Introduction

We have developed a versatile scheme to model the time dependent tectonic deformation and stresses in the Earth. Three dimensional finite elements are used to take into account the heterogeneities in Earth properties. A unified numerical solution approach is incorporated with the wave front technique so that an efficient solution can be implemented on an ordinary size computer, and very general rheological constitutive laws can be used. Detailed procedures are given in the next section. Theoretical model results of the tectonic deformation and stress after a thrust fault earthquake and a strike slip earthquake are given in the last section.

Solution Technique

The central part of the modelling scheme is the finite element method. We used the wave front solution approach (Irons, 1970) to reduce the problem to a tractable size and an efficient solution, and we used a unified numerical solution approach (Zienkiewicz and Cormeau, 1974) to deal with a wide range of possible rheological constitutive laws.

The wave front approach represents an attempt to minimize the in-core storage requirement while giving a relatively efficient solution. Gaussian elimination is the central process of this technique. However, a global displacement-force equation is eliminated as soon as it has received all of the element stiffness and consistent nodal force contributions. The coefficients are moved to outside storage and other equations are updated accordingly. So only a small portion of stiffness matrix is in core at a time, thus achieving a saving in core usage. Assembly and elimination processes are not separated. After completion of assembly and elimination, the coefficeints are returned to core for back substitution in the order opposite to that by which they were saved. The wave front solution technique for static elastic problems has been implemented at MIT and has proved to be quite efficient (Orringer, 1974).

To deal with different rheological constitutive laws and to introduce generality, we divide the total strain $\underset{\sim}{\varepsilon}$ into three parts

$$\underset{\sim}{\varepsilon} = \underset{\sim}{\varepsilon}^{e} + \underset{\sim}{\varepsilon}^{cp} + \underset{\sim}{\varepsilon}^{\circ} \tag{1}$$

where $\underset{\sim}{\varepsilon}^{e}$ is the elastic strain, $\underset{\sim}{\varepsilon}^{\circ}$ the initial strain and $\underset{\sim}{\varepsilon}^{cp}$ the creep strain. Quite generally the constitutive law for creep strain rate and stress can be put into the form

$$\dot{\underset{\sim}{\varepsilon}}^{cp} = \underset{\sim}{\Gamma}\ \underset{\sim}{\sigma} \tag{2}$$

where the dot indicates time derivative. $\underset{\sim}{\Gamma}$ is a symmetric matrix (which may depend on stress) and $\underset{\sim}{\sigma}$ is the stress.

The virtual work principle is

$$\int_{\Omega} \delta\underset{\sim}{\varepsilon}^T \underset{\sim}{\sigma} \, d\Omega - \int_{\Omega} \delta\underset{\sim}{u}^T \underset{\sim}{b} \, d\Omega - \int_{S\sigma} \delta\underset{\sim}{u}^T \underset{\sim}{t} \, d S = 0 \qquad (3)$$

where $\underset{\sim}{b}$ is the prescirbed body force, $\underset{\sim}{t}$ the prescribed boundary traction, $\underset{\sim}{u}$ the displacement and T indicates transpose. Integration is over the volume Ω and traction boundary $S\sigma$ respectively.

$$\text{Let } \underset{\sim}{\varepsilon} = \underset{\sim}{L}\,\underset{\sim}{u}, \quad \underset{\sim}{u} = \underset{\sim}{N}\,\underset{\sim}{a} \qquad (4)$$

$\underset{\sim}{L}$ is the operator relating strain and displacement, $\underset{\sim}{N}$ the shape function and $\underset{\sim}{a}$ the nodal displacements. Then equation (3) becomes

$$\delta\underset{\sim}{a}^T \left[\int_{\Omega} (\underset{\sim}{L}\,\underset{\sim}{N})^T \underset{\sim}{\sigma} \, d\Omega - \int_{\Omega} \underset{\sim}{N}^T \underset{\sim}{b} \, d\Omega - \int_{S\sigma} \underset{\sim}{N}^T \underset{\sim}{t} \, d S\right] = 0$$

or $$\int_{\Omega} \underset{\sim}{B}^T \underset{\sim}{\sigma} \, d\Omega - \underset{\sim}{F} = 0 \qquad (5)$$

where $$\underset{\sim}{B} = \underset{\sim}{L}\,\underset{\sim}{N}, \quad \underset{\sim}{F} = \int_{\Omega} \underset{\sim}{N}^T \underset{\sim}{b} \, d\Omega + \int_{S\sigma} \underset{\sim}{N}^T \underset{\sim}{t} \, d S.$$

Using $\underset{\sim}{\sigma} = \underset{\sim}{D}\,\underset{\sim}{\varepsilon}^e = \underset{\sim}{D}\,(\underset{\sim}{\varepsilon} - \underset{\sim}{\varepsilon}^{cp} - \underset{\sim}{\varepsilon}^{\circ})$ where $\underset{\sim}{D}$ is the set of elastic constants, equation (5) can be put into the standard form

$$\underset{\sim}{K}\,\underset{\sim}{a} = \underset{\sim}{V} \qquad (6)$$

where $\underset{\sim}{K} = \int_{\Omega} \underset{\sim}{B}^T \underset{\sim}{D} \underset{\sim}{B} \, d\Omega$

and $\underset{\sim}{V} = \underset{\sim}{F} + \int_{\Omega} \underset{\sim}{B}^T \underset{\sim}{D} \underset{\sim}{\varepsilon}^{\circ} \, d\Omega - \int_{\Omega} \underset{\sim}{B}^T \underset{\sim}{D} \underset{\sim}{\varepsilon}^{cp} \, d\Omega$

Equation (6) is the set of linear equations to be solved using the wave front solution. ε^{cp} is obtained by stepping in time using equation (2). It can be shown that this procedure can be applied to general visco-plastic problems (Zienkiewicz and Cormeau, 1974), including plasticity and creep problems as two special cases. Strain hardening and the use of non-associate laws do not introduce formulation difficulties. Notice also that in later steps, only nodal forces are changed. We have only to update the forces in the assembly and elimination procedures, and have thus achieved an efficient solution. Depending on the configuration of the problem, the CPU usage for each later time step is only about 5% to 10% of the initial solution.

Three Dimensional Models for a Thrust Fault Earthquake and Strike Slip Earthquake

Using techniques described in the last section, we calculated the quasi-static response for two types of earthquakes, a thrust fault and a strike-slip fault. In these models, we assume that linear viscoelasticity holds. Studies on non-linear models are currently underway.

Figure 1 shows a schematic diagram of the thrust fault model. The model fault is 400 km in length and dips at 30° from the surface to a depth of 40 km. The offset between opposite sides of the fault is assumed to be 10 meters. The assumed rheological properties are given in Table 1. There are five elements in each vertical column. The boundary conditions are: pinned bottom (700 km depth), free top surface, free surfaces at the three sides far from the fault, and a reflection boundary condition (zero normal displacement) for side AA'.

Figure 2 gives the finite element grid on the free surface for half of the model. Due to symmetry, only half of the region needs to be modelled.

Figure 3 shows the horizontal displacement on the free surface along the symmetry line (AA' in Figure 2). There is significant time dependent displacement up to one thousand km away from the source.

Figure 4 gives the horizontal plate velocity as a function of time at selected nodes on the symmetry line AA' (indicated by circles in Figure 2). The plate motion is not uniform; accelerations continue for decades after the event.

Figure 5 gives the normal stress perpendicular to fault strike at selected locations along the symmetry line AA' (indicated by crosses in Figure 2). The stress decays with time near the fault, but increases with time at a distance of several hundred kilometers. This is a rather general

result as long as there is a low viscosity layer beneath the lithosphere. Physically, this is easy to understand: the dislocation introduces high stress in its vicinity. Due to the asthenosphere low viscosity the stresses relax near the dislocation while this load diffuses away from the source. For this thrust fault earthquake this diffusion effect is not very large on the free surface since the fault motion is not purely horizontal. We would anticipate a larger diffusion effect on the free surface for a strike slip earthquake whose fault motion is entirely horizontal.

The schematic diagram for the strike slip earthquake fault is given in Figure 6. The earthquake has a fault length of 200 km and extends from the surface to 15 km depth. The offset along the fault is assumed to be 10 meters. Again, due to symmetry only half of the region needs to be modelled. The finite element grid of half of the free surface region is given in Figure 7. The rheological properties are given in Table 2.

Figure 8 gives the horizontal surface displacement immediately after the earthquake at nodes for a quadrant of the free surface region. Due to symmetry, along the line bisecting the fault (AA' in Figure 7) the displacement is parallel to the fault; while along the line containing the fault (OO' in Figure 7), the displacement is perpendicular to the fault except on the fault. Figure 9 and Figure 10 give the accumulated horizontal displacement 9.5 and 49 years

later, respectively. There is in general an increase in displacement with time, along with some change of direction (except on symmetry lines). This increase in displacement can be understood as a result of transferring the load from the low viscosity layer to the lithosphere as the stresses in the low viscosity layer relax. The parallel displacement along the symmetry line (OA in Figure 7) is given in Figure 11. The detailed time dependence at several locations (indicated by circles in Figure 7) is given in Figure 12, and velocity as function of time is given in Figure 13. Again there is nonuniform plate motion lasting for decades after the event.

Strike slip earthquakes show interesting stress diffusion effects in the lithosphere. Figure 14 shows the time dependence of maximum shear stress at several locations near the fault (indicated by crosses in Figure 7). They decrease with time monotonically as we expect for high stress areas. Away from the fault tip, the stresses drop off with distance rapidly, according to St Venant's Principle, since the earthquake dislocation is a balanced force system. However, in front of the fault tip, viscoelastic interaction causes the stress to increase with time. Figure 15 shows the time dependence of maximum shear stress at some locations in front of the fault tip (indicated by squares in Figure 7). At 160 km away from the fault center, the stress increases rapidly in the first decade. Furthermore, the time dependent stress

due to earthquakes will reinforce the pre-stress there. The obvious conclusion is that the chance of an earthquake happening is greater in the area in front of a fault tip. The triggered earthquake may again generate its own stress perturbation which may cause migration of earthquakes. Although this calculation is not meant to model a specific region, this migration of earthquakes along a strike-slip fault zone is actually observed, for example, along the North Anatolian fault (Dewey, 1976; Toksöz et al., 1979).

Summarizing these viscoelastic models: the results indicate that great earthquakes cause significant motion at distances up to 1,000 km away and that relaxation processes last for decades after the event. These conclusions have a direct effect on the interpretation of geodetic data. The stress diffusion effect can be useful in the analysis of earthquake migration in space and time.

References

Dewey, J.W. Seismicity of northern Anatolia, Bull. Seism. Soc. Am., 66, 843-868, 1976.

Irons, B.M., A Frontal Solution Program for Finite Element Analysis, Int. J. Num. Meth. Eng., 2, 5-32, 1970.

Orringer, O., FRAP: Frontal Analysis Programs, Aero Structural Lab, M.I.T., 1974.

Toksöz, M.N., A.F. Shakal and A.J. Michael, Space-time migration of earthquakes along the north Anatolian fault zone and seismic gaps, Preprint, 1979.

Zienkiewicz, O.C. and I.C. Cormeau, Visco-plasticity - Plasticity and creep in elastic solids - A unified numerical solution approach", Int. J. Num. Meth. Eng., 8, 821-845, 1974.

Table 1

Thrust Earthquake Model

Depth (km)	Viscosity (poise)
0 - 80	1.0×10^{26}
80 - 180	1.0×10^{20}
180 - 400	1.0×10^{21}
400 - 700	1.0×10^{22}

Young's Modulus = 2.00×10^{6} bars, Poisson's ratio = 0.25

Table 2

Strike Slip Earthquake Model

Depth (km)	Viscosity (Poise)
0 - 30	1.0×10^{26}
30 - 180	1.0×10^{20}
180 - 400	1.0×10^{21}

Young's Modulus = 2.00×10^{6} bars, Poisson's ratio = 0.25

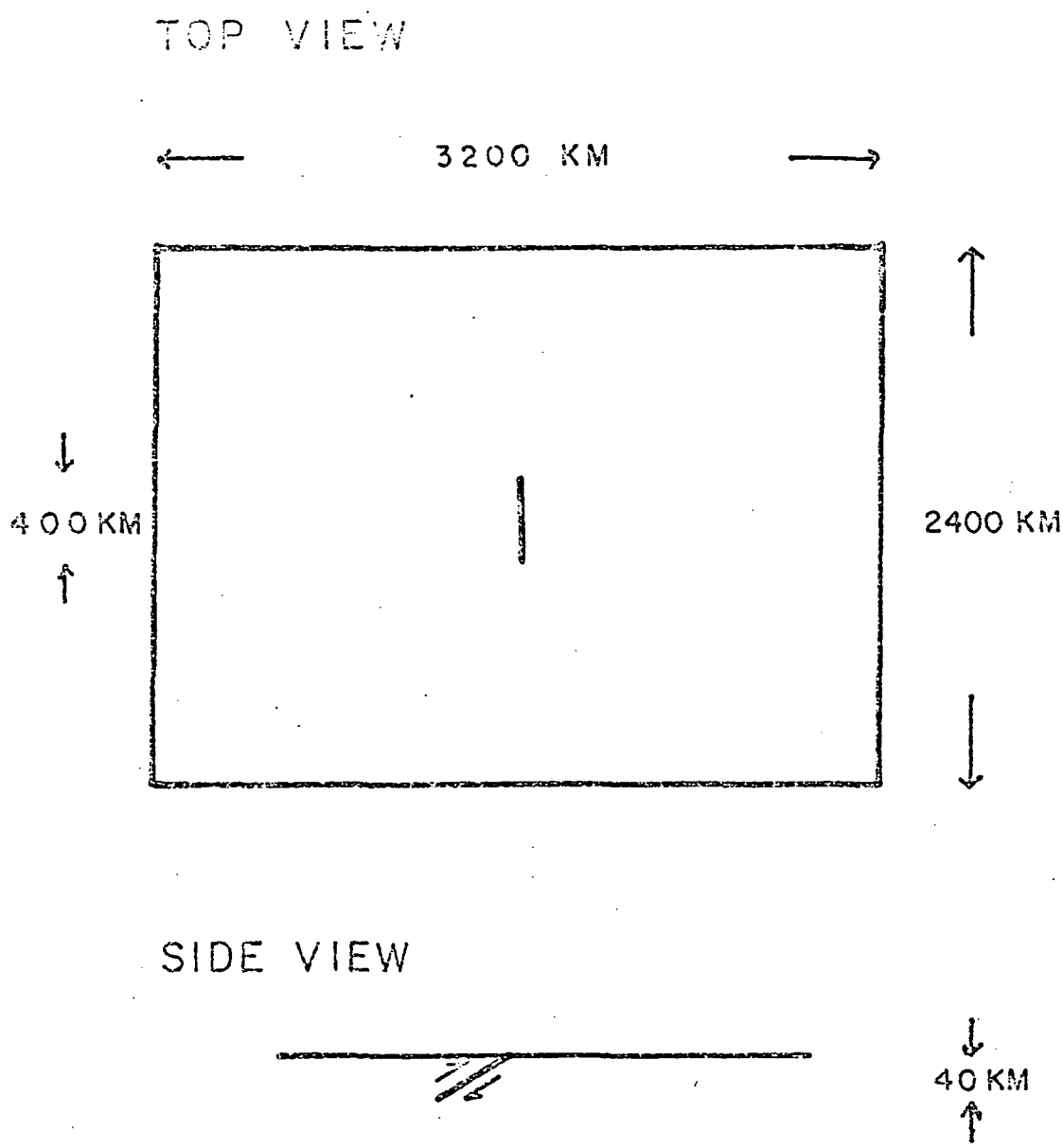

Fig.1.Schematic diagram of thrust fault model

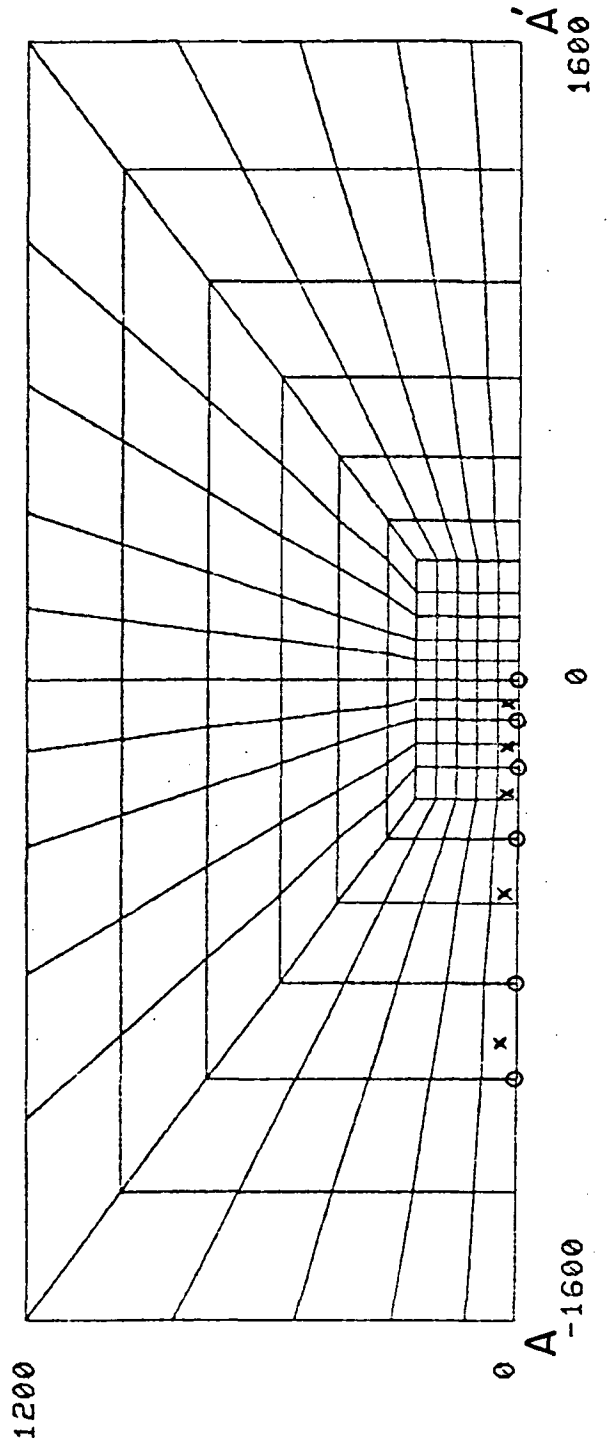

Fig. 2 Finite element grid on free surfact for half the model region

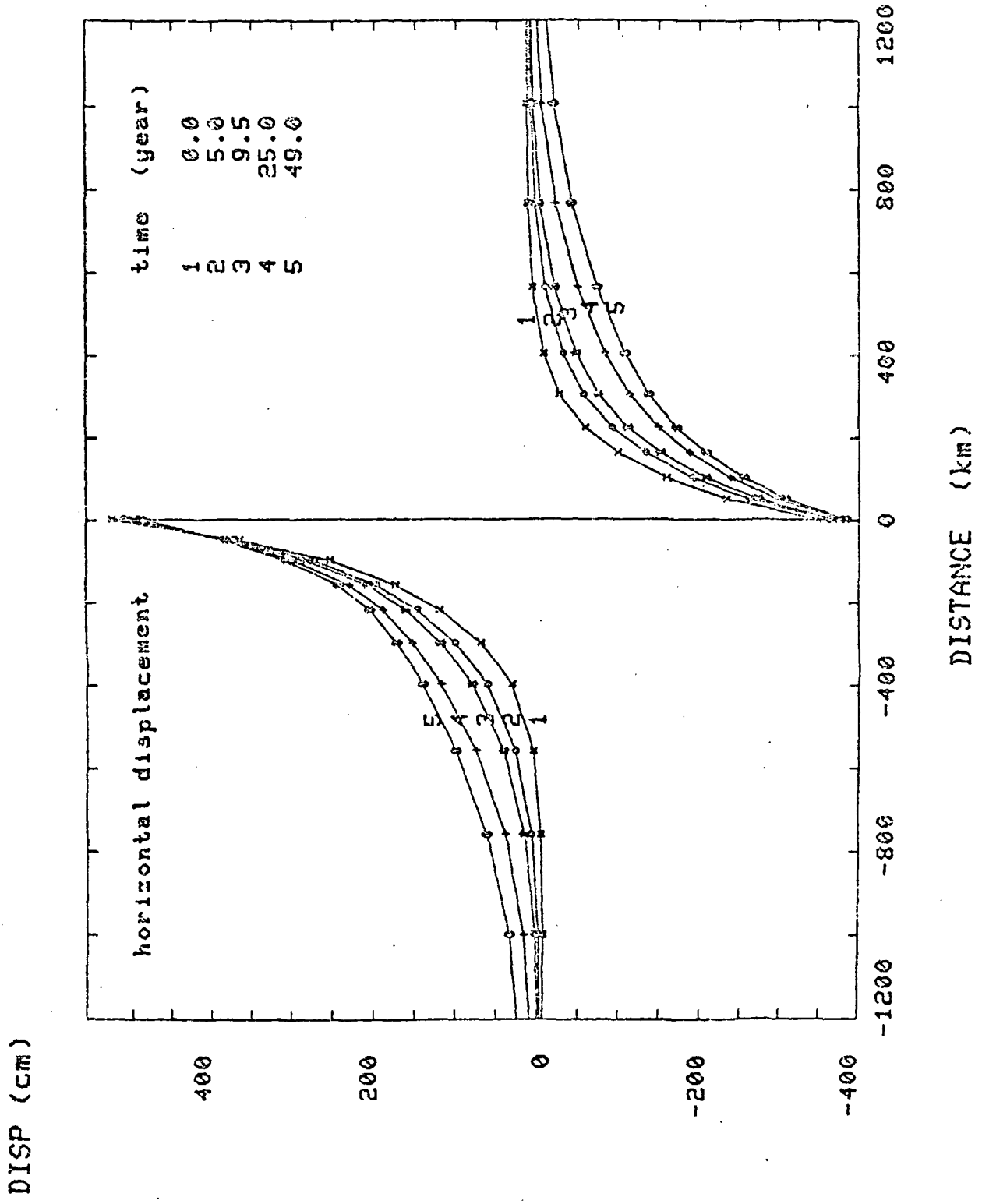

Fig. 3 Horizontal displacement along symmetry line in thrust fault model

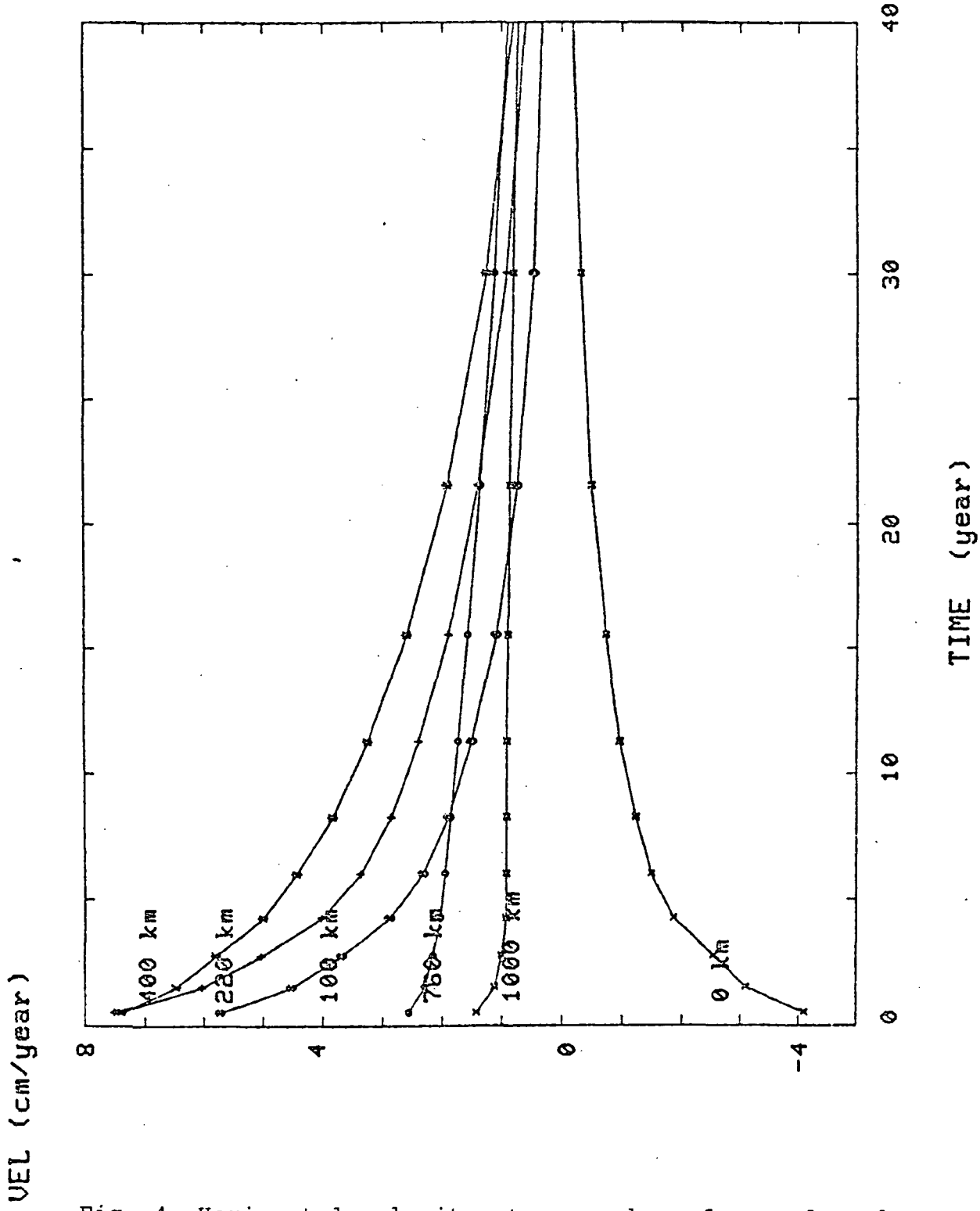

Fig. 4 Horizontal velocity at several surface nodes along symmetry line

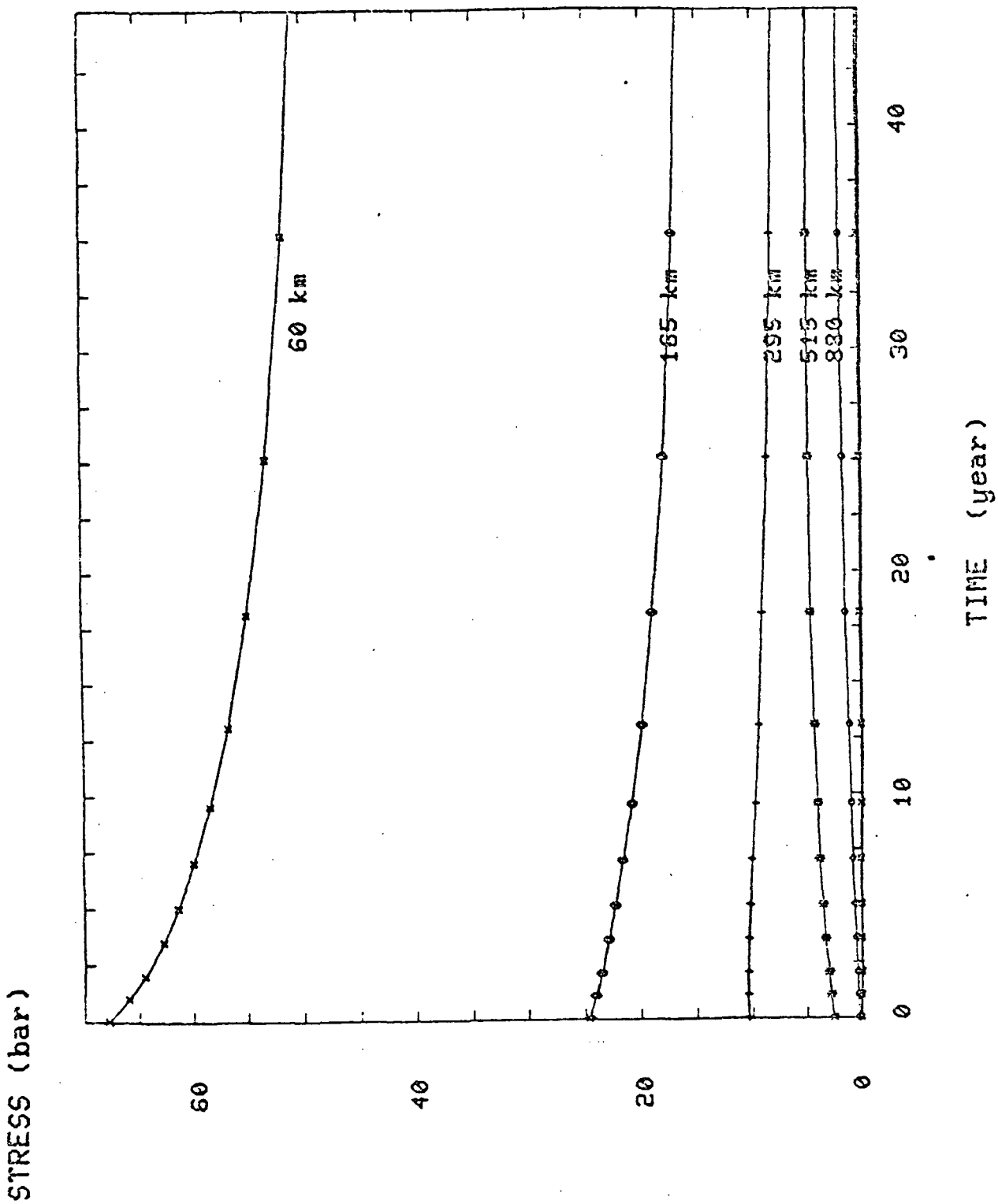

Fig. 5. Normal stress perpendicular to fault strike at locations near symmetry line for thrust fault model

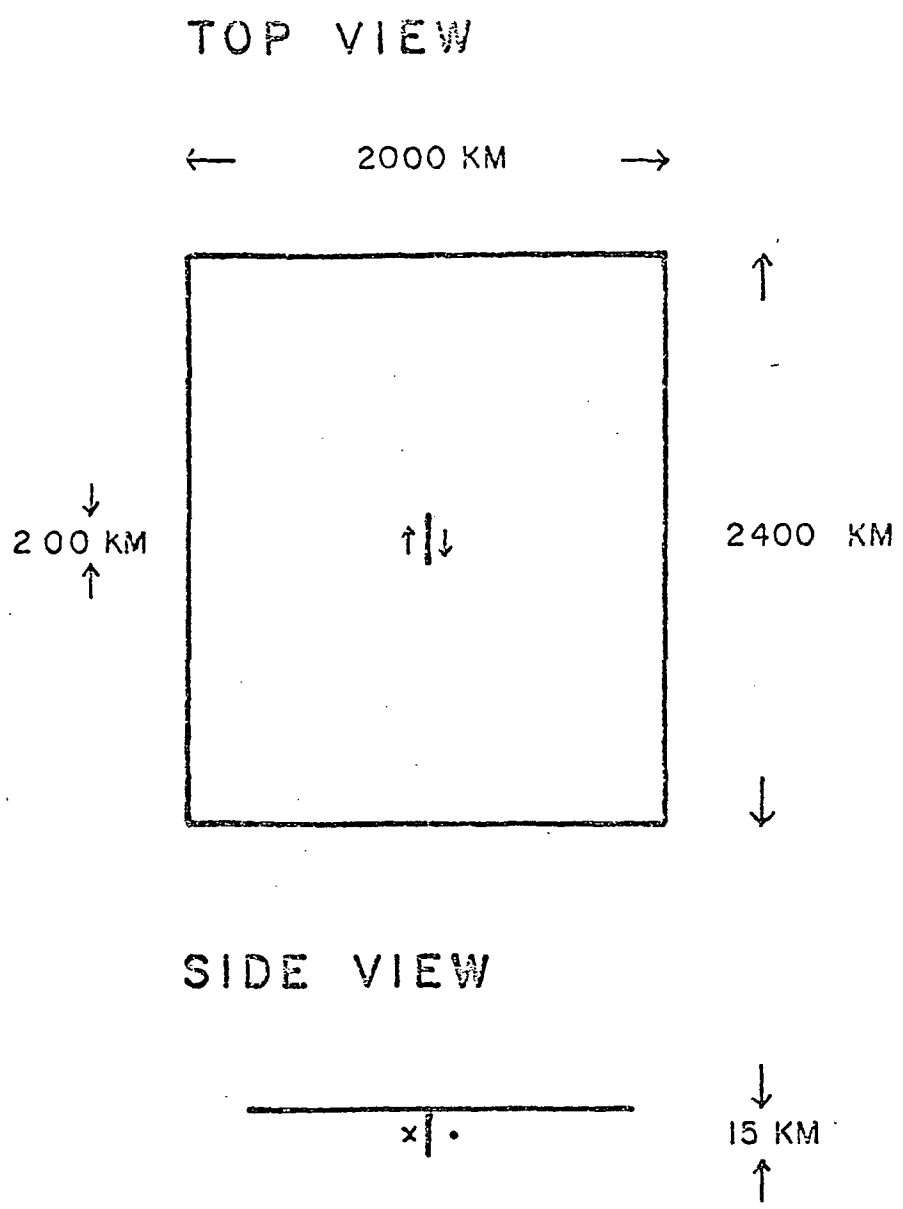

Fig. 6 Schematic diagram of strike slip fault model

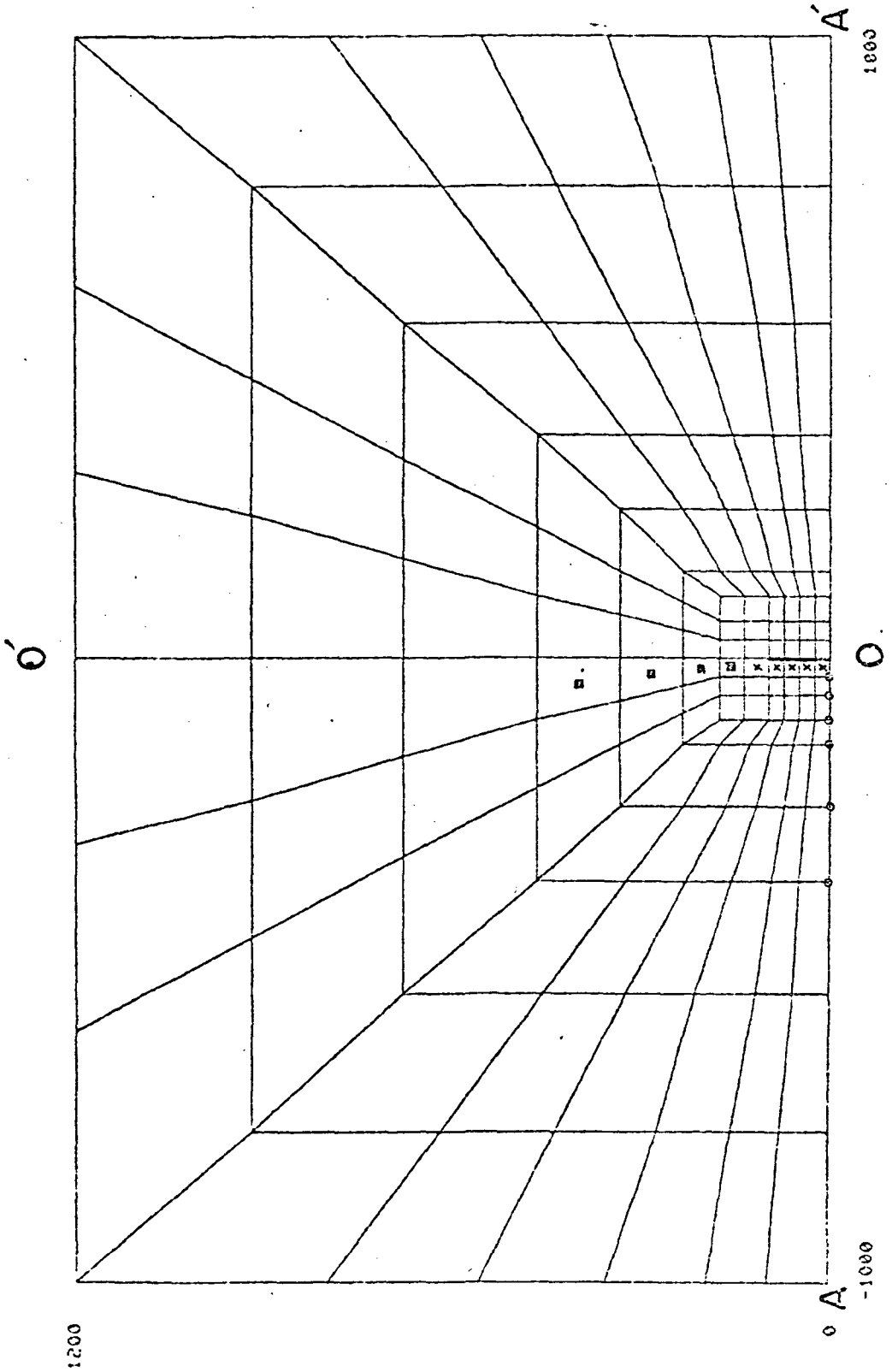

Fig. 7 Grid on free surface for half the region of the strike slip earthquake model

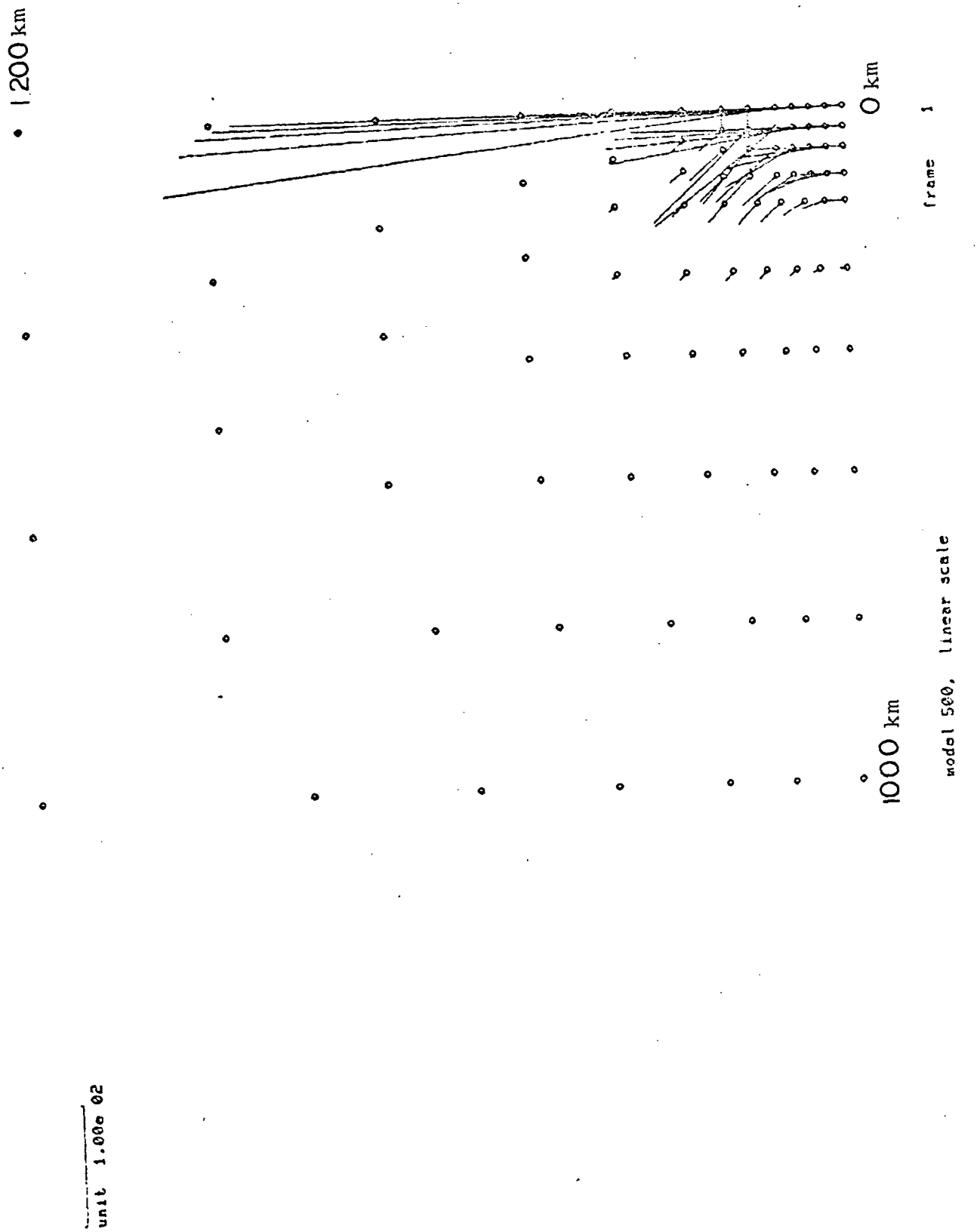

Fig. 8 Initial horizontal displacement on free surface for strike slip earthquake model

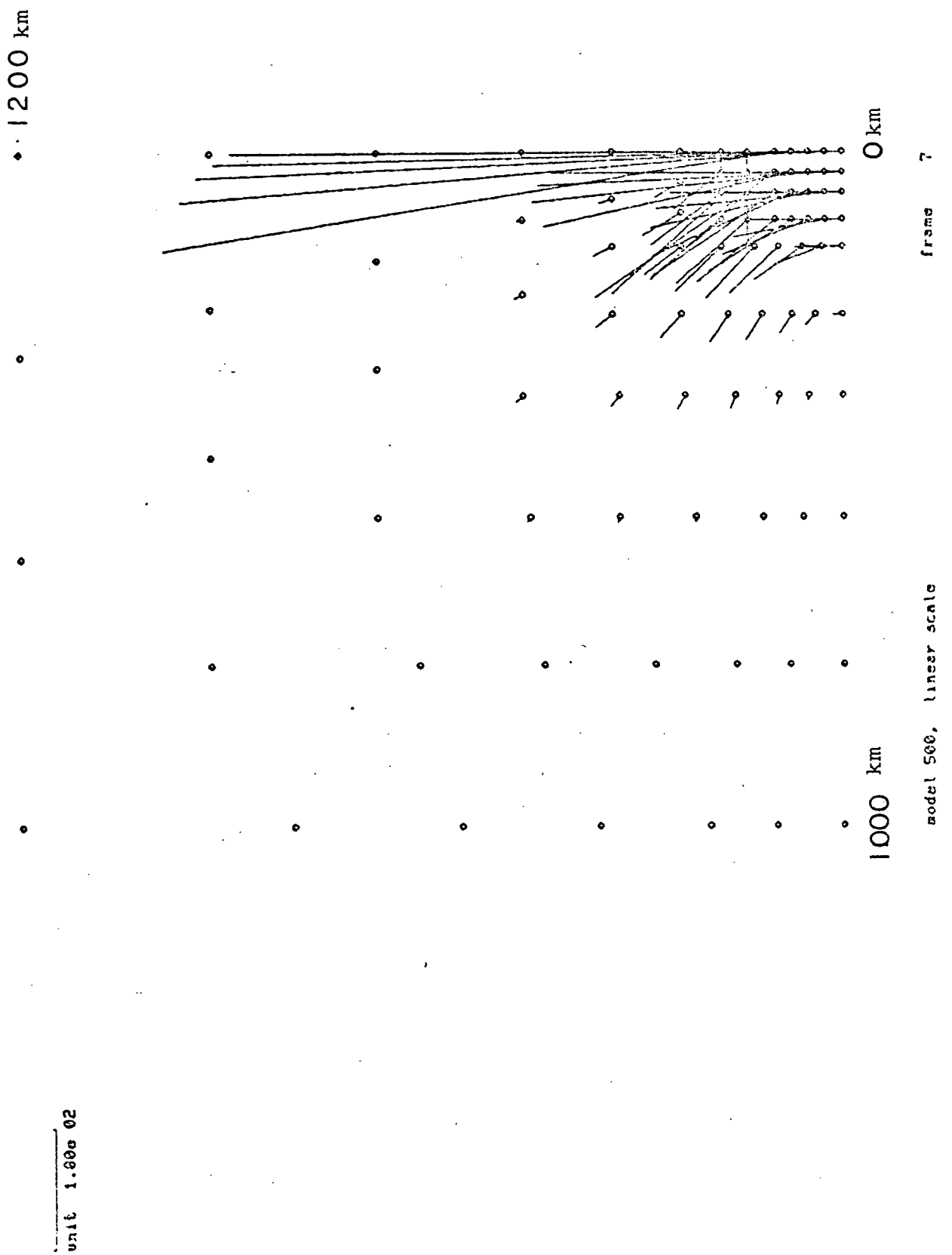

Fig. 9 Same quantity as figure 8 at 9.5 years later

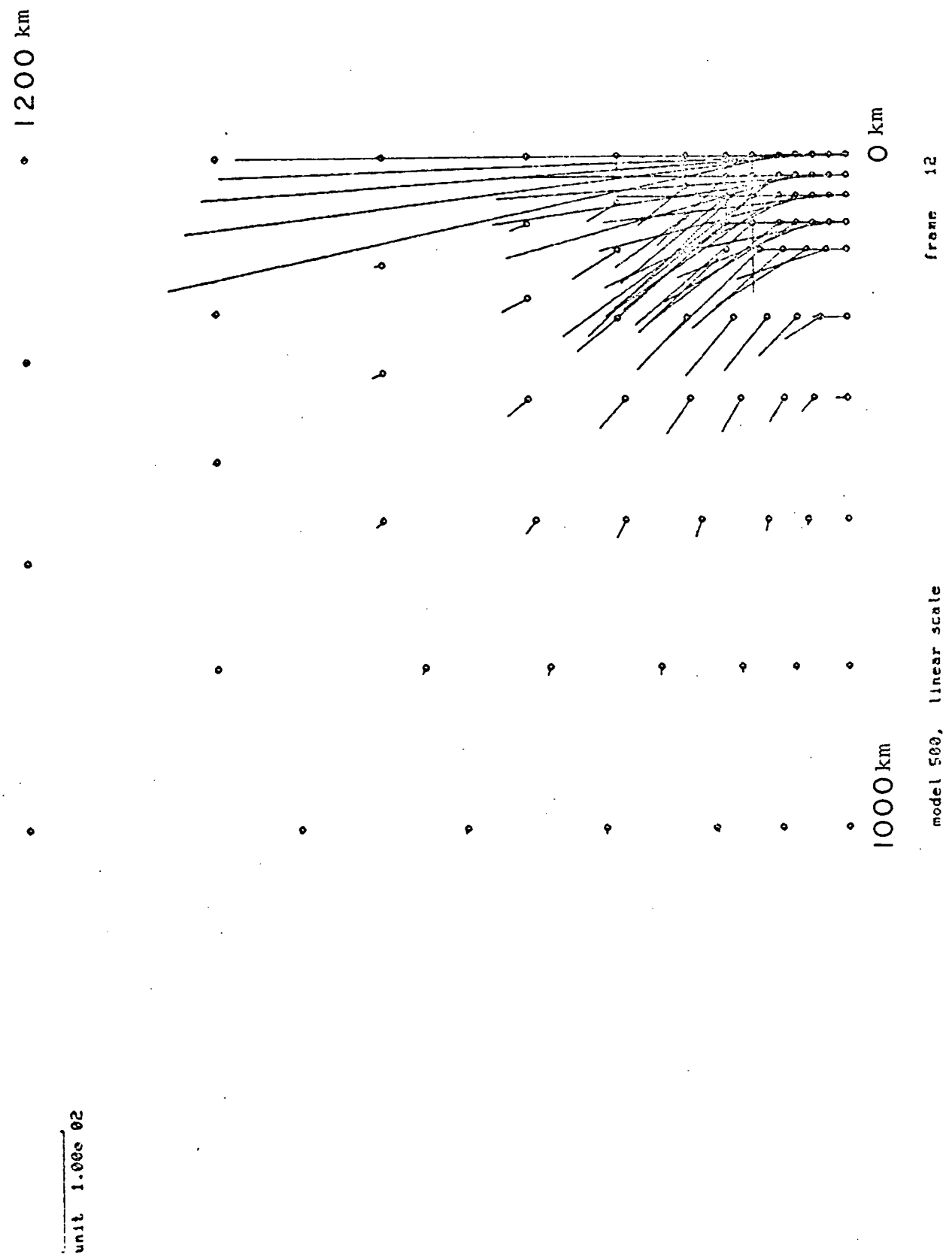

Fig. 10 Same quantity as figure 8 at 49 years later

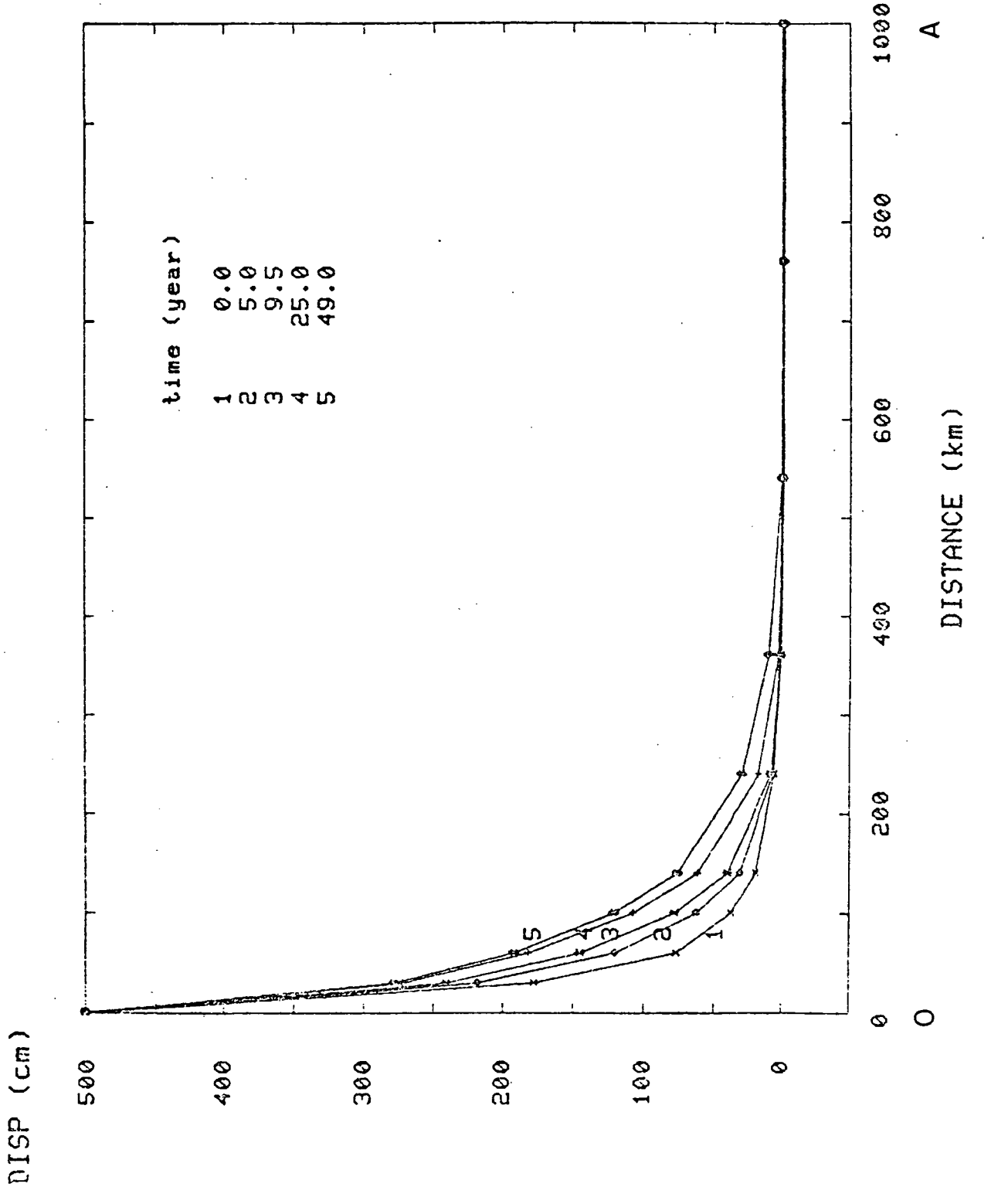

Fib. 11. Displacement parallel to fault length along symmetry line

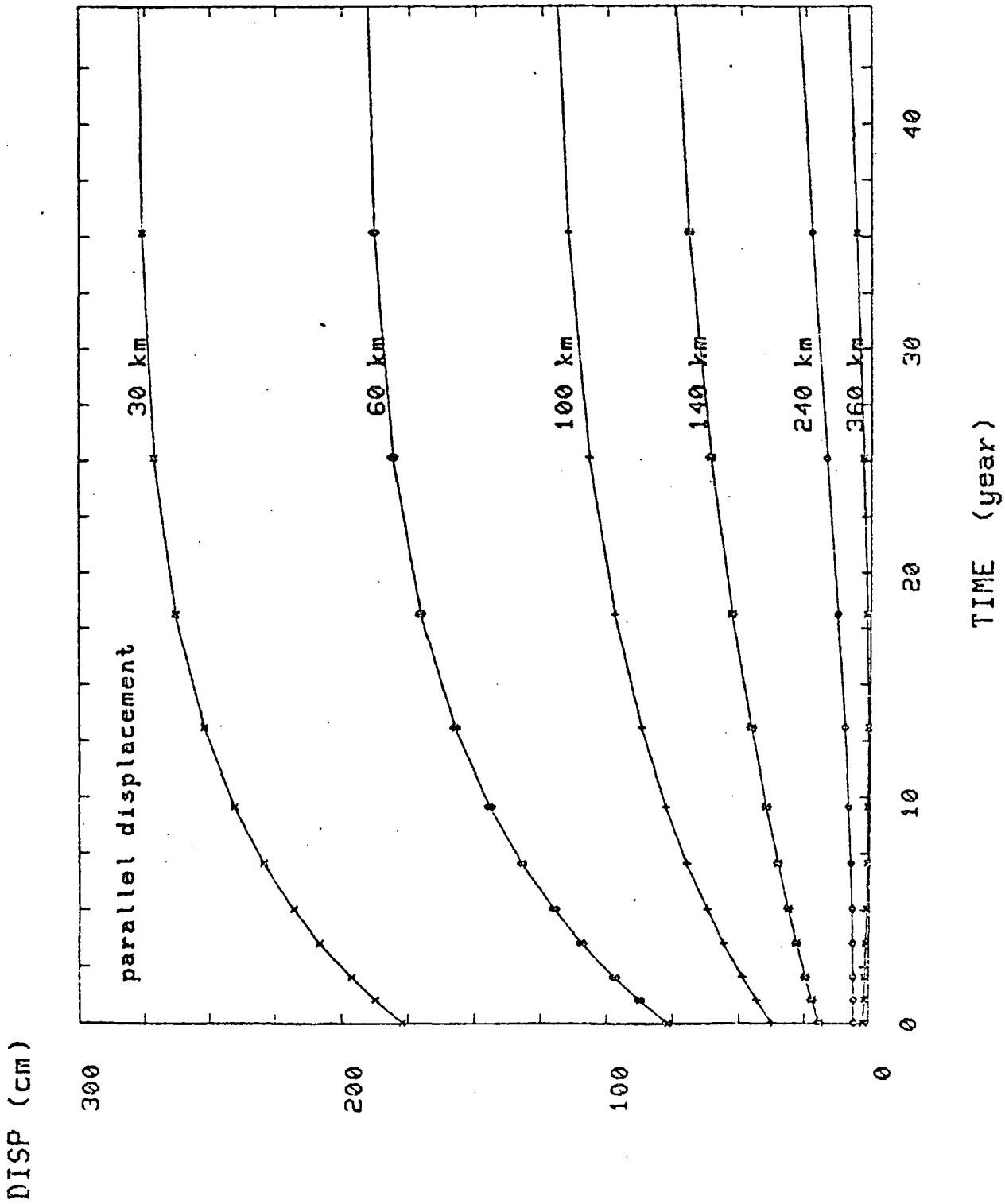

Fig. 12 Time dependence of displacement at several locations along the symmetry line

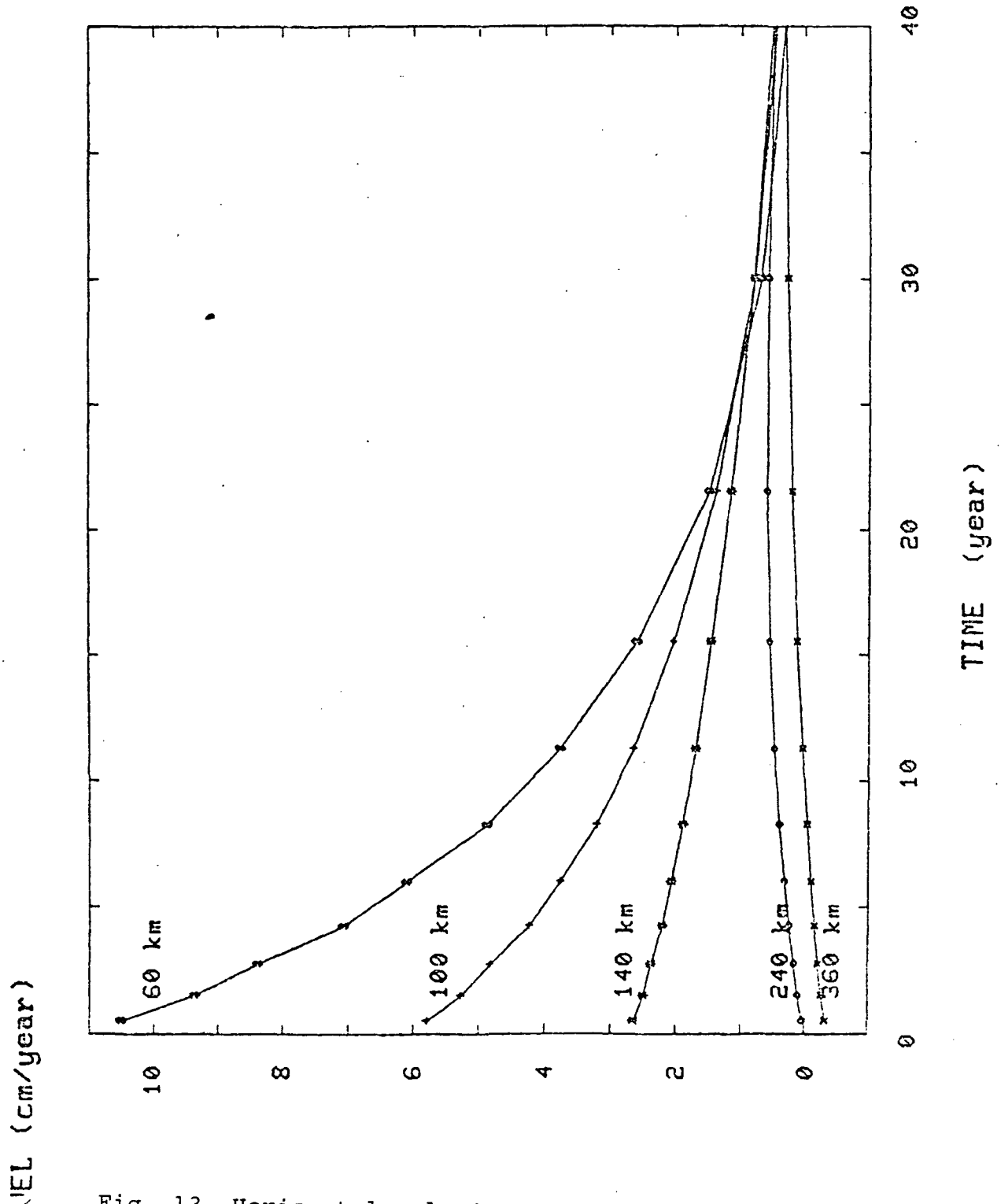

Fig. 13 Horizontal velocity at several locations along the symmetry line

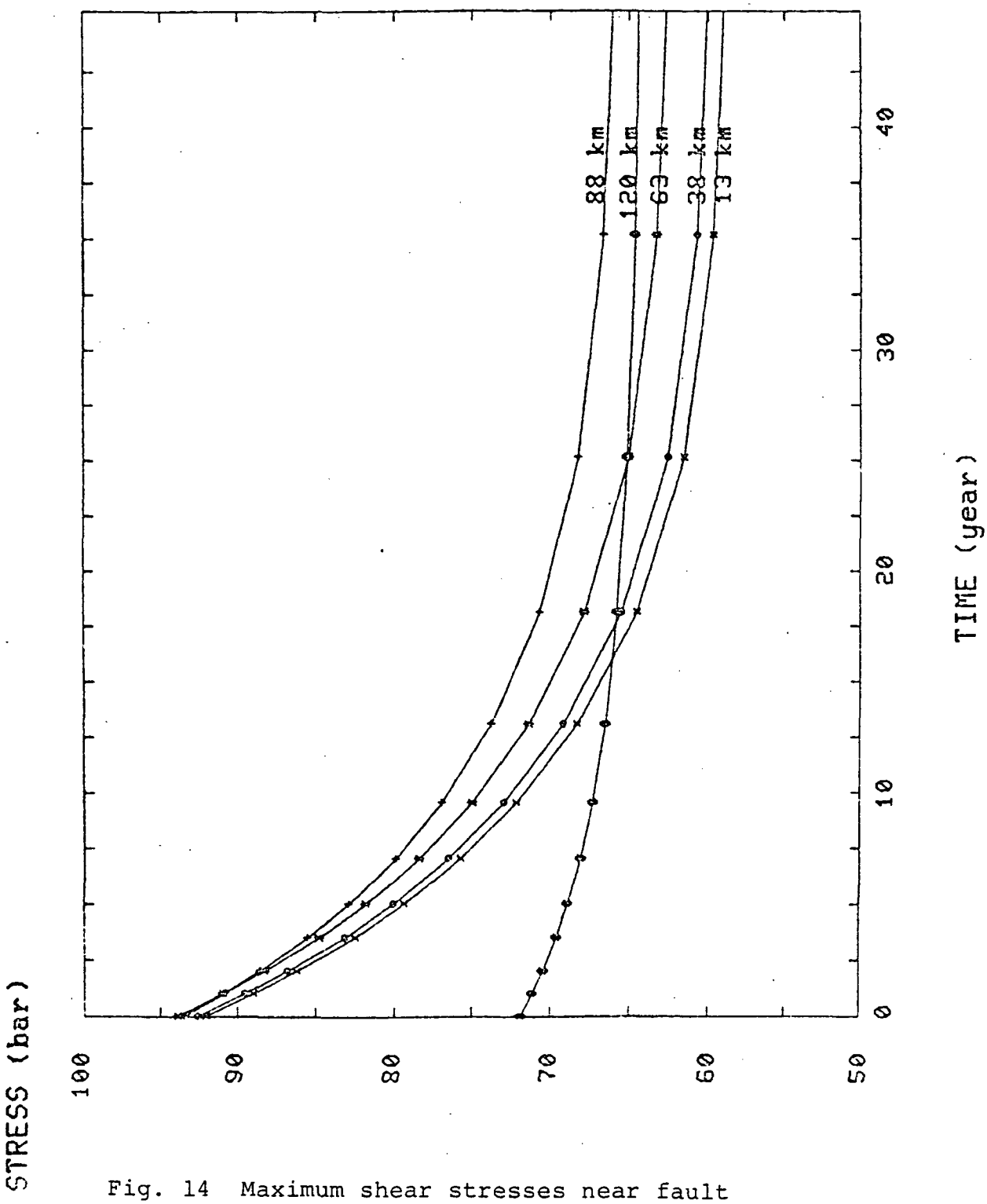

Fig. 14 Maximum shear stresses near fault

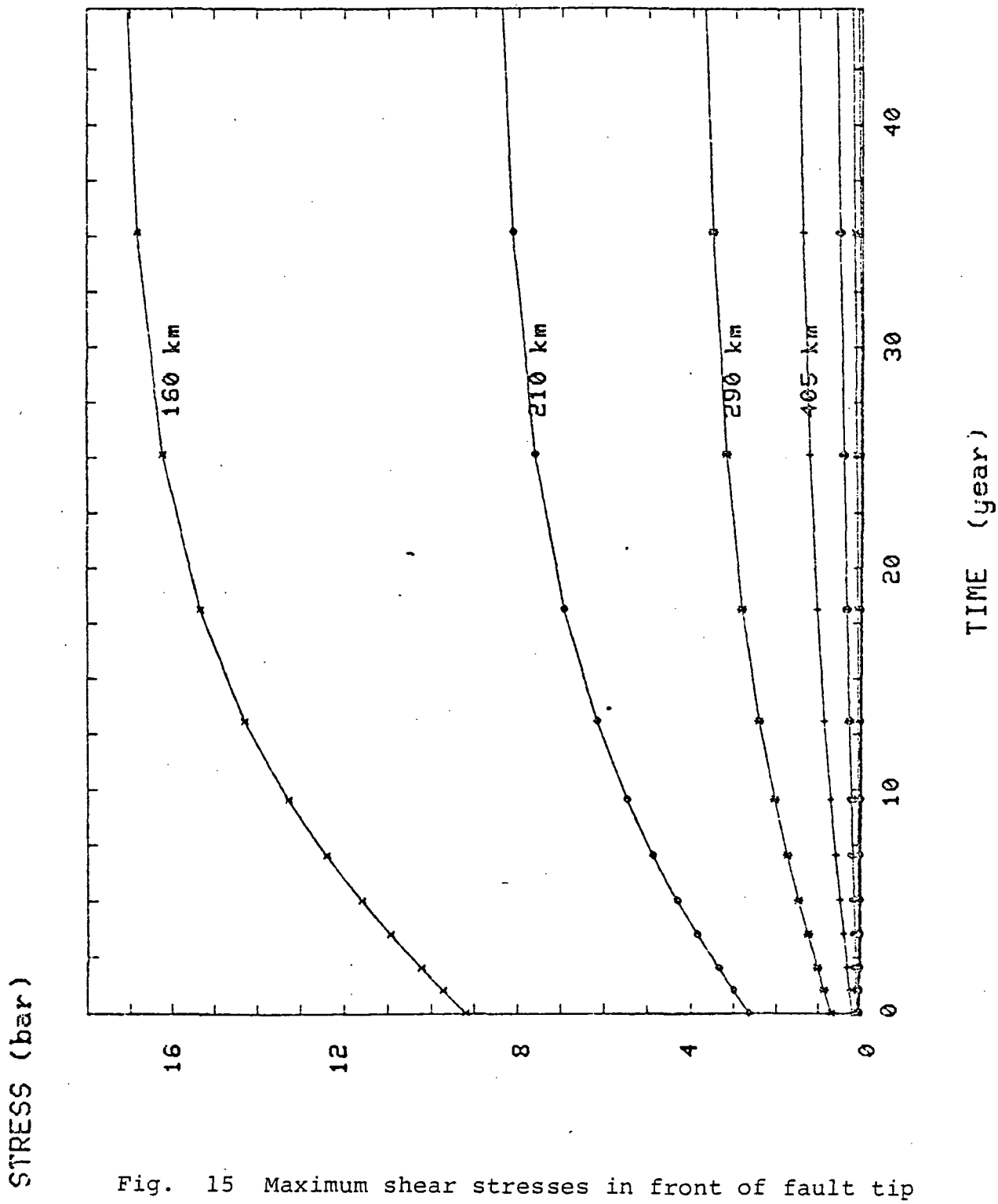

Fig. 15 Maximum shear stresses in front of fault tip